

CASE FILE COPY

NASA CR-114,496
Available to the public

GROUND EFFECT FOR V/STOL AIRCRAFT CONFIGURATIONS
AND ITS SIMULATION IN THE WIND TUNNEL

PART II EXPERIMENTAL STUDIES

By J. E. Hackett, R. A. Boles, and E. B. Praytor

Distribution of this report is provided in the interest of information exchange. Responsibility for the contents resides in the author or organization that prepared it.

Prepared under Contract NAS2-6690 by
LOCKHEED-GEORGIA COMPANY
Marietta, Georgia

for Ames Research Center

NATIONAL AERONAUTICS AND SPACE ADMINISTRATION

GROUND EFFECT FOR V/STOL AIRCRAFT CONFIGURATIONS
AND ITS SIMULATION IN THE WIND TUNNEL

Part II Experimental Studies

by J. E. Hackett,
R. A. Boles,
and E. B. Praytor

Distribution of this report is provided in the interest of information exchange. Responsibility for the contents resides in the author or organization that prepared it.

Prepared under Contract No. NAS2-6690 by

The Lockheed-Georgia Company,
Marietta, Georgia

for Ames Research Center

NATIONAL AERONAUTICS AND SPACE ADMINISTRATION

TABLE OF CONTENTS FOR PART II

<u>Section</u>	<u>Page</u>
SUMMARY FOR PART II.	1
1. INTRODUCTION TO PART II.	3
2. WIND TUNNEL MODELS.	4
2.1 The knee-blowing flap model.	
2.2 The lifting-jet model.	
3. TEST FACILITIES, INSTRUMENTATION AND TECHNIQUES.	5
3.1 The wind tunnel.	
3.2 Ground plane configurations.	
3.3 Instrumentation.	
3.4 Data reduction.	
4. TEST PROGRAM	7
4.1 General Approach.	
4.2 The knee-blown flap model.	
4.3 The lift-jet model.	
5. EXPERIMENTAL RESULTS FOR THE KNEE-BLOWING FLAP MODEL - MOVING AND FIXED GROUND	8
5.1 Static tests.	
5.2 Total lift with fixed and moving ground.	
5.3 Wing and flap surface pressure distributions - moving ground.	
5.4 Fixed-ground effects.	
5.5 Below-speed moving ground tests.	
6. EXPERIMENTAL RESULTS FOR THE KNEE-BLOWING FLAP MODEL - TANGENTIALLY BLOWN GROUND	13
6.1 Pressures at the ground.	
6.2 Pressures at the wing undersurface.	
6.3 Lift coefficients as a function of floor b.l.c. setting: selection of 'N' values.	
6.4 Other slot positions and model heights.	
6.5 Tests with simulated strut shrouds.	
7. EXPERIMENTAL RESULTS FOR THE ROUND-JET MODEL.	17
7.1 Moving and fixed ground.	
7.2 Tangentially-blown ground.	
8. COMBINED FLOOR TANGENTIAL-BLOWING REQUIREMENTS	19
9. CONCLUSIONS	20
9.1 The knee-blowing flap model.	
9.2 The round-jet model.	
9.3 Combined floor b.l.c. requirements.	

	<u>Page</u>
TABLES	22
APPENDIX	25
FIGURES	26

LIST OF FIGURES FOR PART II

<u>Figure Number</u>		<u>Page No.</u>
1.	The knee-blowing flap model, general view.	26
2.	The knee-blowing flap model, dimensions.	27
3.	Pressure orifice locations, in plan view, for the KBF model.	28
4.	Pressure orifice locations and wing section for the KBF model.	29
5.	General arrangement of the lifting jet model.	30
6.	Pressure orifice locations for the lifting jet model.	31
7.	The 42 x 30 inch low speed wind tunnel.	32
8.	The moving belt ground plane.	33
9.	The boundary layer controlled ground plane.	34
10.	Schematic of the data system.	35
11.	Typical flap pressure distributions at zero forward speed.	36
12.	Predicted and measured effective C_{μ} distributions at zero forward speed.	37
13.	Effects of hight and fixed ground flow distortion on lift performance of knee-blowing flap model.	38
14.	Effect of model height on chordwise pressure distribution. $C_{\mu_{nom}} = 0.3, \eta = 0.342$	39
15.	Effect of model height on chordwise pressure distribution. $C_{\mu_{nom}} = 0.3, \eta = 0.643$	40
16.	Effect of model height on chordwise pressure distribution. $C_{\mu_{nom}} = 0.3, \eta = 0.866$	41
17.	Effect of model height on chordwise pressure distribution. $C_{\mu_{nom}} = 3.0, \eta = 0.342$	42
18.	Effect of model height on chordwise pressure distribution. $C_{\mu_{nom}} = 3.0, \eta = 0.643$	43
19.	Effect of model height on chordwise pressure distribution. $C_{\mu_{nom}} = 3.0, \eta = 0.866$	44
20.	Formation of trapped, underwing vortex at low altitude and high jet momentum.	45

21.	Effect of fixed ground flow distortion on surface pressure distributions. $C_{\mu_{nom}} = 1.0, \eta = 0.866.$	46
22.	Effect of fixed ground flow distortion on surface pressure distributions, $C_{\mu_{nom}} = 3.0, \eta = 0.866.$	47
23.	Effect of fixed ground flow distortion on lower surface pressure distributions. $C_{\mu_{nom}}$ between 0.40 and 1.00.	48
24.	Effect of fixed ground flow distortion on lower surface pressure distributions. $C_{\mu_{nom}}$ between 1.00 and 3.00.	49
25.	Results of below-speed moving ground tests.	50
26.	Pressure distributions at the ground for the knee-blowing wing.	51
27.	Effect of blowing b.l.c., at the ground, on wing lower surface pressures. $h = 3", \eta = 0.643$	52
28.	Effect of blowing b.l.c., at the ground, on wing lower surface pressures. $h = 3", C_{\mu_{nom}} = 3.0.$	53
29.	Effect of blowing b.l.c., at the ground, on wing lower surface pressures. $h = 4", \eta = 0.643.$	54
30.	Effect of slot size on performance of ground b.l.c. system.	55
31.	Effect of ground b.l.c. on sectional lift coefficient.	56
32.	Errors in lift coefficient for fixed and b.l.c. ground configurations.	57
33.	Percentage lift errors for fixed and b.l.c. ground configurations.	58
34.	Effect of dummy underwing support strut fairing. (i) $C_{\mu_{nom}} = 1.0, N = 2.$	59
35.	Effect of dummy underwing support strut fairing. (ii) $C_{\mu_{nom}} = 3.0, N = 3$	60
36.	Static pressure distributions for the round jet model, center-tunnel position.	61
37.	Pressure changes, near a round lifting jet, caused by descending into ground effect. (i) $U_{\infty}/U_i = 0.20$	62
38.	Pressure changes, near a round lifting jet, caused by descending into ground effect. (ii) $U_{\infty}/U_i = 0.3$ and $0.4.$	63
39.	Effect of blowing b.l.c., at the ground, on lifting-jet exit plane pressures: (i) Moderate jet penetration cases.	64

40.	Effect of blowing b.l.c., at the ground, on lifting-jet exit plane pressures: (ii) Strong jet penetration cases.	65
41.	Ground simulation techniques for round, lifting-jet configurations.	66
42.	Combined floor tangential-blowing requirements.	67

SYMBOLS FOR PART II

A_D	wing duct cross sectional area (KBF model).
A_{SLOT}	total slot cross sectional area (KBF model).
b	wing span.
C_{REF}	reference chord length.
C_D	slot discharge coefficient.
C_f	developed distance from KBF slot to flap trailing edge.
C_l	lift coefficient.
\bar{C}_l	average lift coefficient based on three chordwise pressure integrations.
C_{l_h}	sectional lift coefficient based on gross lift per foot of wing span and reference length h . See also equation 8.3.
$C_{L_{hb}}$	wing lift coefficient using reference area hb .
C_P	static pressure coefficient.
C_μ	slot or jet blowing momentum coefficient
C_{μ_1}	blowing momentum coefficient based on mass flow rate and slot total pressure.
d	diameter of the lifting jet nozzle at the jet exit plane.
h	height above ground of wing quarter chord or bound vortex.
H_{SLOT}	b.l.c. slot plenum total pressure.
M	b.l.c. floor blowing parameter defined in equation 4.2.
M'	b.l.c. floor blowing parameter defined by equation 7.2.
N	b.l.c. floor blowing parameter, defined by equation 4.1.
P	jet penetration parameter in section 7.1 defined by equation 7.1 (elsewhere local static pressure).
P_{STAG}	stagnation pressure of the lifting jet impinging on the ground plane.
P_∞	freestream static pressure.
t	slot height (actual).

t_{eff} effective slot height.
 U_J lifting jet velocity at the jet exit plane.
 U_{SLOT} blowing slot air velocity at the slot exit plane.
 U_∞ freestream velocity (far field)
 η spanwise wing coordinate, normalized on semispan.
 θ angular deviation of flow (KBF model slot).
 π constant = 3.14159
 ρ air density.



GROUND EFFECT FOR V/STOL AIRCRAFT AND ITS SIMULATION
IN THE WIND TUNNEL.

Part II Experimental Studies.

by J. E. Hackett
and R. A. Boles

SUMMARY

Wind tunnel tests on a finite, knee-blowing-flapped wing and on a direct jet lift configuration were performed in a 30 x 42 inch wind tunnel at the Lockheed-Georgia Company. The objectives of these tests were, in experimental order:

- (i) To obtain definitive fixed-versus-moving ground comparisons on a powered, high-lift finite wing and on a lifting jet configuration as a function of model height and lift.
- (ii) To understand the flow mechanisms which lead to observed differences between moving and fixed-ground results.
- (iii) To discover whether the above effects of a moving ground plane can be simulated by tangential-blowing boundary layer control at the wind tunnel floor.
- (iv) To check the form and the numerical constants for the wall jet blowing equation derived theoretically in Part I of this report. This relates wall jet blowing quantities to model lift coefficient.

All of the above objectives were met. In particular, it was shown that the tangentially-blown ground gives a good approximation to moving ground results for a 20-inch span knee-blowing flap model, up to $C_{L_{hb}}$ values of about six, using the blowing quantities predicted in Part I of this report. Above this value of lift coefficient, flow impingement occurs and higher tangential blowing quantities become necessary. Nevertheless undersurface pressure distributions can still be reproduced, in detail, up to $C_{L_{hb}}$ values approaching nine - the highest tested. In the equation

$$U_{SLOT} = U_{\infty} (1 + N C_{L_{hb}} / 2\pi)$$

the tangential-blowing parameter N was increased progressively from 2, at a $C_{L_{hb}}$ value of six, to approximately 3 at the upper end of the lift range, to give proper moving ground simulation. These values are specific to the particular slot used.

Tests with a simulated underwing support strut shroud showed that fences are required, on the shroud, to prevent floor b.l.c. air from migrating up the shroud and impinging on the wing undersurface. When a trapped, undersurface

vortex is present (as was found even with a moving ground) it appears possible that suppression of spanwise flow, by a strut shroud, may modify the vortex strength and lead to incorrect results.

With a round lifting-jet model, both floor-induced interference and floor b.l.c. effectiveness were found to depend largely upon a jet penetration parameter, p , defined as $(U_j d)/(U_\infty h)$. There were no measurable ground effects, at the exit surface, when p was less than 1.25. When the exit plane was three diameters from the ground, or more, it was immaterial whether the ground was fixed or moving. At an altitude of one diameter or more and with p between 1.25 and 2.5, the tangentially-blown ground provided a good simulation of moving ground results. However, as p increased beyond 2.5, the boundary-layer-controlled ground was decreasingly effective. Beyond p -values of 4 or 5, there appears to be little alternative to using a moving ground.

1. INTRODUCTION TO PART II

In Part I of this report, the provision of wall-jet boundary layer control at the floor surface below a lifting model was suggested as a means of replacing a moving ground by a more acceptable device. Suitable wall-jet blowing velocities and slot heights were predicted and a function of model lift coefficient, CL_{hb} , was suggested which defines blowing velocity as a function of model lift.

The purpose of the experiment described here is to determine the feasibility of this wall jet scheme and find the limits of application. It is of additional interest to investigate the use of the system with a typical jet or fan-lift configuration: a single, fuselage-mounted, round jet configuration was chosen.

Base data obtained with a moving ground and with a fixed ground provided information concerning when special ground treatment is required. The general philosophy throughout was to provide conditions extending beyond the limits of normal STOL testing. To this end an unswept, 20-inch span, low-winged model was designed with a full-span, highly-deflected, knee-blown jet flap. The model support sting, which was tubular with one square inch internal cross sectional area, allowed high mass flow and momentum coefficients to be attained. The sting height could be continuously varied from a condition with the flap trailing edge almost touching the floor to a position above the wind tunnel centerline. The available test ranges were consequently much more demanding, for the tunnel floor simulation, than most STOL high lift test conditions.

A round, lifting-jet model was also tested: configuration details are given in Section 2. Moving-versus fixed ground phenomena for this model are regarded as less important than for the finite wing. For this reason, the jet model was more lightly instrumented and was tested less.

A suitable sting balance was available, but the associated air bridge lacked capacity for the present experiments. A pressure-tapped model was therefore designed, which allowed ground-induced effects to be seen as changes in pressure distribution. This caused a significantly increased data load but lead to a much better understanding of flow mechanisms, particularly under the wing.

Sections 3 and 4 will be devoted to descriptions of the models and test techniques. Fixed-versus-moving ground comparisons and tangentially-blown floor results will be discussed in Sections 5 and 6 respectively. Section 7 will be devoted to the round-jet model while Sections 8 and 9 will be used to summarize the results and draw conclusions.

2. WIND TUNNEL MODELS

2.1 The Knee-blowing Flap Model

Figures 1 and 2 show the rectangular, low-mounted wing and basic fuselage. The wing span and area are 20 inches and 0.556 square feet respectively and there is a full span slat and a full span, highly-deflected flap with a blowing slot at the knee. A half-circle fairing along the top of the fuselage covers pressure tubes and instrumentation wires. Air is supplied through the sting into the fuselage and then to a plenum in the wing. The slot height used was 0.045 inches. At a tunnel dynamic pressure of 10 psf, momentum coefficients up to 3.0 were available.

In addition to 109 external static pressure orifices on the wing, there were four static orifices in the wing plenum and four total pressure tubes pointing towards the fuselage. Details of the layout are given in Figures 3 and 4.

Incidence was measured using an accelerometer mounted within the nose of the model. Additional physical characteristics of this model may be found in Table I.

2.2 The Lifting-jet Model.

The same fuselage is used as before, but additional flow straighteners and screens are included which give the desired jet flow quality. A flat-plate, high wing is fitted with a span of 13 inches and an area of 0.417 square feet (See Figure 5). The jet diameter is 1.75 inches and velocities up to 370 ft/sec are available. Further details are given in Table I.

The exit plane surrounding the round jet contains 46 pressure orifices arranged as shown in Figure 6. Except for the accelerometer in the nose, there was no other instrumentation.

3. TEST FACILITIES, INSTRUMENTATION AND TECHNIQUES

3.1 The Wing Tunnel (See Figure 7)

The tunnel is located at the Lockheed-Georgia Company Research Laboratory. The test section dimensions of 30 x 42 inches give a height-to-width ratio of 0.7 and an area of 9 square feet. There is a 6-foot diameter, 400 horsepower, 1200 rpm fan with speed variations via an eddy current variable speed unit. The empty test section top speed is 310 feet/second, however ground belt limitations made about 100 ft/sec desirable for the present tests.

The model sting is mounted on a sector pitch mechanism giving a range of incidence from -14 to +24 degrees. The entire pitch mechanism is mounted on a hydraulic lift table which allows model altitude to be changed conveniently, while retaining the center of rotation at the model position. The available height range is from 1.75 inches above the floor to beyond the tunnel centerline. At the lower altitudes, the incidence range becomes limited by sting interference with the tunnel floor.

3.2 Ground Plane Configurations

Three ground plane configurations are available in the test section, the normal solid floor, a moving belt ground plane and a tangentially-blown, boundary-layer-controlled floor. Configuration change is accomplished in about four hours.

The moving ground spans 30 inches of the 42 inch test section width and has an effective length of 38 inches, between roller centers. The belt is powered by a hydraulic motor rated at approximately 20 H.P. which is adequate up to more than 100 ft/sec. The belt speed, which is continuously variable, is monitored via the voltage output of a 'Globe' D.C. motor coupled to the driven roller and used as a tachogenerator. Calibration was made using a pulse counter and a digital voltmeter.

Tracking of the belt is currently monitored and adjusted manually. Tension adjustments are made at one end of the non-driven roller, the other end being permanently set. Principal adjustments are found to be necessary during start-up and shut down, though some changes have to be made when model lift is increased under near-to-ground conditions. Significant increases in power are usually also required in these circumstances.

The boundary-layer-controlled ground plane (Figure 9) is provided with five 30-inch-long blowing slots spaced 4, 8, 12, 16 and 20 inches forward of the center of the test section. Spacers in the slots make available heights of 0.032, 0.051 and 0.067 inches. Each slot has a large, separate plenum and a separate control valve. Each plenum has a static pressure tapping which is used to measure and set slot pressure ratio. Slot velocities up to 460 feet/second are available. There are also surface static pressure orifices and Preston tubes arranged as shown in Figure 9.

3.3 Instrumentation

Test section dynamic and total pressures are monitored using Statham temperature-compensated pressure transducers, which have good linearity over a ± 0.3 psi range.

Auxilliary air supply, ground plane pressure data, model pressure data and other pressure data (boundary layer rakes, total pressure probes, etc.) were all measured using Stratham 48-port, type D3 Scanivalves, of which there were seven. These were arranged in three gangs and, with the exception of a single 150 psi transducer used for internal flows, all were used with 2.5 psi transducers. At any one time, no more than five scanivalves were in use, since all were left coupled to a particular model or to the b.l.c. box.

Flow-Dyne, critical-flow nozzles were used for mass-flow measurement. The mass-flow requirement of the jet model was sufficiently different from the wing model that a smaller critical flow nozzle had to be used.

The accelerometer mounted in the nose of the model, already mentioned, was calibrated against a Hilger and Watts, Model B vernier angle gauge.

3.4 Data Reduction (See Figure 10)

Raw data counts were recorded on magnetic tape by a Hewlett-Packard data acquisition system located next to the wind tunnel. The tapes were taken to the CDC 1700 computer, located at the Lockheed-Georgia low speed wind tunnel, where appropriate conversion and data reduction routines were applied. Initial output was in tabulated form and plot-tapes could be made where required. Plots of selected runs were made using a Calcomp plotter associated with a Univac 1106 computer.

Originally, fast data turn-around was planned, so that test runs could be made very selectively. In practice, priority conflicts and other difficulties prevented this and resort had frequently to be made to the use of raw data counts printed on a strip record during tests.

Both dynamic and free stream static pressure were recorded at each scanivalve step, which eliminated slow-drift errors during the 40-second scanivalve stepping cycle. Calculated pressure coefficients were integrated routinely at spanwise stations of 34.2%, 64.3% and 86.6% of semispan.

The momentum coefficient of the slot was calculated on the basis of the mass flow measurement using the critical nozzle together with the total pressure: atmospheric pressure ratio, based on wing plenum conditions, which gave slot velocity. No measurement of slot area was involved in this calculation. The designation $C_{\mu 1}$ is used for momentum coefficients calculated in this way. This differs from the nominal, setting value $C_{\mu \text{nom}}$ because momentum coefficient could only be set approximately.

In the case of the round jet model, critical flow nozzle inlet pressure was used for monitoring purposes. This was calibrated using total pressure rake measurements at the jet exit plane.

4. TEST PROGRAM

4.1 General Approach

The procedure used was first to determine under what combinations of test variables ground effect is significant, then determine within this range where differences arise between moving and fixed ground test conditions and finally determine the regimes in which a boundary-layer-controlled ground is a viable alternative to a moving ground.

The major test variables were model height, moving ground belt speed, flap or jet momentum coefficient, angle of attack and floor b.l.c. quantities where appropriate.

Tuft observations on the model and/or the ground plane were made routinely.

4.2 Tests with the Knee-Blowing Flap Model

Test heights were 3, 4, 5, 10 and 15 inches giving height-to-chord ratios (based on 4-inch nominal chord) of 0.75, 1.0, 1.25, 2.5 and 3.75 respectively relative to the wing datum line.

When employed, the moving ground speed was set equal to tunnel speed. With slot momentum coefficient above 2.0 and heights below 5-inches, there was undue belt wear and some control difficulty at 10 psf dynamic pressure. Consequently, these tests were run at 5 psf dynamic pressure. Otherwise the belt was run routinely at approximately 96 ft/sec.

In the equation for floor b.l.c. blowing,

$$U_{\text{SLOT}} = U_{\infty} (1 + N C_{L_{hb}} / 2\pi) \quad (4.1)$$

the parameter N was varied from 0 to 4.0. Choice of blowing slot location was made so as to place it as close as possible to the position where C_p was 0.3, as suggested in Part I of this report.

4.3 Tests with the Jet-lift Model.

Test heights were at 1, 2, 3, 4 and 8.6 times the 1.75-inch jet diameter, the latter being at the tunnel center. Height measurements were to the exit-plane datum. In order to cover the full range of forward speed ratios, down to $V_{\infty}/V_j = 0.1$, decreased tunnel speed was used in some cases.

The floor b.l.c. equation employed for the jet model was

$$(H_{\text{SLOT}} - p_{\infty}) = M(p_{\text{STAG}} - p_{\infty}) \quad (4.2)$$

where p_{STAG} was the zero-forward-speed stagnation pressure where the jet impinged on the wind tunnel floor. This form was used because the problem was seen as one of obtaining a total pressure balance between the forward-moving part of the impinging jet and the wall jet originating at the blowing slot.

5. EXPERIMENTAL RESULTS FOR THE KNEE-BLOWING FLAP MODEL - MOVING AND FIXED GROUND.

5.1 Static Tests

Since no balance measurements were available, model static performance was determined using flap upper-surface pressure measurements. For these experiments, the wind tunnel floor was completely removed and maximum possible venting was provided in the walls and in the roof. The table below shows values of isentropic thrust, jet velocity etc. which are typical of model test conditions:

	$C_{\mu_{nom}} = 0.7$		$C_{\mu_{nom}} = 3.0$	
Tunnel 'q'	5 psf	10 psf	5 psf	10 psf
Calc. isentropic Thrust	1.88 lbs	3.84 lbs	3.45 lbs	17.15 lbs
H/P	1.082	1.256	1.398	1.837
Slot velocity*	380	620	750	1000
	ft/sec	ft/sec	ft/sec	ft/sec

* 0.045 - inch slot

Figure 11 shows flap upper surface static pressure distributions for the third of the above examples. The rapid local pressure changes at each end of the radiused region are attributable to the discontinuities in curvature there. Detailed differences near the slot, probably in pressure hole position, may have caused the suction peak to be missed for the two inboard stations. The intensity of the suction peak is less at lower C_{μ} values than for the example shown.

There is also a more general decrease in flap suction in the inboard direction. This is caused by a spanwise flow component which is quite noticeable near the wing root but which decreases rapidly outboard.

To determine the effect of spanwise flow on the slot discharge coefficient, a simple analysis may be made based on considerations of continuity. The angular deviation of the flow out of the slot is obtained as:

$$\theta = \left(\frac{t}{A_D} \right) \left(\frac{b}{2} \right) (1 - \eta) \quad (5.1)$$

where A_D is the duct cross-sectional area within the wing and t is the slot height. For the present model this yields

$$\theta = 43.0 (1 - \eta) \text{ degrees} \quad (5.2)$$

Further development gives the slot discharge coefficient, C_D , as

$$C_D = \frac{A_D}{A_{SLOT}} \sin\left(\frac{A_{SLOT}}{A_D}\right) \quad (5.3)$$

This has a value of 0.91 in the present case. Measurements of plenum pressure, mass flow and slot dimensions gave a value of 0.87 over a wide range of blowing conditions. A two-dimensional discharge coefficient of 0.96 is implied, which seems very reasonable.

The above approach may also be extended to determine the distribution of lifting C_{μ} . We may write:

$$C_{\mu_{eff}} = C_{\mu_1} \cos^2 \theta \quad (5.4)$$

Since the chordwise velocity is reduced by the factor $\cos \theta$. θ is given by equation (5.1) or (5.2)

At the flap trailing edge, spanwise flow migration has occurred in such a way that no flow reaches a small inboard segment. The remaining flow focuses at the trailing edge in a manner described by the equation:

$$t_{eff} = t \left\{ 1 - \frac{t}{A_D} C_f \sec^2 \theta \right\}^{-1} \quad (5.5)$$

where C_f is the developed distance from the slot to the trailing edge.

We may combine flow inclination effects (Equation (5.4)) and focussing effects (Equation (5.5)) to obtain the effective trailing-edge distribution of momentum coefficient, i.e.

$$C_{\mu_{eff_{te}}} = C_{\mu_1} \frac{t_{eff}}{t} \cos^2 \theta \quad (5.6)$$

Figure 12 shows theoretical C_{μ_1} , distributions obtained on applying the above equations at the slot, at the downstream end of the flap radius and at the trailing edge. The C_{μ_1} value is evidently a function not only of spanwise position but also of chordwise position. Integrated surface pressure measurements will therefore comprise weighted averages, with bias toward the radiused region. The experimental points in Figure 12 confirm that this is so. The agreement is quite surprising considering that there have been no allowances for turning efficiency or for scrubbing loss.

The broken line, in Figure 12, is appropriate for use when interpreting the results in the following sections.

5.2 Total Lift with Fixed and Moving Ground

Chordwise experimental pressure distributions were integrated routinely using techniques which included special measures for the sudden pressure rise at the flap knee and for extrapolation to the trailing edge. Computer integrations of early runs were found to agree well with hand plots and planimeter readings.

Local normal force, chordwise force and sectional pitching moment were available at the three pressure plotted stations. \bar{C}_L was calculated as an arithmetic mean of these three values and gave a measure of overall performance. Under elliptic load, this is a reasonably good measure of total lift: an area of 1.47 is obtained for a unit-radius semicircle, compared with the correct value of $\pi/2$ for a distribution uninterrupted by fuselage interference effects.

Forces on the slat are not directly available, because it is too small for a meaningful number of pressure tubes to be installed. However, studies using the Lockheed-Georgia multiple airfoil program, making cross-reference to experimental pressure distributions, show that slat lift was small at zero incidence.

Chordwise pressure integrals for the knee blowing flap model include all of the jet turning and, since the exit plane of the blowing slot is vertical, the normal force integral requires no addition of a thrust component. Though these integrals are of considerable general interest, no attempt will be made to describe the results comprehensively.

Figure 13 summarizes the lift performance of the wing, as a function of the slot momentum coefficient, at various heights above the ground. Here, as in the remainder of this report, moving ground data is taken as the norm and fixed ground deviations are viewed as experimental error. It is evident from Figure 13 that $C_{L_{hb}}$ values extend well into the range where image-induced counterflow reduces lift. (see section 2 of Part I of this report). With moving ground there is a lift decrease of up to 15% between center tunnel and the smallest height in Figure 13. At this lowest height, there is a further decrement, at a C_{μ_1} of 2.0, of 20% on stopping the belt.

The upper part of the C_{μ_1} range is admittedly high relative to most aircraft applications. Nevertheless, significant errors have also been demonstrated in the lower C_{μ_1} regime. The tests therefore provide a broad basis for testing the effectiveness of floor boundary layer control as an alternative to a moving ground.

5.3 Wing and Flap Surface Pressure Distributions - Moving Ground

Pressure distributions at the three span stations are shown in Figures 14, 15 and 16. At this C_{μ_1} value (0.3) the flap flow was fully attached at all spanwise stations. Flap loads continue to reflect the span-load gradients found statically, but leading-edge loads follow the more-familiar decline outboard. The flow is virtually stagnant on most of the undersurface inboard.

At the 86.6% span stations there is only a moderate decline in total lift coefficient.

Figures 14, 15 and 16 include data for heights of 3", 5", 10" and 15". A continuous decline in upper surface suction is seen as height is decreased, which is most marked at the flap suction peaks and is of increasing severity inboard. Pressures on the undersurface (at $C_{\mu 1} = 0.3$) show very little change with height for these, moving ground, cases. However there is a slight increase in undersurface lift near the nose as the ground is approached and it seems likely that slat loads are also changing. Lift coefficients on the wing/flap decrease by about 13½% between center-tunnel and the 3" model height.

Figures 17, 18 and 19 represent the high $C_{\mu 1}$ range. Here, the blowing effects predominate and the span loading becomes more uniform. Ground effect is more severe (about 18½% average) with most of the increase arising inboard. Undersurface pressures near the nose behave much as before but decreases in static pressure under and ahead of the flap now become evident as the ground is approached. These are especially significant with the moving ground present because the ability to repeat the effect will be a very sensitive test of the abilities of the boundary layer controlled ground.

Figure 20 shows the wing section, drawn at full scale, situated 3" above the ground. Streamlines have been added to illustrate the flow near the 85% semispan station. Data employed in preparing the figure include slat flow computations, wing pressure distribution (Figure 19, Run 350 and others) tuft wand observations and data measured on the boundary layer controlled ground when set correctly. Figure 20 is believed to be both qualitatively and quantitatively accurate. What is not evident are the strong spanwise flows which were superimposed upon the flow depicted in Figure 20. The flow beneath the wing is evidently both viscous and three-dimensionally complex.

5.4 Fixed-Ground Effects

With the ground fixed, the free stagnation points (Figure 20) became attached to the surface, the front one moving much further forward, even at moderate $C_{\mu 1}$ values. The jet sheet impinged upon the ground and split, with some fluid moving forward, some aft. The forward moving fluid was, in effect, a wall jet which decayed until sufficient total pressure loss had occurred that mainstream stagnation/separation could occur. The separated region enclosed a strong vortex which induces significant undersurface suction and lift loss. In Figure 21, it is clear that most of the undersurface has become involved: the attendant lift loss, beyond the moving ground value, is about 18½% at this station. Conditions on the upper surface, in contrast, appear to be virtually the same, at $C_{\mu 1} = 1.0$, whether the ground is fixed or moving.

Increasing $C_{\mu 1}$ to 3.0 (Figure 22) increases the fixed-versus-moving-ground lift loss to 23½%, even though fixed ground flap lift increases slightly and moving ground undersurface lift loss is now present. Failure to employ a moving ground, or its equivalent, under these conditions would give an apparent ground effect of 12% (see Figure 19) plus 23½% due to fixed ground flow distortion. (Figure 22)

Figures 23 and 24 extend the wing undersurface data to other $C_{\mu 1}$ values and to one chord height. At 3" height ($h/c = 0.75$) differences occur between fixed and moving ground undersurface pressures at a $C_{\mu 1}$ value of 0.3, but only reach significant size at $C_{\mu 1}$ of 0.7 and above. At one chord height, the effects are similar, but less intense. Fixed and moving ground distributions separate little until $C_{\mu 1}$ values somewhat greater than 1.0. Even so, both fixed and moving ground results indicate the trapped vortex phenomenon at 4" height for the high end of the $C_{\mu \text{ nom}}$ range.

5.5 Below-Speed Moving Ground Tests

Tests with a belt surface moving at less-than-mainstream speed are interesting in their own right because of moving belt mechanical limitations. In the present context, however, such tests can be viewed as having under-active boundary layer control. The sensitivity of the phenomena just described to belt speed reduction is an indicator of the likely success of the boundary layer controlled ground under intractible conditions such as ground impingement. Figure 25 shows that belt speed may be halved, almost with impunity, up to $C_{\mu 1} = 1.0$. This remains substantially true at a momentum coefficient of 2.0 and even at 3.0, the fixed ground error is reduced to one third. Until the more extreme conditions are encountered, the flow is more dependent upon the presence of a moving belt (i.e. at half-speed or above) than upon its running at full speed. This gives encouragement concerning the prospects of boundary layer control at the floor.

6. EXPERIMENTAL RESULTS FOR THE KNEE-BLOWING FLAP MODEL: TANGENTIALLY-BLOWN GROUND

6.1 Pressures at the Ground

Figure 26 shows the development of the centerline pressure distribution at the ground as the model momentum coefficient is increased, with no floor boundary layer control applied. At a model momentum coefficient of 0.1 it is evident that the peak C_p of 0.5 is sufficient to provoke separation: tufts confirmed this. However, the separation was mild, the trapped-vortex-induced suction was weak and there was no floor impingement of the jet sheet.

At a momentum coefficient to 2.0, in contrast, the trapped-vortex-induces strong suction at the ground with high impingement pressures immediately downstream of this. Juxtaposed between these two model blowing conditions, the ground pressure distribution at unit momentum coefficient is somewhat surprising. Tufts showed strong separation, yet C_p 's of 0.7 and above were recorded and no suction region was evident.

It will be recalled from Section 4.2, here, and from Part I of this report that the floor b.l.c. blowing slot should be positioned near the 0.3 pressure coefficient contour. Most conveniently, this lay very close to the 8" slot location, for the 3" model height, and remained there over almost the entire test range, even with floor b.l.c. applied.

Floor b.l.c. plenum pressure was calculated using equation (4.1) together with C_{1h} values from Figure 13. Tangential blowing at the floor varied the measured floor pressure peaks progressively, as 'N' was increased, until mainstream stagnation occurred. The classical, double-peaked floor pressure distribution was then observed, corresponding to the classical potential flow bubble and trapped vortex described early in Part I of this report. A theoretical pressure distribution, using a point vortex and the same C_1 , was remarkably similar to measurements but was more compressed in the streamwise direction.

6.2 Pressures at the Wing Undersurface

Figure 27 shows pressures at the wing undersurface, for various values of 'N' and representative values of model momentum coefficient. Up to and including unit model momentum coefficient, it is clear that a range of 'N' values is possible, with a preference for $N=2$ to avoid unwanted trailing-edge increments. At higher 'N'-values the higher-than-mainstream-stagnation pressures suggest that the top of the wall jet impinges on the bottom of the flap, which is only about 1.4 inches from the ground in this condition. This is in general agreement with wall jet thickness calculations of Part I of this report.

At the higher C_{1h} values, which are beyond the reach of analytical prediction, increasing 'N' forces both the front stagnation point on the ground and the trapped vortex progressively further back and an "overblowing" situation can occur, relative to the moving ground results. Trailing edge impingement at this altitude prevents a true match between b.l.c ground and moving ground results. However, a compromise here will obviously still significantly improve upon fixed-ground results. It should be emphasized that the model altitude for the case discussed here is untypically low compared with most STOL aircraft configurations.

Figure 28 shows that, at a nominal C_{μ} of 3.0, flap impingement is quite marked inboard but much less so at the 86.6% station. The more severe pressure gradients and higher pressure maxima inboard evidently thicken the wall jet more there. At the 86.6% station the match between the $N=3$ or 3.5 curves and the moving ground result is quite remarkable.

Results for one-chord altitude, which is more representative of practical STOL configurations, are given in Figure 29. In this case, the 12" ground blowing slot position was the best approximation to the 0.3 pressure coefficient contour. Once again an 'N' value of 2 is adequate up to unit momentum coefficient and continues to provide a reasonable match up to a C_{μ} of 2. It is apparent that flap impingement is no longer present. Reference to the more-sensitive, inboard station shows flat aft undersurface pressure distributions throughout, despite the use of a further-back slot. In much of Figures 28 and 29, it was difficult to plot the boundary-layer-controlled ground results because of coincidences with moving-ground points.

The results just described confirm both the general hypothesis of Part I, concerning the peak wall jet velocity below the model and the wall jet calculations which lead to the prediction of 'N'. In addition, it has been demonstrated that, on raising 'N' to 3, extrapolation is possible well into the (analytically intractible) separated-flow regime.

The tests described so far all employed the 0.067-inch high slots, which require much less power than the smaller slots available. Late in the test program, design studies brought up questions concerning smaller slots so limited checks were made with the 8-inch slot set at 0.032 inches height. Figure 30 shows similar performance to previously except at a nominal C_{μ} of 3.0. These differences are thought to be due to using the 8" slot position rather than the 12" position used for the base runs. However, it appears that using the smaller slot, at the same momentum coefficient, does not seriously distort the former conclusions.

6.3 Lift Coefficients as a Function of Floor b.l.c. Setting: Selection of 'N' Values

Inconsistencies found on forming C_L increments for the inboard and outboard stations were eventually traced to two faulty pressure holes. For this reason, the discussion in this subsection will be based upon the 0.643 station, with cross-reference to the other two stations as appropriate.

Figure 31 again illustrates the wide discrepancies between fixed and moving ground results, also seen in Figure 13, and adds data for the boundary-layer-controlled ground. At the low end of the C_{μ} range, it appears that the presence of boundary layer control is more significant than any particular value of 'N'. At flap blowing and lift coefficient increase, however, the trapped, underwing vortex forms and the choice of 'N' becomes important, particularly at the 3-inch model height.

Figure 32 shows the data in incremental form as a function of C_{μ} . Lower surface contributions, at 3 inch height, have been isolated using hand integrations. The undersurface lift contributions are evidently larger than those for the whole section. Further investigation showed progressively decreased upper surface sections as 'N' was increased. At $N=2$, however, the b.l.c. ground and the moving ground upper surface pressure distributions were indistinguishable.

Figures 31 and 32 show that moving-ground lift coefficients may be exceeded at high blowing rates on the b.l.c. ground. This is caused by flap undersurface impingement and does not occur with the model at the 4-inch height.

Figure 33 converts the previous results to a percentage basis, using moving ground results as the norm. In choosing a suitable value of 'N', the lowest possible value is always preferable because less power is required. With this in mind, and considering Figures 27, 28, 29, 32 and 33 together with other supporting data, we reach the following conclusions:

- (i) If an 'N' value of 4 is used, serious impingement occurs on the lower surface of the flap at 3 inches altitude. There are no improvements relative to $N=3$.
- (ii) An 'N' value of 3 is desirable for $C_{l_{hb}}$ values of approximately six and above. For the present model, this held lift errors within $\pm 4\%$. The maximum fixed-ground error exceeded 30%.
- (iii) $N=2$ is desirable for $C_{l_{hb}}$ less than six. Errors decreased, from about 4%, at the lower $C_{l_{hb}}$ values. The corresponding low- $C_{l_{hb}}$ fixed-ground error was 17%.
- (iv) Though N-values less than 2 are effective at lower lift coefficients there is no gain in accuracy and the use of $N=2$ is recommended for simplicity's sake.

6.4. Other slot positions and model heights

Fairly extensive tests were carried out with the model at 3-inch height, but using other blowing slots than the "correct" 8-inch one. It was found that slot positions upstream of this gave unsatisfactory results regardless of 'N' value. The 4-inch slot was equally unsuccessful. In the former cases, it is thought that too-thick a wall jet had developed; in the latter, boundary layer separation may have occurred upstream of the slot.

No floor boundary layer control tests were carried out with model altitudes of 5-inches or above. However, the rules derived for the lower altitudes are expected to apply provided that $C_{l_{hb}}$, rather than C_l , is used where appropriate.

It is worth noting that, with the model at 10-inch altitude, the separation point on the floor was aft of the flap trailing edge and little effect was apparent at the model. Nevertheless, the preceding rules still apply: the prevention of floor separation certainly does no harm.

6.5 Tests with simulated strut shrouds

A 2.5-inch high, 30% thick, simulated strut shroud was mounted on the tunnel floor midway between the 0.643 and the 0.866 span stations. A 2.8-inch chord at the base tapered to 2.34 inches at the top. With the model set at the 3-inch height, there was approximately 0.2 inches clearance between the shroud and the wing. The shroud could be yawed about its quarter-chord, which coincided with the wing quarter-chord.

For these tests, which were conducted last, the wing was in a basic condition, with no fuselage, and the slot at the flap knee had been reduced from 0.045 inches to 0.016 inches.

Figure 34 shows lower surface pressure distributions with the strut absent (the datum case for present purposes), with the strut set at zero-yaw, and with it set at 45 degrees yaw. The latter setting aligned the strut with the flow direction observed with no strut installed. Ground tangential blowing was set with $N=2$, the correct value at this knee-blowing momentum coefficient. The figure shows the familiar vortex-induced under-wing suction with no strut installed. However, this disappears when the unyawed strut is added (see the 0.643 station). Yaw is helpful at this station, but fails to provide a complete remedy. Yaw also gives some improvement at the 0.866 station, but only for the first 50% of chord. Aft of this, there is a strong interaction because the strut trailing edge lies directly below the wing pressure taps (see also Figure 35). It is apparent that high-total-pressure air, most likely from the floor b.l.c. system, has impinged upon the undersurface of the wing. This confirms the need for the present check-tests. Further experiments are required directed at the following questions:

- (i) how serious is the impingement problem for larger strut/wing clearances?
- (ii) is relief possible using boundary layer fences on the strut shroud?
- (iii) with impingement prevented, is there a more-optimum yaw setting?
- (iv) with (i) to (iii) resolved, is proper simulation possible?

There is a definite possibility that, with the underwing vortex present, the answer to (iv) is no. This is because axial flow in the vortex core is blocked, which may have a fundamental effect on its character and strength. Nevertheless, the use of floor boundary layer control will still provide a very significant improvement in ground simulation compared with fixed-ground testing.

7. EXPERIMENTAL RESULTS FOR THE ROUND-JET MODEL

7.1 Moving and fixed ground

With the ground fixed, the main measurements were of pressures in the exit plane surrounding the jet, though some tuft studies were also made. A survey of the pressure data showed that pressures on the jet centerline were surprisingly insensitive to ground effect. However, the line of orifices just outboard of the edge of the jet (Line 'EE' in Figure 6) responded quite strongly to ground effect and pressures here were used in assessing moving ground and boundary layer controlled ground performance.

Figure 36 shows center-tunnel pressure distributions along EE. These were subtracted from in-ground results in preparing subsequent figures. In Figure 36, it is possible that the true suction peak lies just aft of the transverse center line, but comes between pressure orifices.

At a velocity ratio, U_∞/U_j , of 0.1, there was considerable unsteadiness for most tests and pressure readings showed undue scatter. Results for U_∞/U_j of 0.2 are shown in Figure 37. The jet impinged on the fixed ground for most of the heights shown and the familiar "U"-shaped, aft-facing vortex was present on the floor. The interference increment for one diameter altitude virtually removes the center-tunnel suction peak with the ground fixed. There is also a general increase in static pressure aft and a decrease forward of the transverse center line.

Application of the moving ground almost halved the interference aft, but further increased the suction ahead of the jet position. There was evidently a venturi effect between the lower fuselage and the ground, which was increased by the pumping action of the moving belt. As model height was increased, Figure 37 indicates a rapid decrease in ground effect, which was almost zero by four diameters altitude.

At higher forward speed ratios (Figure 38) the ground interference declined rapidly, though the general trends were similar to before. It was found that the boundary for zero ground effect was described quite well by the expression:

$$p = \frac{U_j/U_\infty}{h/d} = 1.25 \quad (7.1)$$

The form of (7.1) is not altogether surprising since a very similar equation is a good approximation to free air jet penetration. The above equation implies that ground interference is a function of the model altitude expressed as a proportion of the free air jet penetration at the same velocity ratio.

7.2 Tangentially-blown ground

Round-jet impingement represents a particularly severe test for the ground b.l.c system, especially at the lowest altitudes described in the previous subsection. Figures 39 and 40 include curves for boundary layer controlled ground experiments. The figures are arranged with 'p' (Equation 7.1) increasing monotonically and similarly increasing ground effects are evident. As 'M' (Equation 4.2) was increased the match with the moving ground curve became better at the lower 'p' values, but deteriorated for higher 'p' values until, in Figure 40(b), there was only marginal improvement due to applying b.l.c. at the ground.

Figure 41 summarizes the previous results. In this figure, lines of constant penetration parameter, 'p', are rays from the origin. There are five significant regions:

Region 'A' ($p < 1.25$ and $h/d \geq 1$)

There is no measurable ground effect at the jet exit plane whether the ground is fixed or moving.

Region 'B' ($1.25 < p < 2.5$ and $h/d > 3$ approximately)

Ground effect is mild, but measurable, and the same for both fixed and moving ground.

Region 'C' ($1.25 < p < 2.5$ and $h/d \geq 1$)

Tangential blowing at the ground provides good simulation of moving ground conditions. If tangential blowing is applied for h/d greater than 3, it does no harm.

Region 'D' ($2.5 < p < 5.0$ and $h/d > 1$)

The application of floor b.l.c. gives some improvement over the fixed ground results, but a moving ground is desirable.

Region 'E' ($p > 5.0$)

For meaningful results, a moving ground is a necessity.

Fortunately the last condition is likely to occur very infrequently in practical cases owing to performance penalties and interference with the lift fan or engine.

The experimental values of 'M' for matching the moving ground results did not form a consistent pattern. The data consequently were reanalyzed in terms of 'M' defined by:

$$M' = \frac{H_{\text{SLOT}} - p_{\infty}}{H_{\text{JET}} - p_{\infty}} \quad (7.2)$$

This correlated the results far more satisfactorily, with a constant value of between 1.4 and 1.5 for all but a single case. Somewhat surprisingly, there was no discernable trend with altitude. As with N, previously, M' is specific to the slot height used. Converting to a more convenient form gives:

$$\frac{C_{\mu_{\text{slot}}}}{C_{\mu_{\text{jet}}}} = \frac{(H_{\text{SLOT}} - p_{\infty})^t}{(H_{\text{JET}} - p_{\infty})^d} = 0.027 \quad (7.3)$$

Where $C_{\mu_{\text{jet}}}$ is a two-dimensional quantity corresponding to the center plane of the jet. Equation (7.3) is applicable for a slot position 5-diameters ahead of the jet exit and may be applied throughout Figure 41, except for region E.

8. COMBINED FLOOR TANGENTIAL-BLOWING REQUIREMENTS.

Though the parameters 'N' and 'M' have physical relevance and are convenient for particular test set-ups such as those described previously, the floor tangential blowing momentum coefficient is the more convenient form from a general operational viewpoint.

Equation (4.1), for the knee-blowing flap model, leads to:

$$C_{\mu_{\text{slot}}} = \frac{\frac{1}{2} \rho_{\text{slot}} U_{\text{SLOT}}^2 t}{\frac{1}{2} \rho_{\infty} U_{\infty}^2 C_{\text{REF}}} = \frac{t}{C_{\text{REF}}} \left(1 + N \frac{C_{l_h}}{2\pi} \right)^2 \quad (8.1)$$

$$\text{where } C_{l_h} = C_l \frac{C_{\text{REF}}}{h} \text{ and } C_{l_h} < 5.0$$

Substitution of the relevant slot height and reference chord gives the curves marked "N=2" and "N=3" in the $C_{\mu_{\text{slot}}} \sim C_{l_h}$ plot shown in Figure 42. It has already been shown that the "N=2" condition is applicable up to a C_{l_h} value of approximately five. Beyond this, analyses of pressure plots and Figures 32 and 33 shows a good, high- C_{l_h} match when:

$$C_{\mu_{\text{slot}}} = 0.088 \frac{C}{h} (C_{l_h} - 3.5) \quad (8.2)$$

In the above equations, slot placement at $C_p = 0.3$ is assumed.

It is also possible to include lifting-jet results in Figure 42 using the definition:

$$C_{l_h} = \frac{(H_{\text{JET}} - \rho_{\infty})d}{\frac{1}{2} \rho_{\infty} U_{\infty}^2 C_{\text{REF}}} \quad (= C_{\mu_{\text{jet}}}) \quad (8.3)$$

Here, C_{l_h} (like $C_{\mu_{\text{jet}}}$) is a sectional lift coefficient based on the gross lift, per foot of span on the longitudinal center plane of the jet. Substituting from Equation (7.3) gives:

$$C_{\mu_{\text{slot}}} = 0.027 C_{l_h} \quad (8.4)$$

The above equation is for slot placement 5-diameters ahead of the jet.

Figure 42 shows that Equation (8.4) and the "N=2" curve are very similar. At the low end of the C_{l_h} range the round jet and the jet sheet from the wing are both strongly deflected by the mainstream and evidently affect the ground to an equivalent degree so far as their b.l.c. requirements are concerned. Near $C_{l_h}=5$, the more-two-dimensional nature of the wing flow appears to become significant and the larger tangential-blowing quantities given by Equation (8.2) become necessary. The spread between the Equation (8.2) (jet) curves and the Equation (8.4) (wing) curves is thus attributable to three-dimensional differences between the two flows. Requirements for intermediate configurations can be expected to lie in the region marked "I", in Figure 42.

9. CONCLUSIONS

9.1 The knee-blowing flap model

A 20-inch span, 4-inch nominal chord, unswept, pressure-tapped wing, low-mounted on a single fuselage (see Figures 1 and 2), was tested in a 30 x 42 inch wind tunnel using fixed, moving and boundary-layer-controlled floor configurations. The model included a full-span slot and a full-span, highly-deflected, knee-blowing flap. The mean of these sectional C_l values, measured at center-tunnel, rose from 3.6 at a momentum coefficient of 0.3 to 8.9 at 3.0. No tunnel corrections were applied.

Tests in ground effect lead to the following conclusions:

1. At values of sectional lift coefficient, based on model height, below about six, moving-ground-induced lift loss was a distributed effect with an almost-constant percentage loss any any one altitude. Above this lift range, a spanwise vortex formed below the aft 50% of chord which intensified as lift was further increased and caused noticeable additional lift loss.
2. With a fixed ground, there were serious lift errors caused by the trapped underwing vortex forming prematurely and extending over almost the whole chord. At one chord altitude and less, undersurface contributions were pessimistic by more than a unit increment in C_l for high flap-blowing cases. (See Figure 13). This causes the ground-induced lift loss to appear to be between 1.7 times and twice the correct value. Local errors exceeding 30% of total lift occurred with a blowing momentum coefficient of 3.0 at h/C_{nom} of 0.75. (See Figure 33).
3. The onset of underwing vortex flow, with the ground moving, corresponds fairly closely with the occurrence of the potential flow bubble discussed in Part I of this report, despite the very simple nature of that model.
4. Below values of lift coefficient, based on model height, of about six, the application of tangential blowing at the ground provided successful simulation of moving ground conditions using a blowing parameter, N , of two. This is the value predicted theoretically in Part I of this report. Application of ground boundary layer control in these cases removed both ground separation and the under-wing vortex. (See Figures 27 and 29).
5. Larger and more-carefully-chosen floor tangential blowing rates were needed in cases where the occurrence of the under-wing vortex was correct. (See Figure 28). An 'N' value of three was found to produce good results at C_{lh} values of six and above (See Figures 32 and 33). The 'N' values quoted here are specific to the slot height used, which was 1.7% of reference chord.
6. Below - speed moving ground belt runs showed that, in the sub-trapped-vortex range, reasonably good full speed ground simulation was achieved at half belt speed (see Figure 25). Beyond this range, proper belt speed became increasingly necessary to ensure correct under-wing effects.

7. Limited tests with a simulated under-wing support strut shroud showed that boundary layer fences on the shroud are desirable to prevent upward migration of floor b.l.c. air and impingement on the wing undersurface. However, even with this precaution and the shroud correctly toed-in, there are doubts whether the trapped vortex condition can be correctly simulated. This is because the shroud blocks axial flows in the vortex core and may modify fundamentally the very-three-dimensional flow field. Further work is needed on the interference of under-wing support-strut shrouds under close-to-ground conditions. However, application of floor b.l.c. still gives much improved ground simulation compared with fixed ground testing.
8. Conclusion 4, above, confirms the hypothesis of Part I, that the wall jet maximum velocity just below the model should equal the mainstream velocity at infinity. The applicability of the wall jet program, used to predict wall jet velocity decay along the floor, is also confirmed by implication. Conclusion 5, above, shows that extension is possible into the trapped vortex regime if 'N' is suitably altered. These confirmations lend confidence to wider use of the theory.

9.2 The round-jet model

A simple, lifting-jet model with a high-mounted, flat-plate wing and a 1.75-inch diameter jet emergent from the flat lower surface of the 2.75-inch wide fuselage (see Figure 5) was tested under similar conditions to those for the wing model, above. Lower surface pressure measurements were made, around the jet exit, at center tunnel and at altitudes down to one diameter. The forward-speed-ratio range was from 0.1 to 0.6. The effects of the three ground configurations were assessed on the basis of pressure distributions, but no pressure integrations were attempted for this model.

Tests in ground effect lead to the following conclusions:

9. There were no measurable ground effects on the fuselage lower surface when the penetration parameter, p , defined as $(U_J d / U_\infty h)$ was less than 1.25 (Region 'A', Figure 41).
10. When the exit plane was three diameters or more above the ground, it was immaterial whether the ground was fixed or moving (Region 'B', Figure 41).
11. At an altitude of one diameter or more and with 'p' between 1.25 and 2.5, the tangentially-blown ground provided good simulation of moving ground results. (Region 'C', Figure 41). The blowing slot position was five diameters ahead of the jet exit; the blowing momentum was as given by Equation (7.3).
12. Beyond a 'p' value of 2.5, tangential blowing at the floor provided decreasingly effective simulation of the moving ground (Region 'D', Figure 41) until, with 'p' greater than four or five, there was no alternative to the use of a moving ground. (Region 'E').

9.3 Combined floor b.l.c. requirements

13. The momentum coefficient for floor tangential blowing may be plotted on the same basis for both the knee-blowing and the round-jet models (see Figure 42). In the low lift-coefficient range, the two requirements follow almost the same curve. Higher up, three dimensionality causes the two sets of results to diverge. The ability to express the results in the same form for two widely-differing models has important implications regarding simple operation for floor tangential-blowing systems.

TABLE I
Model Dimensions

Knee-blowing flap model

Wing:

area	0.556 ft ²
aspect ratio (on nominal chord)	5.0
span	20.0"
nominal chord (constant)	4.0"
quarter chord location:	
fuselage station	10.50
water line	3.94
twist, sweep,	Zero

Leading Edge Slat:

area (projected onto maximum chord)	0.111 ft ²
span	20.0"
chord (maximum)	0.80"
slot width	0.050"
deflection	80.0 degrees

Trailing Edge Flap:

area (projected onto maximum chord)	0.252 ft ²
span	20.0"
chord (maximum)	1.81"
slot width *	0.045", 0.016"
deflection (wing chord to flap upper surface)	78.0 degrees

*0.016" slot used for under-wing-strut tests only.

Lifting-Jet Model

Wing:

area	0.417 ft ²
aspect ratio	2.8
span	12.96"
mean aerodynamic chord	4.92"
taper ratio	0.40
0.25 M.A.C. location:	
fuselage station	13.56
water line	5.84
butt line	2.78
quarter-chord sweep	34.5 degrees
twist,	Zero

Lifting Jet

diameter	1.750"
location	
fuselage station	14.00
water line	4.06
butt line	0.00

Fuselage (both models)

length	21.50"
maximum width	2.75"
maximum height	2.625"
maximum cross section	6.92 in ²
equivalent diameter	2.97"
fineness ratio	7.24
centerline location	
waterline	5.00
buttline	0.00

Origins of reference system

fuselage station zero:	front point of fuselage
waterline zero:	lower fuselage surface, in jet configuration
butt line zero:	longitudinal center plane

APPENDIX

Flow Calibration and Control

Test Section Calibration.

Test section dynamic pressure, measured using a 5/8 inch diameter pitot-static tube and a precision water manometer, was calibrated against the piezometer rings in the tunnel contraction. Check points were at tunnel stations 10", 24" (test section center-point) and 38.25". There was a -1.3% dynamic pressure gradient along the test section centerline. The static pressure gradient varied from 0.0036 per foot in the forward part of the test section to -0.028 at the rear.

The center-tunnel dynamic pressure was used in data reduction. Static pressure was calculated as the difference between total pressure and compressible dynamic pressure. No corrections were made for tunnel longitudinal pressure gradients or for constraint effects.

Blown-Flap Calibrations

The total pressure distribution along the slot was checked using a hand held total-pressure probe. Internal biasing was required to equalize flow to the right and left wings. Wing plenum pressure was set by monitoring total pressures within the wing plenum. Further details are given in Section 5.1.

Boundary Layer Control Slots in the Tunnel Floor.

Checks showed that the internal, plenum, static pressures approximated very closely to hand-held pitot readings at the slots. Slot velocity was set using plenum pressure ratio. Plenum pressures were measured on a water manometer, up to 25", and on a calibrated Bourdon-type gauge beyond this.

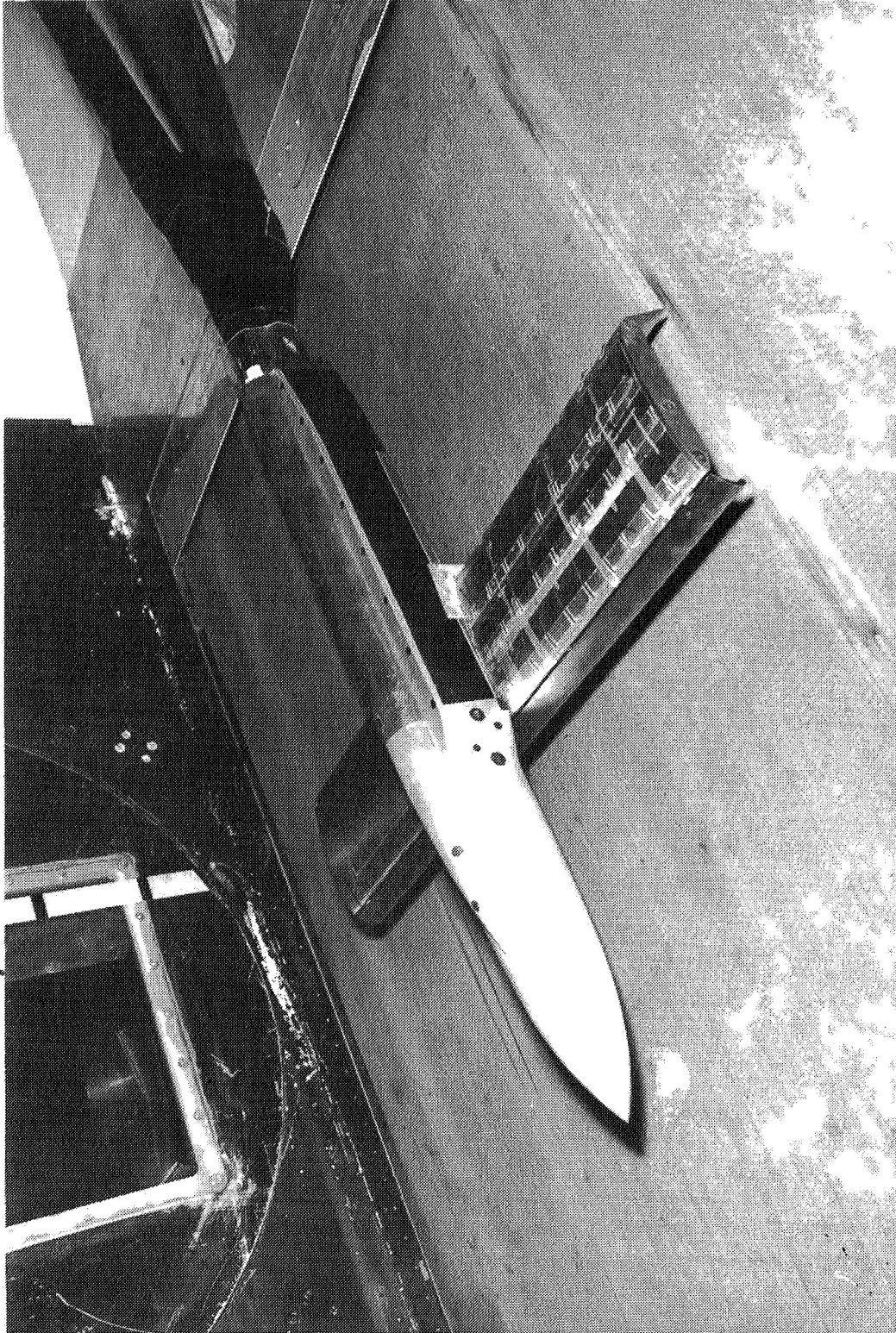


FIGURE 1 THE KNEE BLOWING FLAP MODEL, GENERAL VIEW

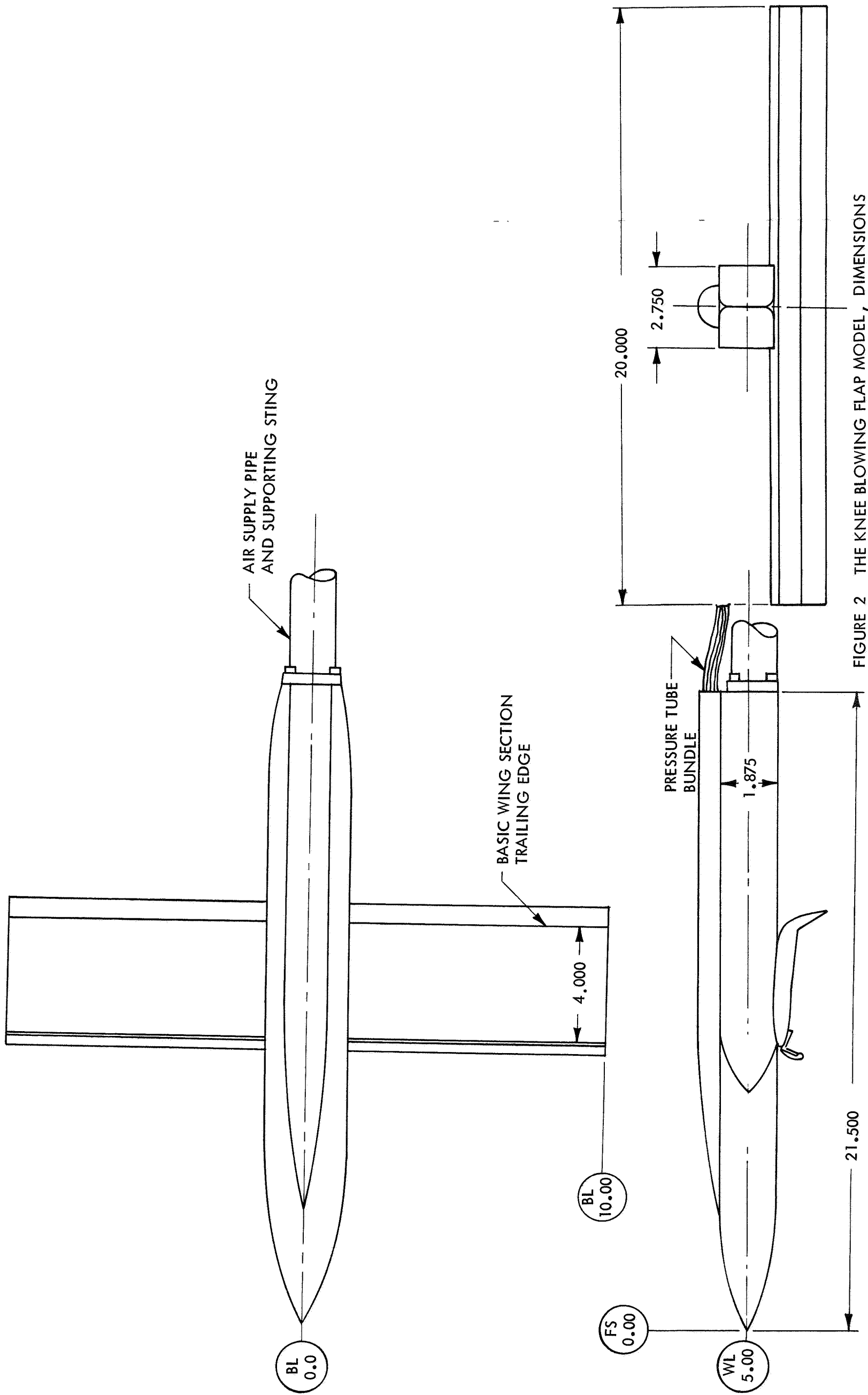
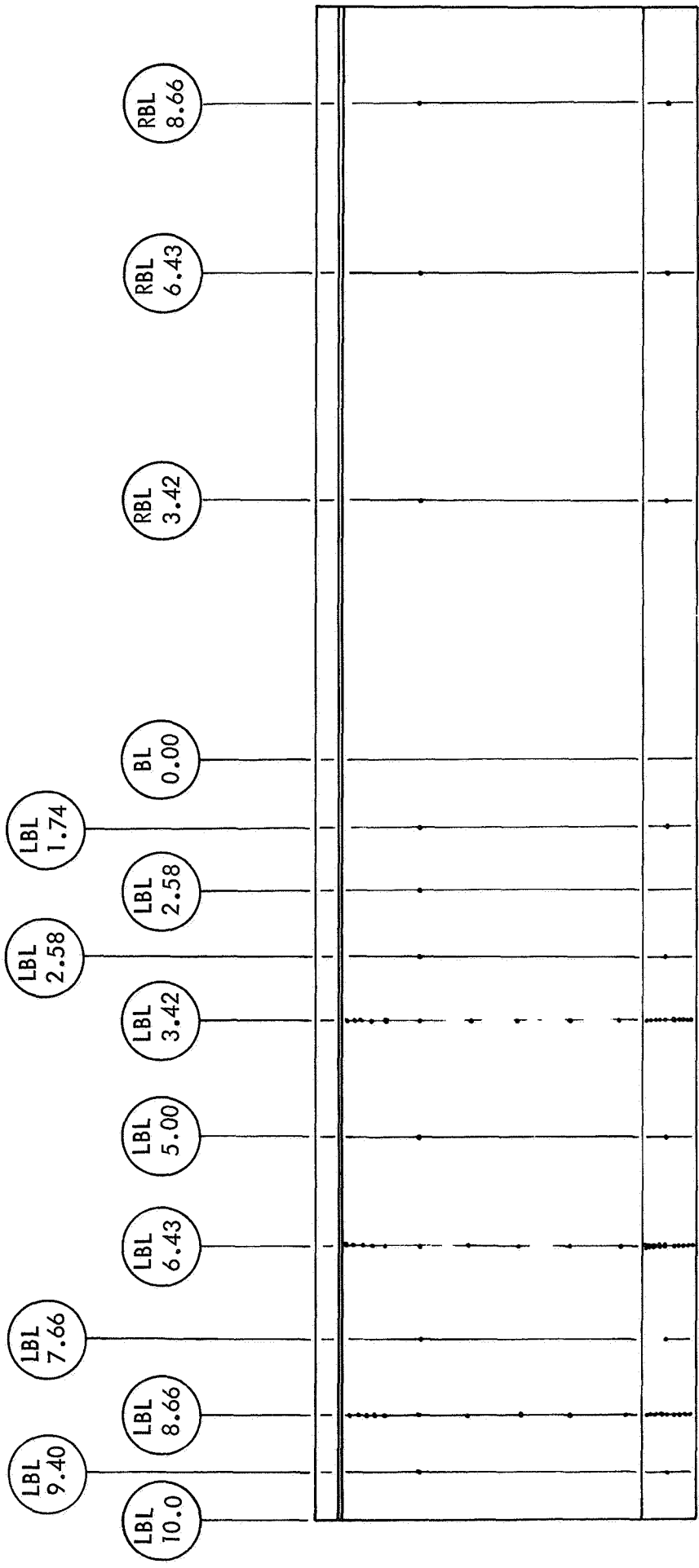


FIGURE 2 THE KNEE BLOWING FLAP MODEL, DIMENSIONS

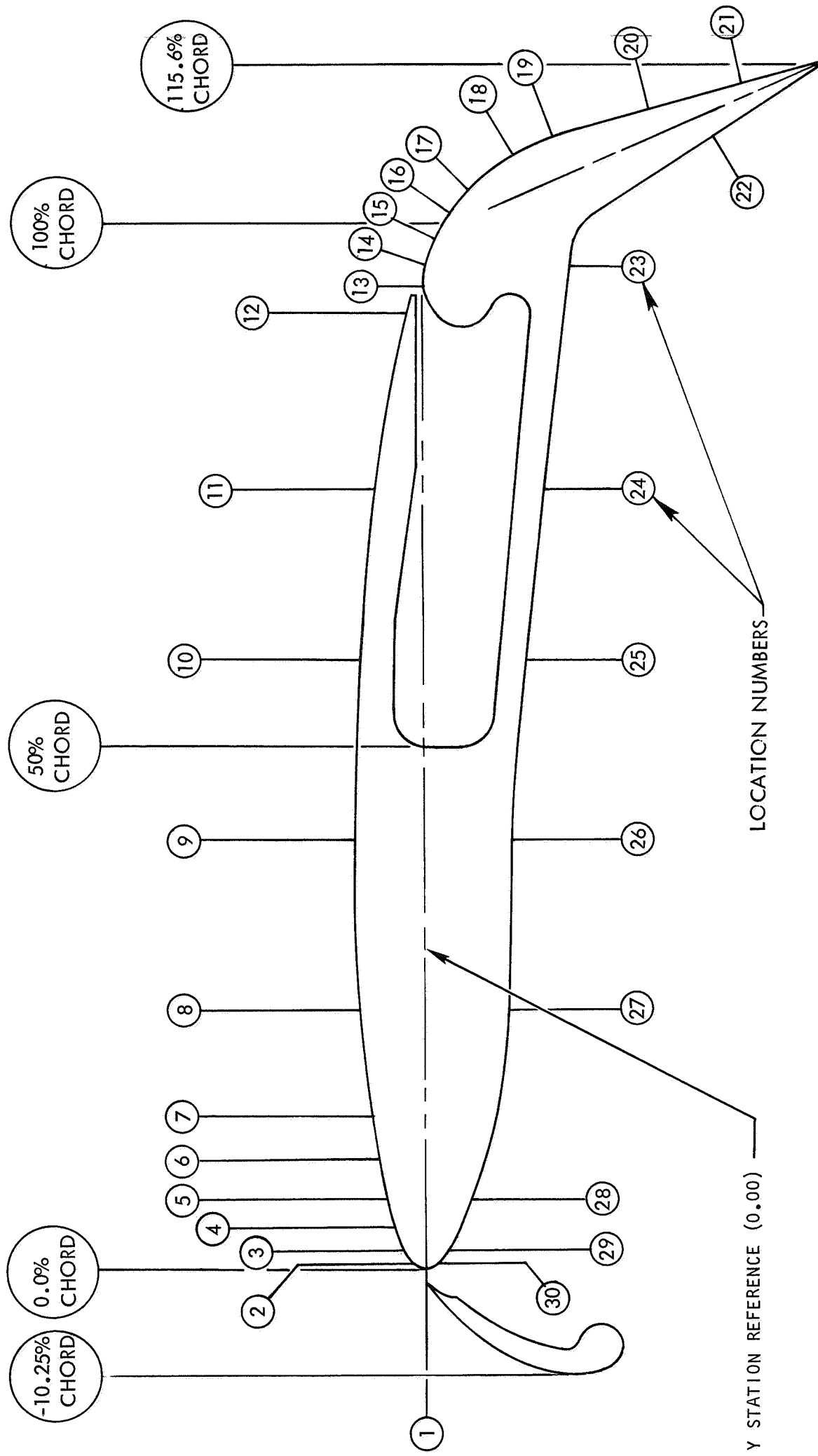
NOTE:
 BUTT LINE LOCATIONS ARE AS SHOWN.
 SEE FIGURE B FOR EXACT CHORDWISE LOCATIONS



ORIFICE IDENTIFICATION

BL LOC	TUBE LOC	TUBE NO.	BL LOC	TUBE LOC	TUBE NO.	BL LOC	TUBE LOC	TUBE NO.
1.74L	8	85	6.43L	12	39	8.66L	26	81
1.74L	17	86	6.43L	13	40	8.66L	27	82
2.58L	8	87	6.43L	14	41	8.66L	28	83
2.58L	17	88	6.43L	15	42	8.66L	29	84
3.42L	1	1	6.43L	16	43	9.40L	8	93
3.42L	3	2	6.43L	17	44	9.40L	17	94
3.42L	4	3	6.43L	18	45	3.42R	8	95
3.42L	5	4	6.43L	19	46	3.42R	17	96
3.42L	6	5	6.43L	20	47	6.43R	8	97
3.42L	7	6	6.43L	21	48	6.43R	17	98
3.42L	8	7	6.43L	22	49	8.66R	8	99
3.42L	9	8	6.43L	23	50	8.66R	17	100
3.42L	10	9	6.43L	24	51			
3.42L	11	10	6.43L	25	52	3.42L	2	101S
3.42L	12	11	6.43L	26	53	3.42L	2	102T
3.42L	13	12	6.43L	27	54	3.42R	2	107S
3.42L	14	13	6.43L	28	55	3.42R	2	108T
3.42L	15	14	6.43L	29	56	6.43L	2	103S
3.42L	16	15	7.66L	8	91	6.43L	2	104T
3.42L	17	16	7.66L	17	92	8.66L	2	105S
3.42L	18	17	8.66L	1	57	8.66L	2	106T
3.42L	19	18	8.66L	3	58	0.00	2	109S
3.42L	20	19	8.66L	4	59			
3.42L	21	20	8.66L	5	60			
3.42L	22	21	8.66L	6	61			
3.42L	23	22	8.66L	7	62			
3.42L	24	23	8.66L	8	63			
3.42L	25	24	8.66L	9	64			
3.42L	26	25	8.66L	10	65			
3.42L	27	26	8.66L	11	66			
3.42L	28	27	8.66L	12	67			
3.42L	29	28	8.66L	13	68			
5.00L	8	89	8.66L	14	69			
5.00L	17	90	8.66L	15	70			
6.43L	1	29	8.66L	16	71			
6.43L	3	30	8.66L	17	72			
6.43L	4	31	8.66L	18	73			
6.43L	5	32	8.66L	19	74			
6.43L	6	33	8.66L	20	75			
6.43L	7	34	8.66L	21	76			
6.43L	8	35	8.66L	22	77			
6.43L	9	36	8.66L	23	78			
6.43L	10	37	8.66L	24	79			
6.43L	11	38	8.66L	25	80			

FIGURE 3 PRESSURE ORIFICE LOCATIONS, IN PLAN VIEW FOR KBF MODEL



TUBE LOC	X/C	Y/C
1	0.000	0.004
2	Not Used	
3	0.017	0.019
4	0.038	0.028
5	0.067	0.038
6	0.103	0.045
7	0.147	0.053
8	0.250	0.062
9	0.414	0.069
10	0.585	0.063
11	0.750	0.047
12	0.913	0.020
13	0.936	-0.001
14	0.968	-0.003
15	0.990	-0.010
16	1.015	-0.021
17	1.037	-0.037
18	1.074	-0.080
19	1.088	-0.120
20	1.111	-0.211
21	1.134	-0.302
22	1.082	-0.275
23	0.965	-0.138
24	0.750	-0.114
25	0.585	-0.096
26	0.414	-0.081
27	0.250	-0.076
28	0.067	-0.044
29	0.017	-0.019
30	Not Used	

FIGURE 4 PRESSURE ORIFICE LOCATIONS AND WING SECTION FOR KBF MODEL

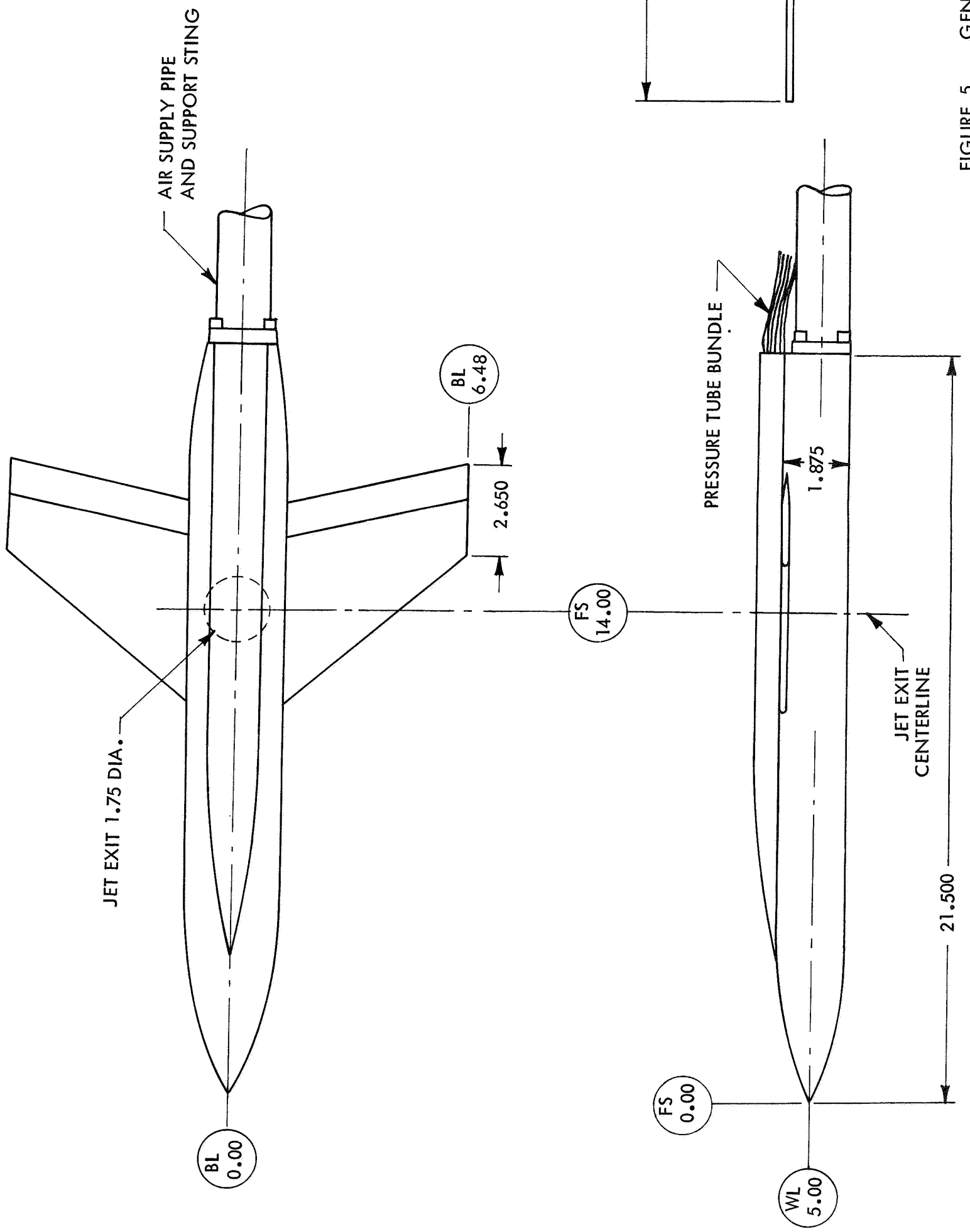
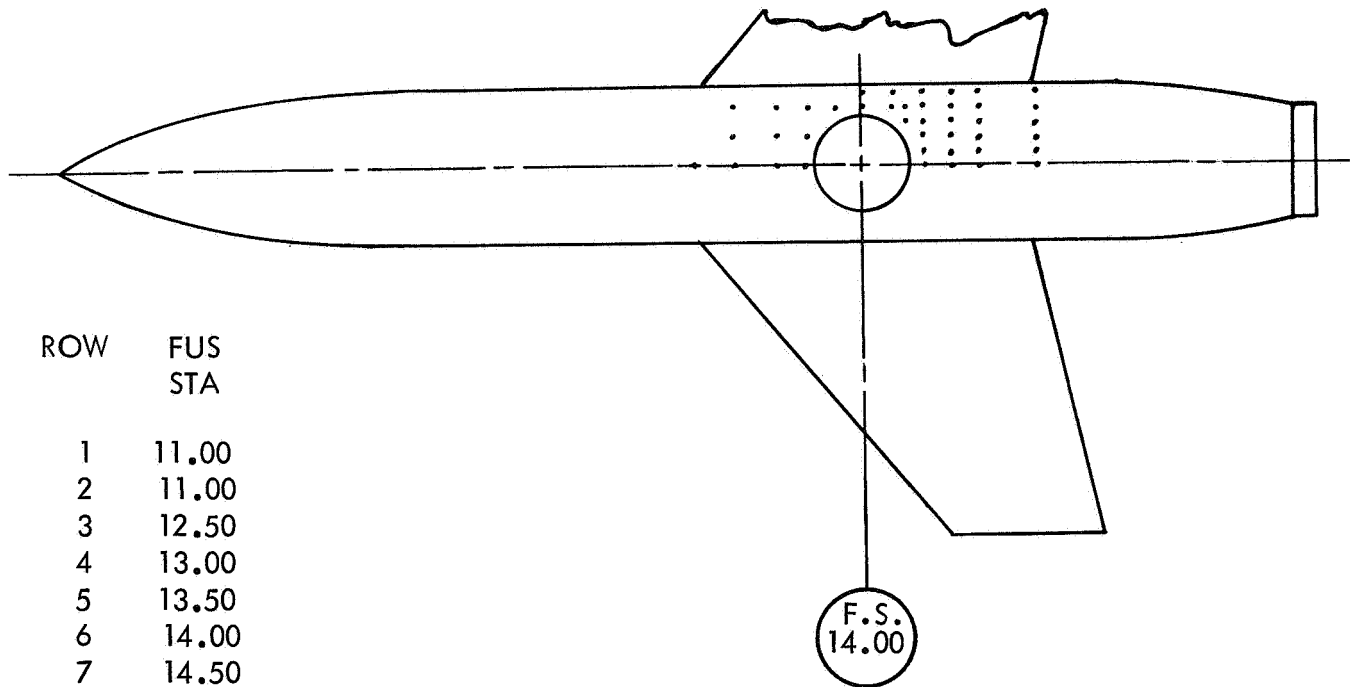
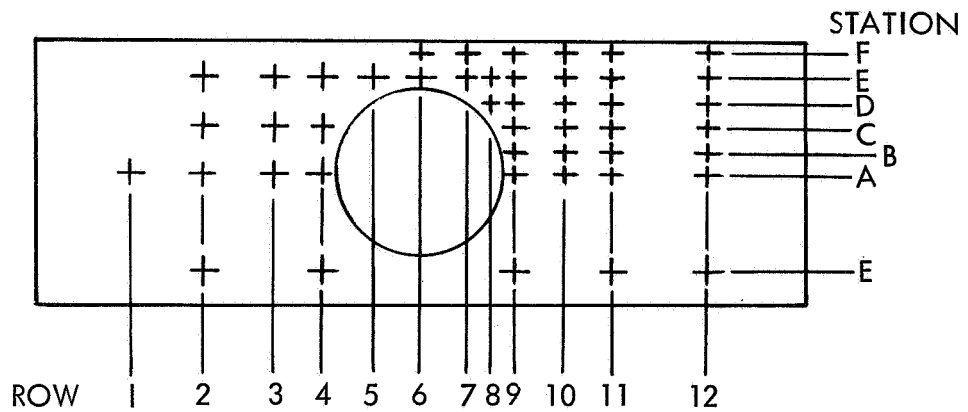


FIGURE 5 GENERAL ARRANGEMENT LIFTING JET MODEL



ROW	FUS STA
1	11.00
2	11.00
3	12.50
4	13.00
5	13.50
6	14.00
7	14.50
8	14.75
9	15.00
10	15.50
11	16.00
12	17.00



VIEW LOOKING UP

STATIONS A THROUGH F 0.25 PITCH

FIGURE 6 PRESSURE ORIFICE LOCATIONS FOR LIFTING - JET MODEL

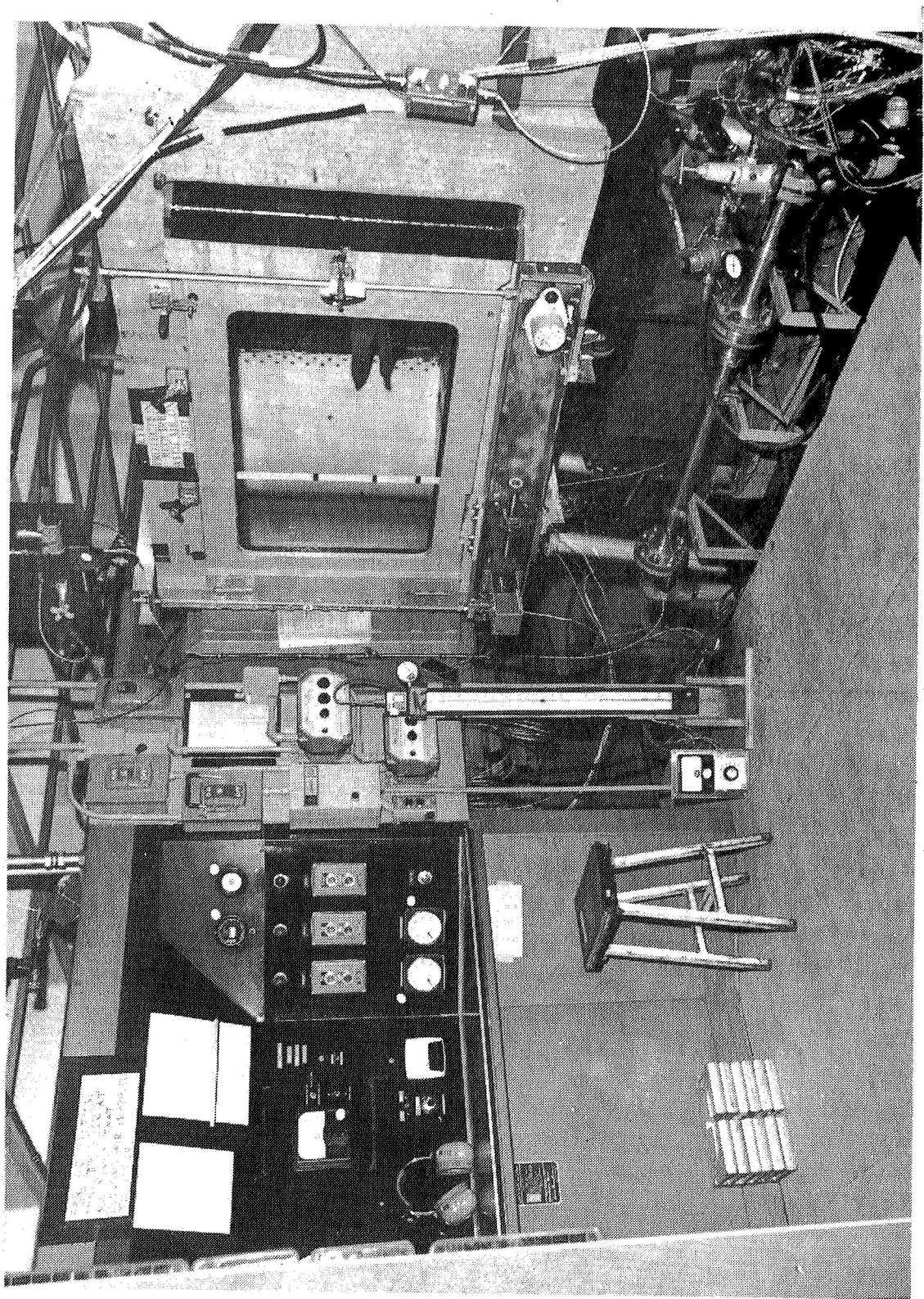


FIGURE 7 THE 42 X 30 INCH LOW SPEED WIND TUNNEL

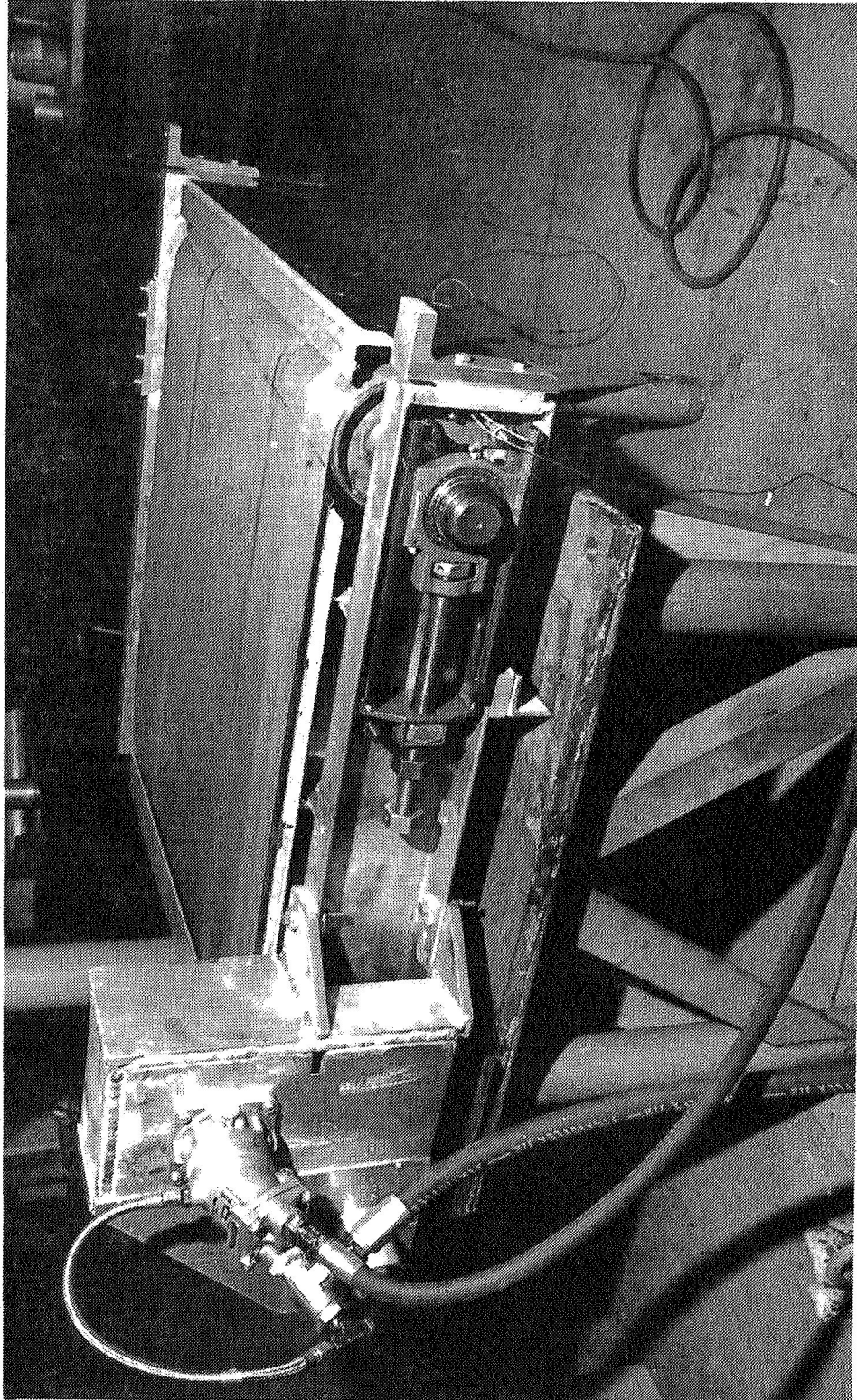
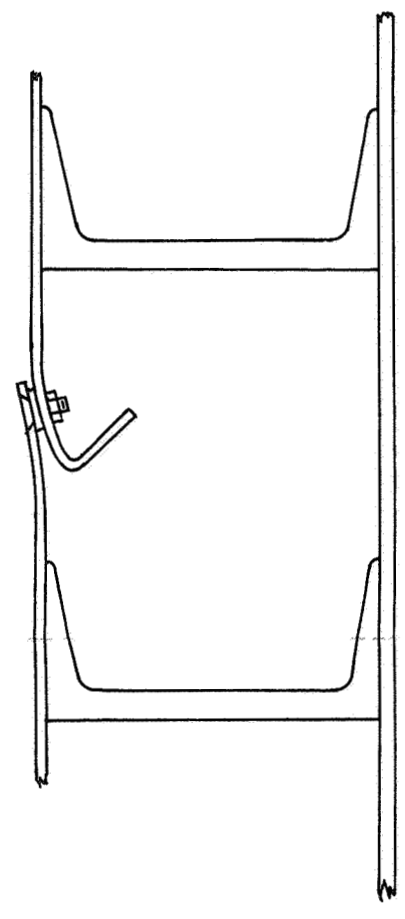
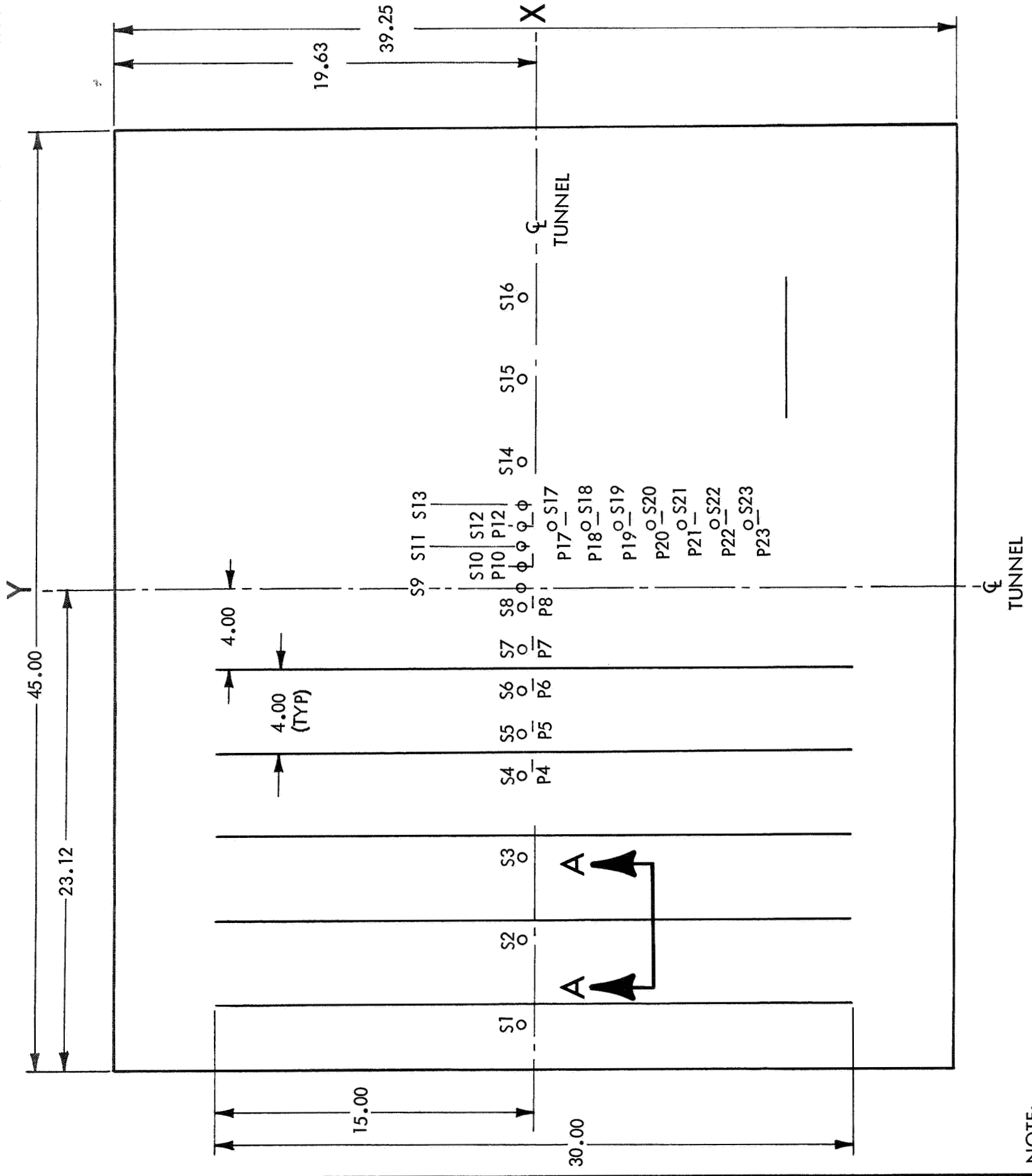


FIGURE 8 THE MOVING BELT GROUND PLANE



GROUND PLANE PRESSURE ORIFICE LOCATIONS					
ORIFICE NUMBER	X	Y	ORIFICE NUMBER	X	Y
S1	-21	0.50	S13	4	0.50
S2	-17	0.50	S14	6	0.56
S3	-13	0.50	S15	10	0.50
S4	-9	0.50	S16	14	0.50
P4	-9	0.00	S17	3	-1.00
S5	-7	0.50	P17	3	-1.50
P5	-7	0.00	S18	3	-2.50
S6	-5	0.50	P18	3	-3.00
P6	-5	0.00	S19	3	-4.00
S7	-3	0.50	P19	3	-4.50
P7	-3	0.00	S20	3	-5.50
S8	-1	0.50	P20	3	-6.00
P8	-1	0.00	S21	3	-7.00
S9	0	0.50	P21	3	-7.50
P9	0	0.00	S22	3	-8.50
S10	1	0.50	P22	3	-9.00
P10	1	0.00	S23	3	-10.00
S11	2	0.50	P23	3	-10.50
P11	2	0.00			
S12	3	0.50			
P12	3	0.00			

ORIGIN LOCATED AT INTERSECTION OF TUNNEL CENTERLINES

NOTE:
S IS THE STATIC PORT AND P IS THE PRESTON TUBE.

FIGURE 9 THE BOUNDARY LAYER CONTROLLED GROUND PLANE

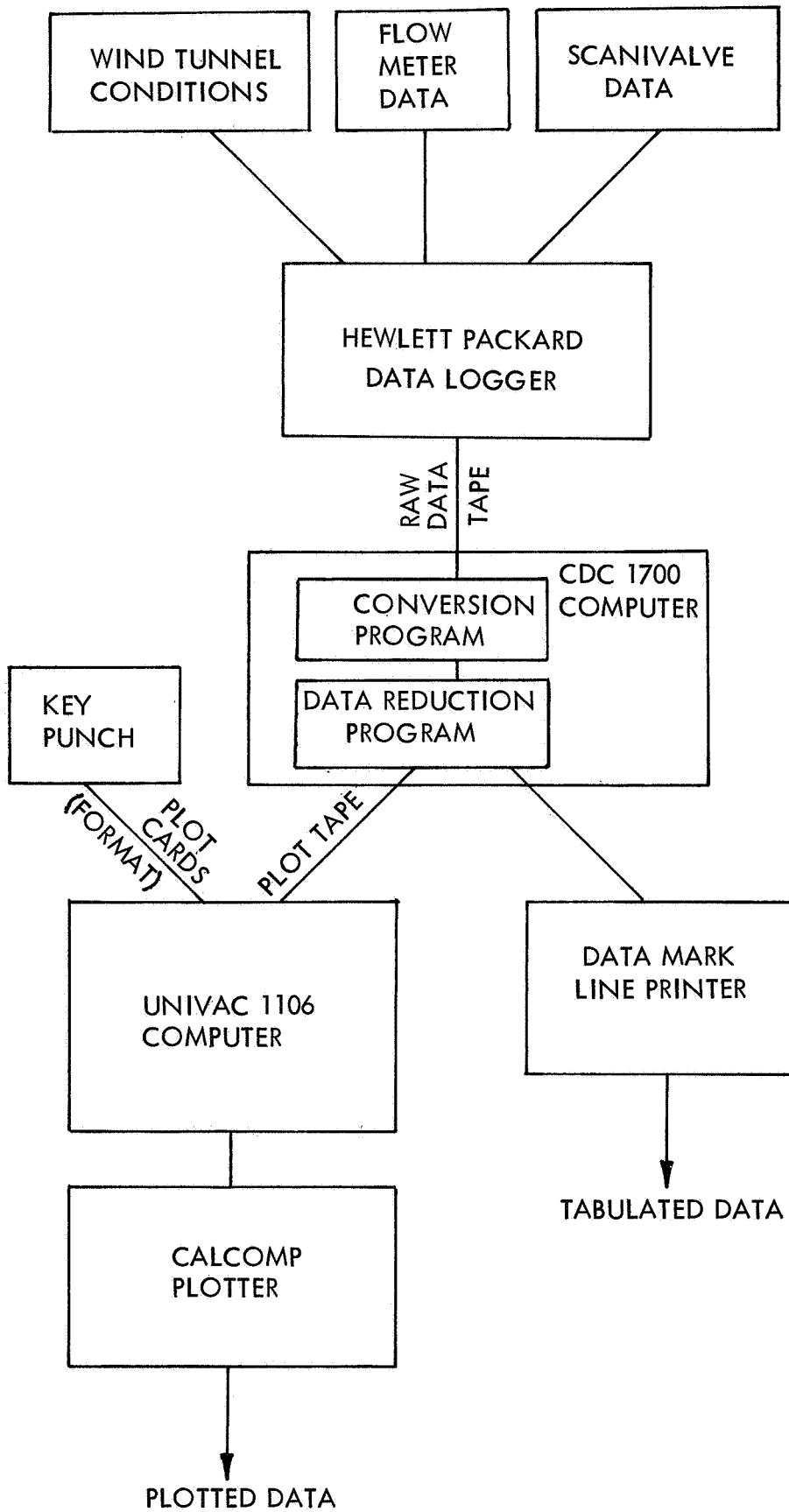


FIGURE 10 SCHEMATIC OF DATA SYSTEM

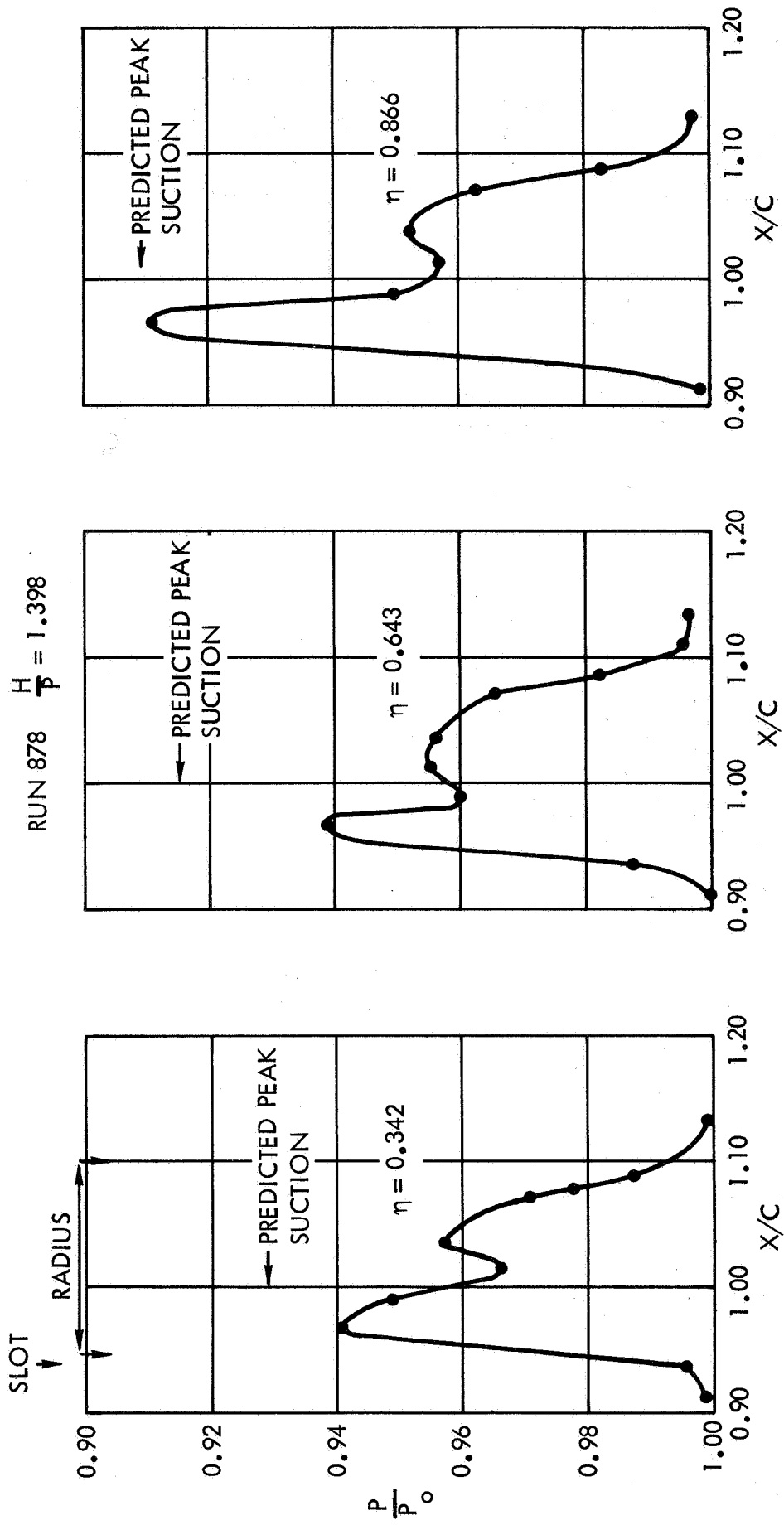


FIGURE 11. TYPICAL FLAP PRESSURE DISTRIBUTIONS AT ZERO FORWARD SPEED

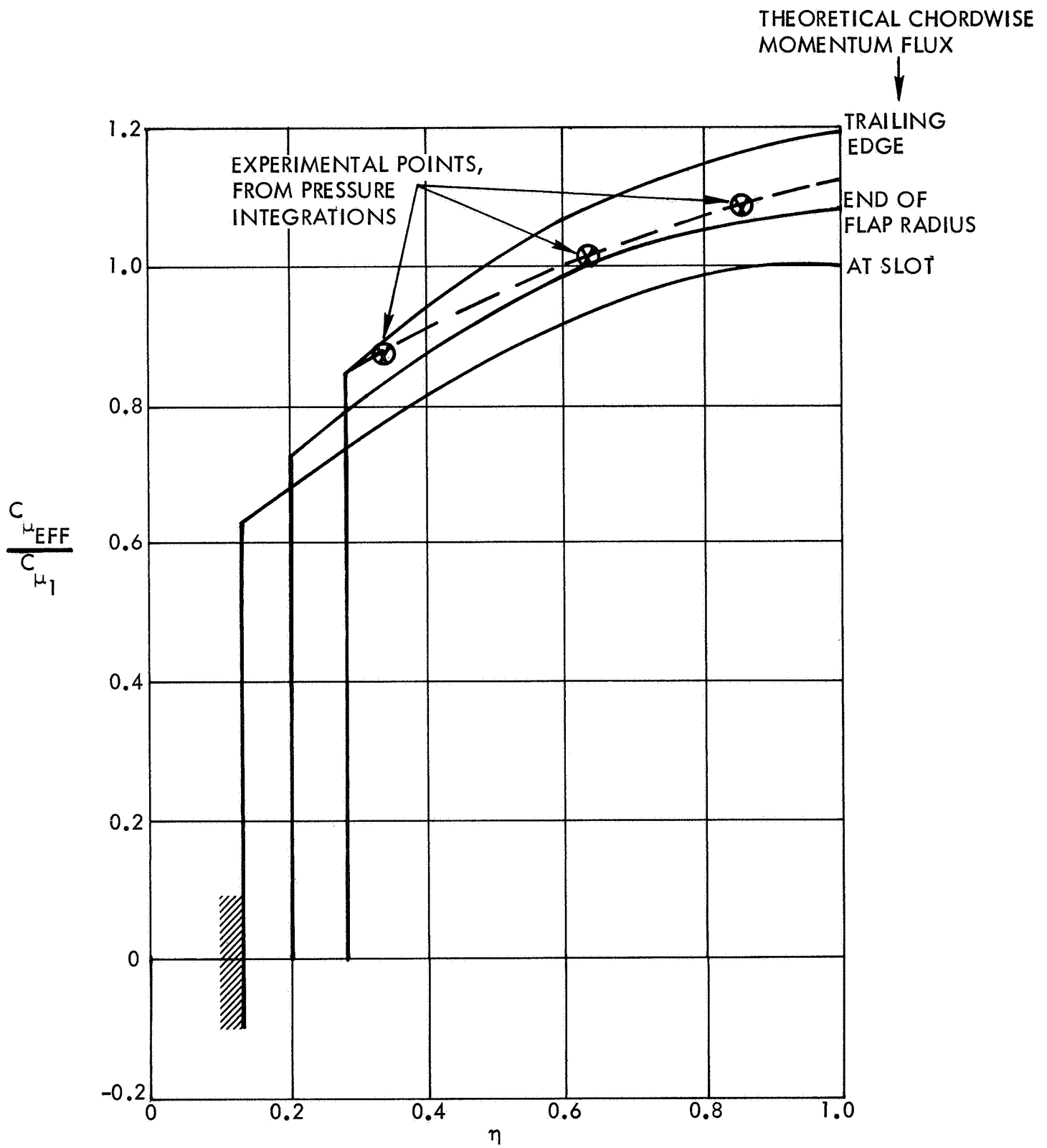


FIGURE 12. PREDICTED AND MEASURED EFFECTIVE C_{μ} DISTRIBUTIONS AT ZERO FORWARD SPEED

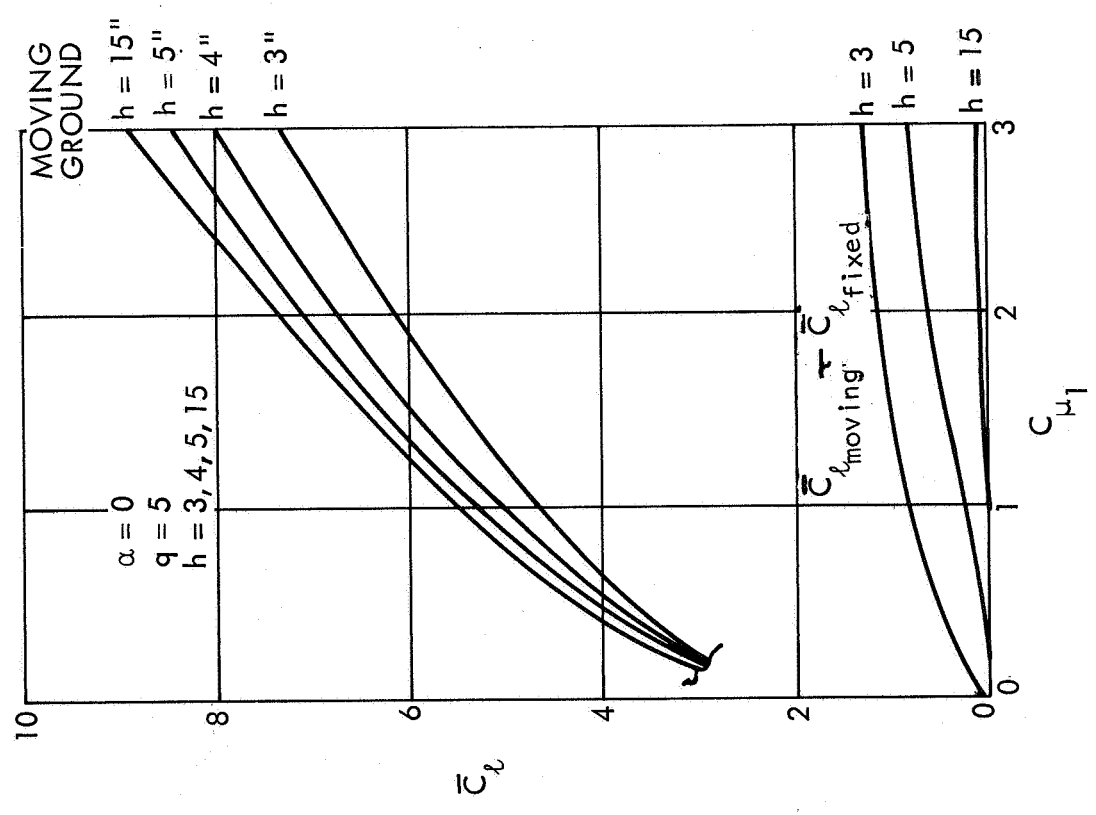
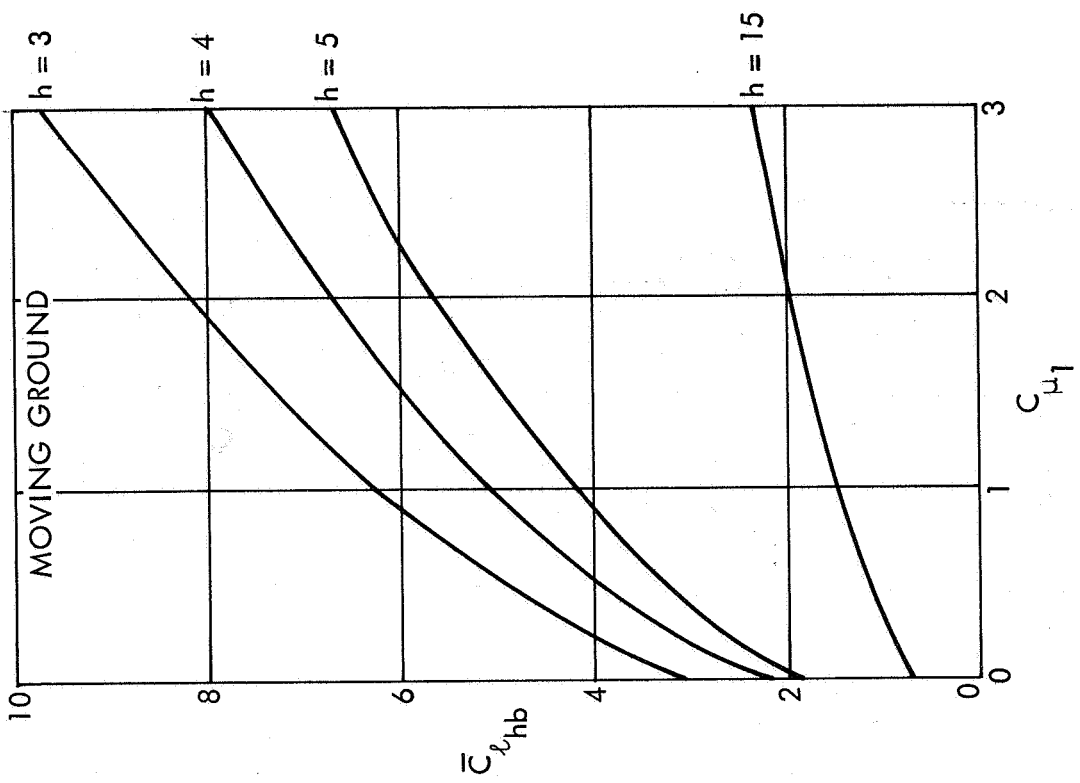


FIGURE 13. EFFECTS OF HEIGHT AND FIXED GROUND FLOW DISTORTION ON LIFT PERFORMANCE OF KNEE BLOWING FLAP MODEL

SYMBOL	h	$C_{\mu\text{NOM}}$	$C_{\mu 1}$	C_l	TUNNEL q - PSF	RUN NO.
⊙	3"	0.30	0.276	3.215	10.13	410
X	5"	0.30	0.282	3.576	9.99	414
+	10"	0.30	0.294	3.856	10.02	419
⊕	15"	0.30	0.290	3.705	10.00	427

NOTE: "FLAGGED" SYMBOLS ARE USED TO DENOTE LOWER SURFACE WHERE NECESSARY

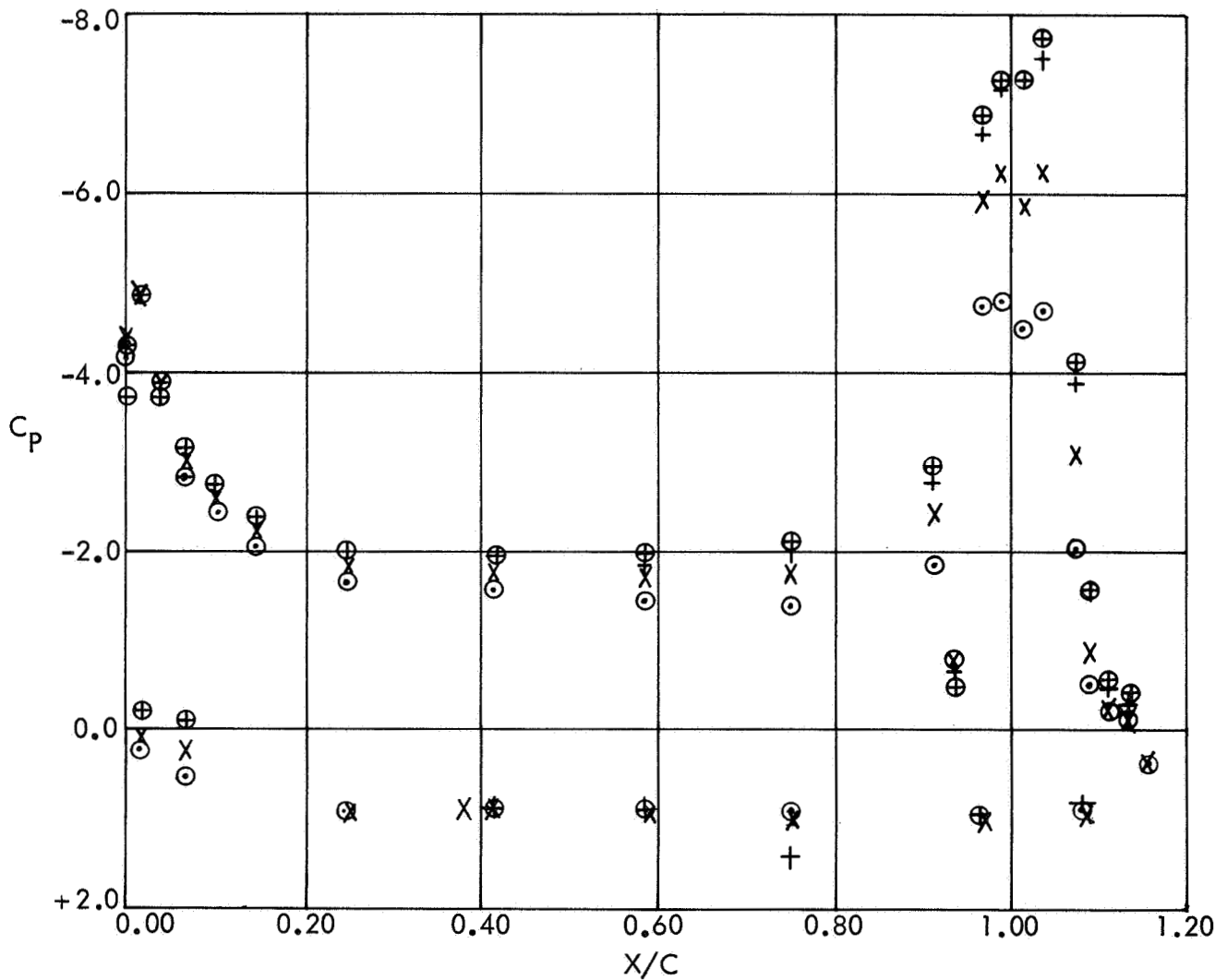


FIGURE 14. EFFECT OF MODEL HEIGHT ON CHORDWISE PRESSURE DISTRIBUTION
 $C_{\mu\text{NOM}} = 0.3$ $\eta = 0.342$ TUNNEL DYNAMIC PRESSURE = 10 PSF

SYMBOL	h	$C_{\mu\text{NOM}}$	$C_{\mu 1}$	C_l	TUNNEL q - PSF	RUN NO.
⊙	3"	0.30	0.276	3.333	10.13	410
X	5"	0.30	0.282	3.588	9.99	414
+	10"	0.30	0.294	3.683	10.02	419
⊕	15"	0.30	0.290	3.725	10.00	427

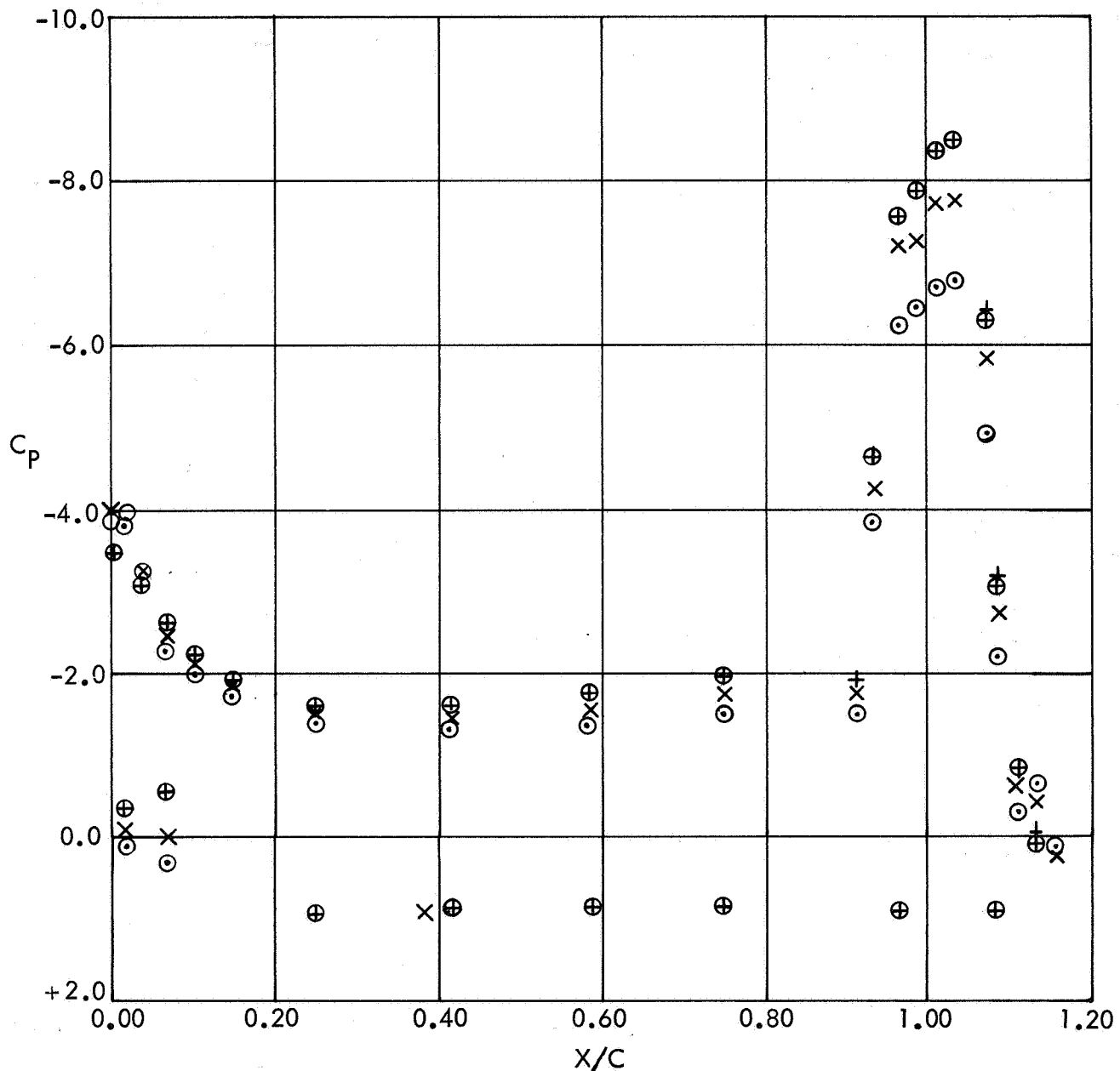


FIGURE 15. EFFECT OF MODEL HEIGHT ON CHORDWISE PRESSURE DISTRIBUTION
 $C_{\mu\text{NOM}} = 0.3$ $\eta = 0.643$ TUNNEL DYNAMIC PRESSURE = 10 PSF

SYMBOL	h	$C_{\mu\text{NOM}}$	$C_{\mu 1}$	C_l	TUNNEL q - PSF	RUN NO.
⊙	3"	0.30	0.276	2.696	10.13	410
△	5"	0.30	0.282	2.978	9.99	414
×	10"	0.30	0.294	3.131	10.02	419
⊕	15"	0.30	0.290	3.142	10.00	427

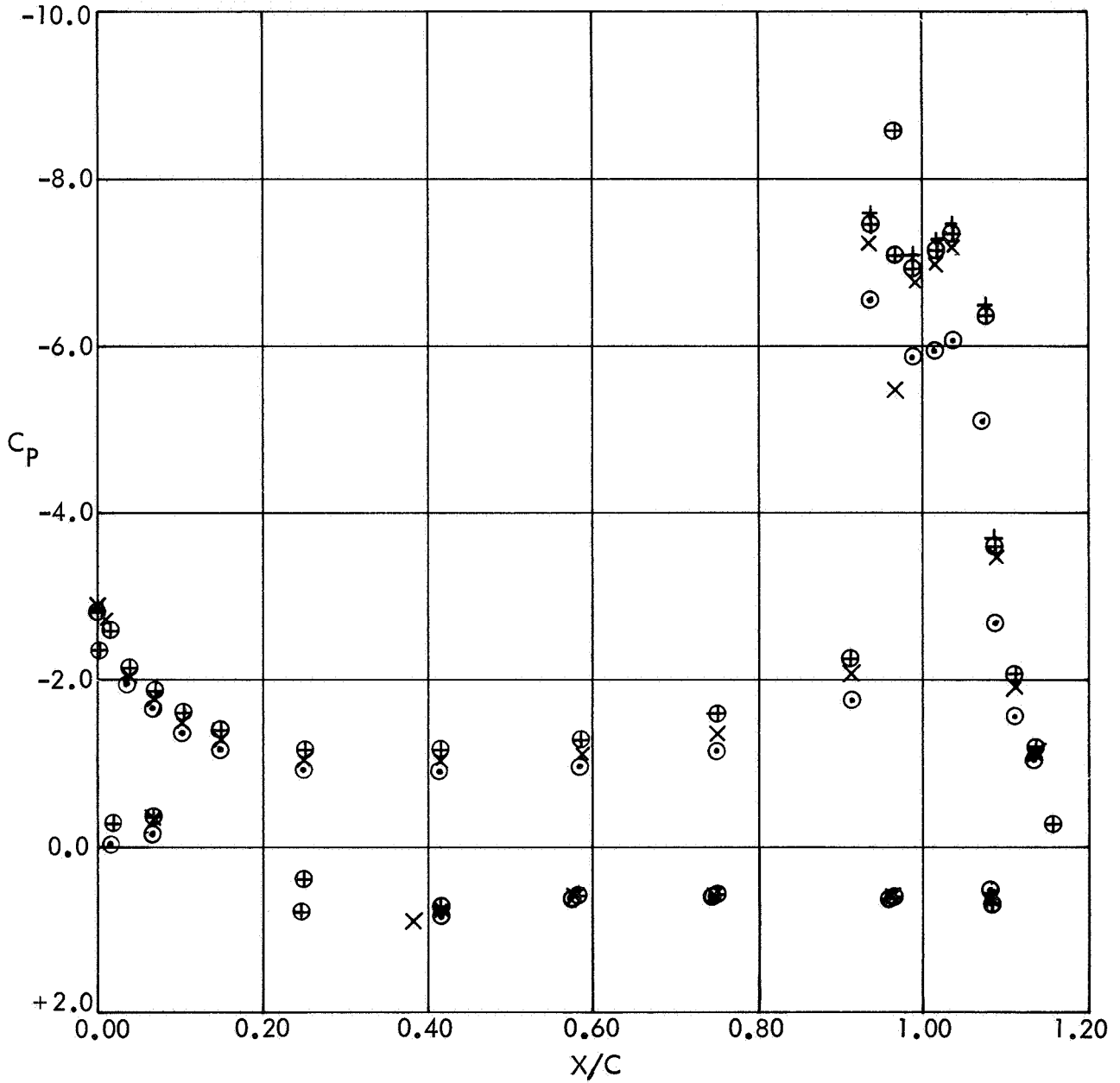


FIGURE 16. EFFECT OF MODEL HEIGHT ON CHORDWISE PRESSURE DISTRIBUTION
 $C_{\mu\text{NOM}} = 0.3$ $\eta = 0.866$ TUNNEL DYNAMIC PRESSURE = 10 PSF

SYMBOL	h	$C_{\mu\text{NOM}}$	$C_{\mu 1}$	C_l	TUNNEL q - PSF	RUN NO.
⊙	3"	3.00	2.860	7.267	4.96	350
△	4"	3.00	2.890	7.919	5.00	603
×	5"	3.00	2.712	7.961	4.86	293
⊕	15"	3.00	2.912	9.138	4.94	544

NOTE: WHERE SYMBOLS ARE OMITTED, CLOSELY COINCIDENT POINTS
MAY BE ASSUMED

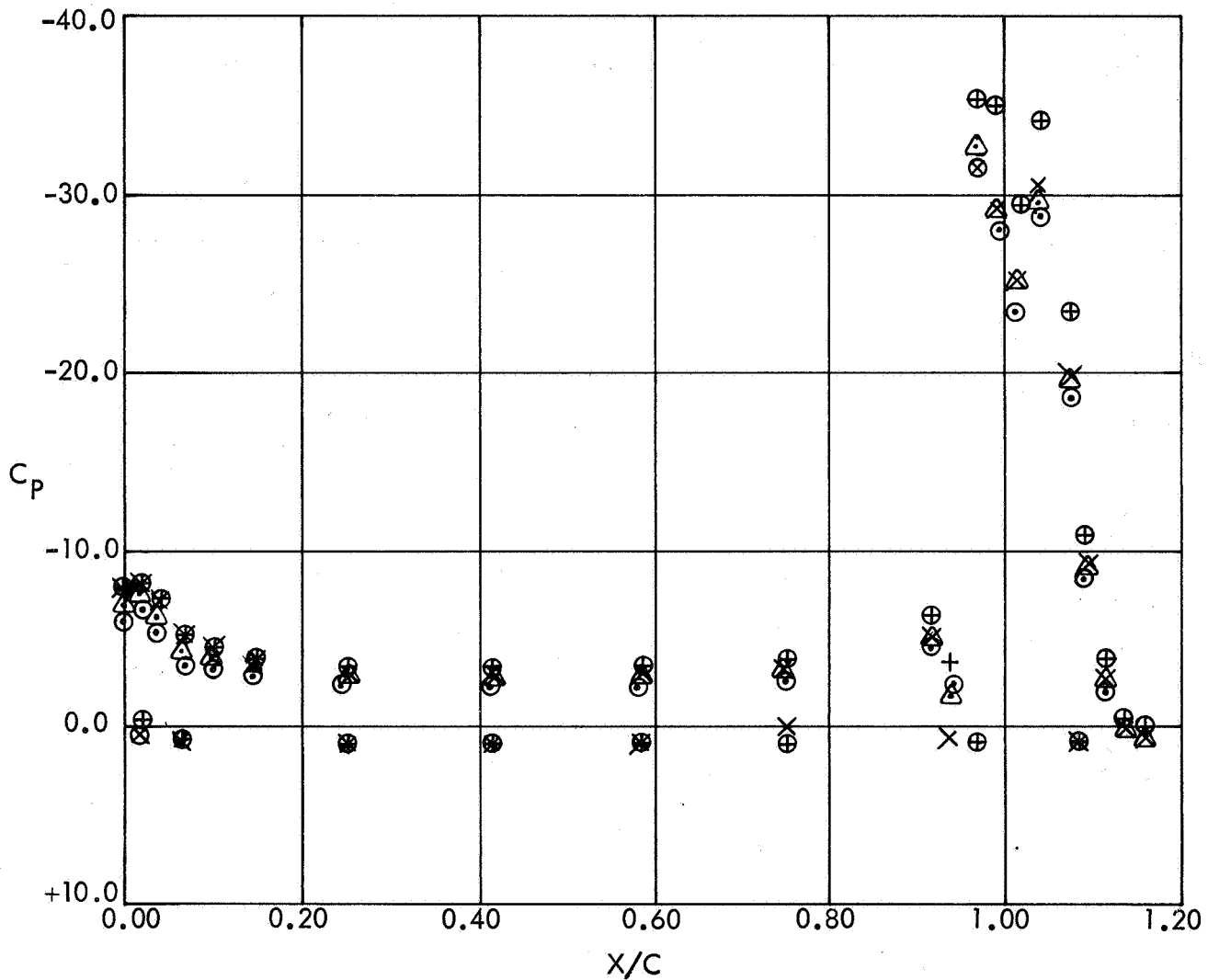


FIGURE 17. EFFECT OF MODEL HEIGHT ON CHORDWISE PRESSURE DISTRIBUTION
 $C_{\mu\text{NOM}} = 3.0$ $\eta = 0.342$ TUNNEL DYNAMIC PRESSURE = 5 PSF

SYMBOL	h	$C_{\mu\text{NOM}}$	$C_{\mu 1}$	C_l	TUNNEL q - PSF	RUN NO.
⊙	3"	3.00	2.860	6.517	4.96	350
△	4"	3.00	2.890	7.292	5.00	603
×	5"	3.00	2.712	7.875	4.86	293
⊕	15"	3.00	2.912	8.502	4.94	544

NOTE: WHERE SYMBOLS ARE OMITTED, CLOSELY COINCIDENT POINTS
MAY BE ASSUMED

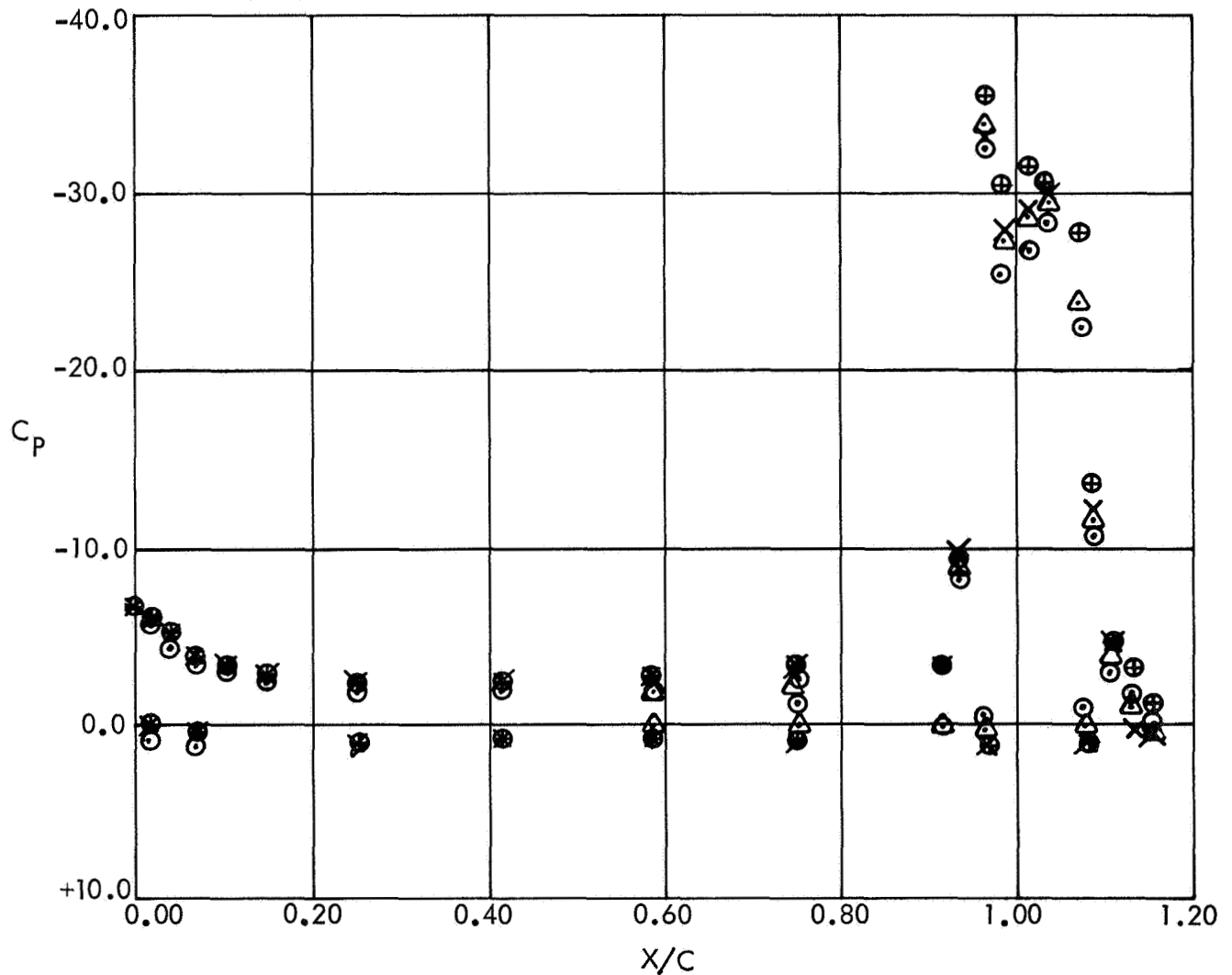


FIGURE 18. EFFECT OF MODEL HEIGHT ON CHORDWISE PRESSURE DISTRIBUTION
 $C_{\mu\text{NOM}} = 3.0$ $\eta = 0.643$ TUNNEL DYNAMIC PRESSURE = 5 PSF

SYMBOL	h	$C_{\mu_{NOM}}$	C_{μ_1}	C_t	TUNNEL q - PSF	RUN NO.
⊙	3"	3.00	2.860	7.689	4.96	350
△	4"	3.00	2.890	8.320	5.00	603
×	5"	3.00	2.712	8.337	4.86	293
⊕	15"	3.00	2.912	8.726	4.94	544

NOTE: WHERE SYMBOLS ARE OMITTED, CLOSELY COINCIDENT POINTS
MAY BE ASSUMED

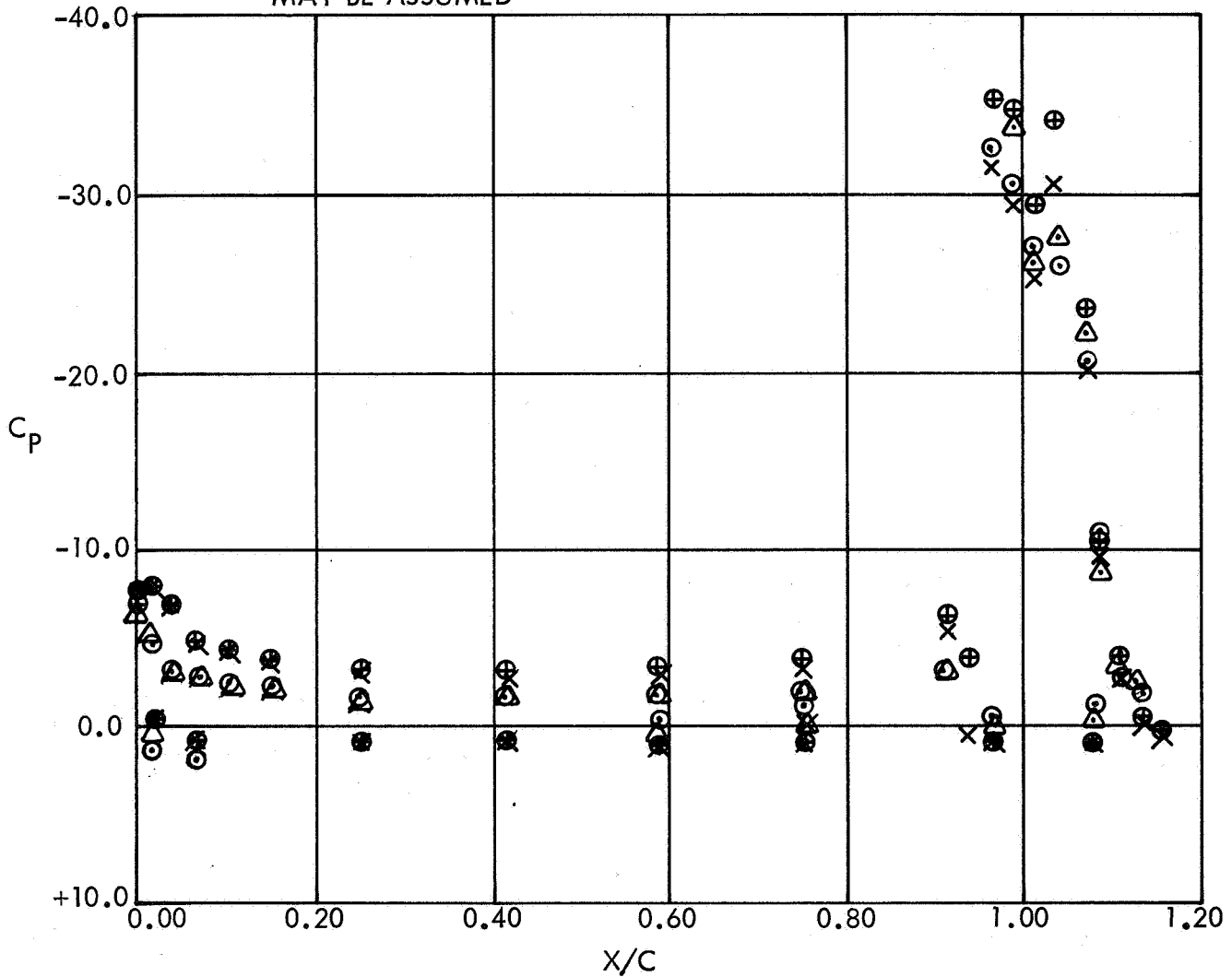


FIGURE 19. EFFECT OF MODEL HEIGHT ON CHORDWISE PRESSURE DISTRIBUTION
 $C_{\mu_{NOM}} = 3.0$ $\eta = 0.866$ TUNNEL DYNAMIC PRESSURE = 5 PSF

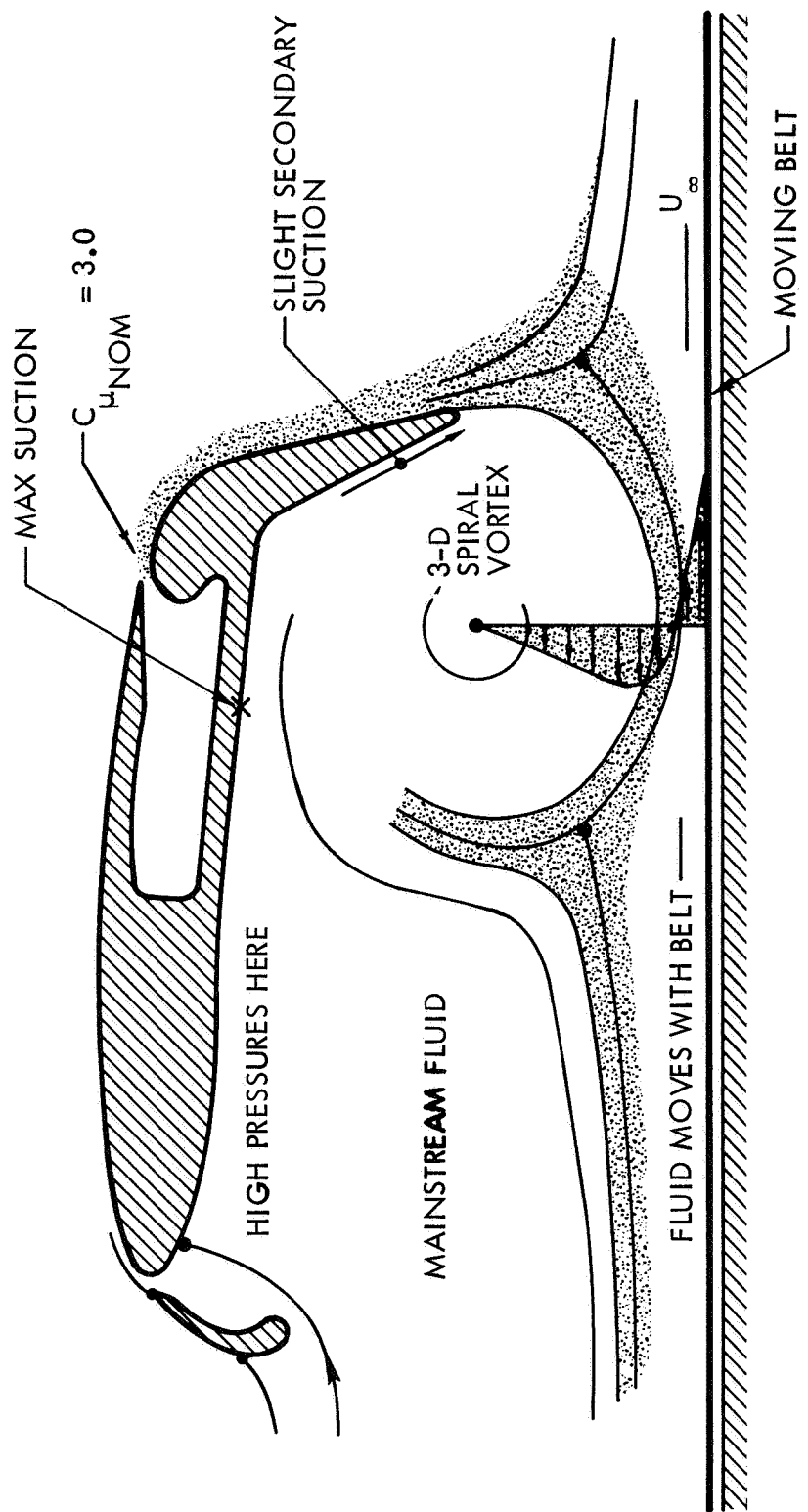


FIGURE 20. FORMATION OF TRAPPED, UNDERWING VORTEX AT LOW ALTITUDE AND HIGH JET MOMENTUM

SYMBOL	GROUND	h	$C_{\mu_{NOM}}$	C_{μ_1}	C_l	η	RUN
⊙	MOVING	3"	1.0	0,891	3,292	4.96	387
X	FIXED	3"	1.0	0.876	4.055	4.92	396

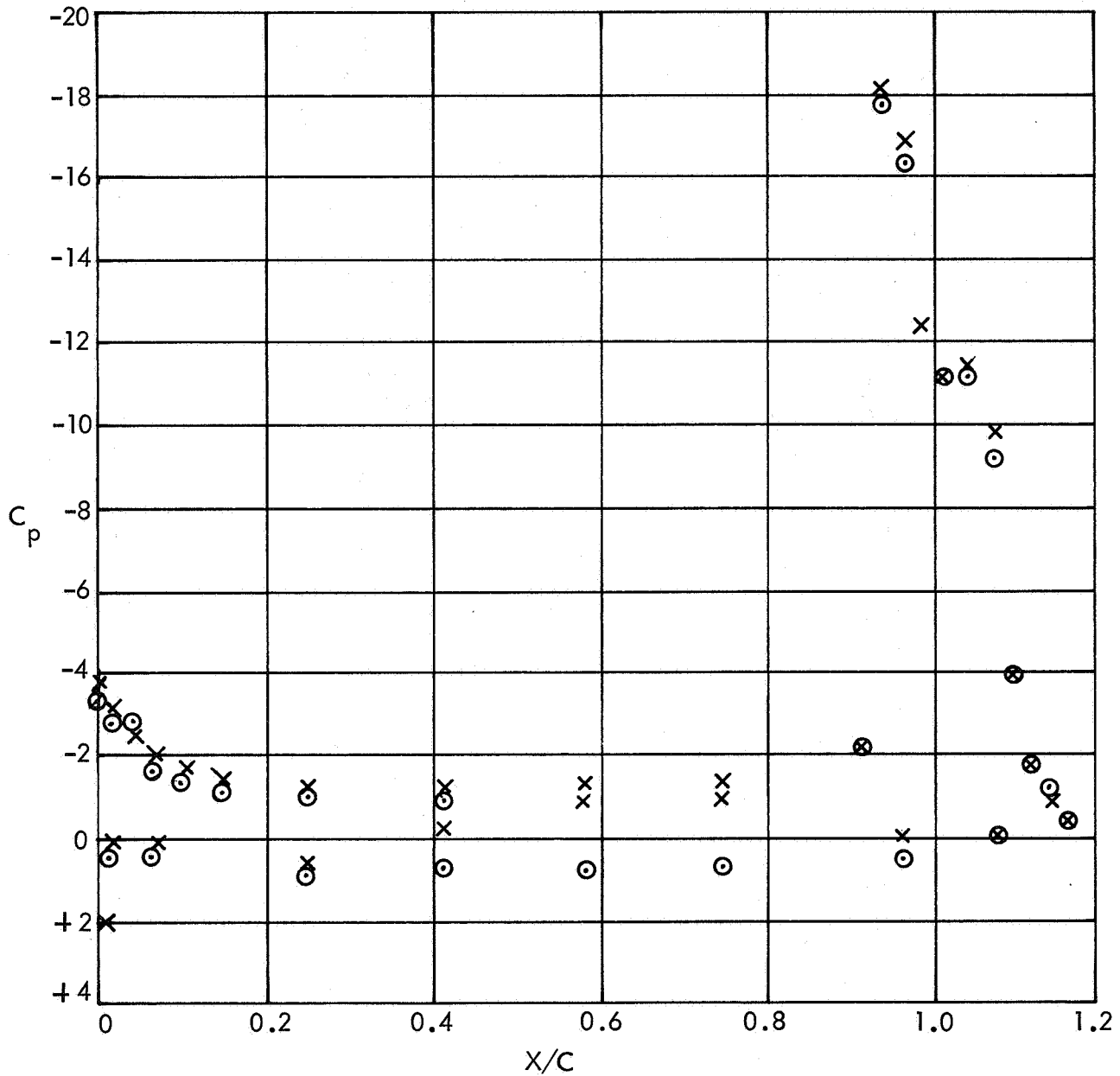


FIGURE 21. EFFECT OF FIXED - GROUND FLOW DISTORTION ON SURFACE PRESSURE DISTRIBUTIONS,
 $C_{\mu_{NOM}} = 1.0 \quad \eta = 0.866$

SYMBOL	GROUND	h	$C_{\mu\text{NOM}}$	$C_{\mu 1}$	C_l	q	RUN
⊙	MOVING	3"	3.0	2.399	5.563	4.95	389
X	FIXED	3"	3.0	2.467	7.262	4.88	398

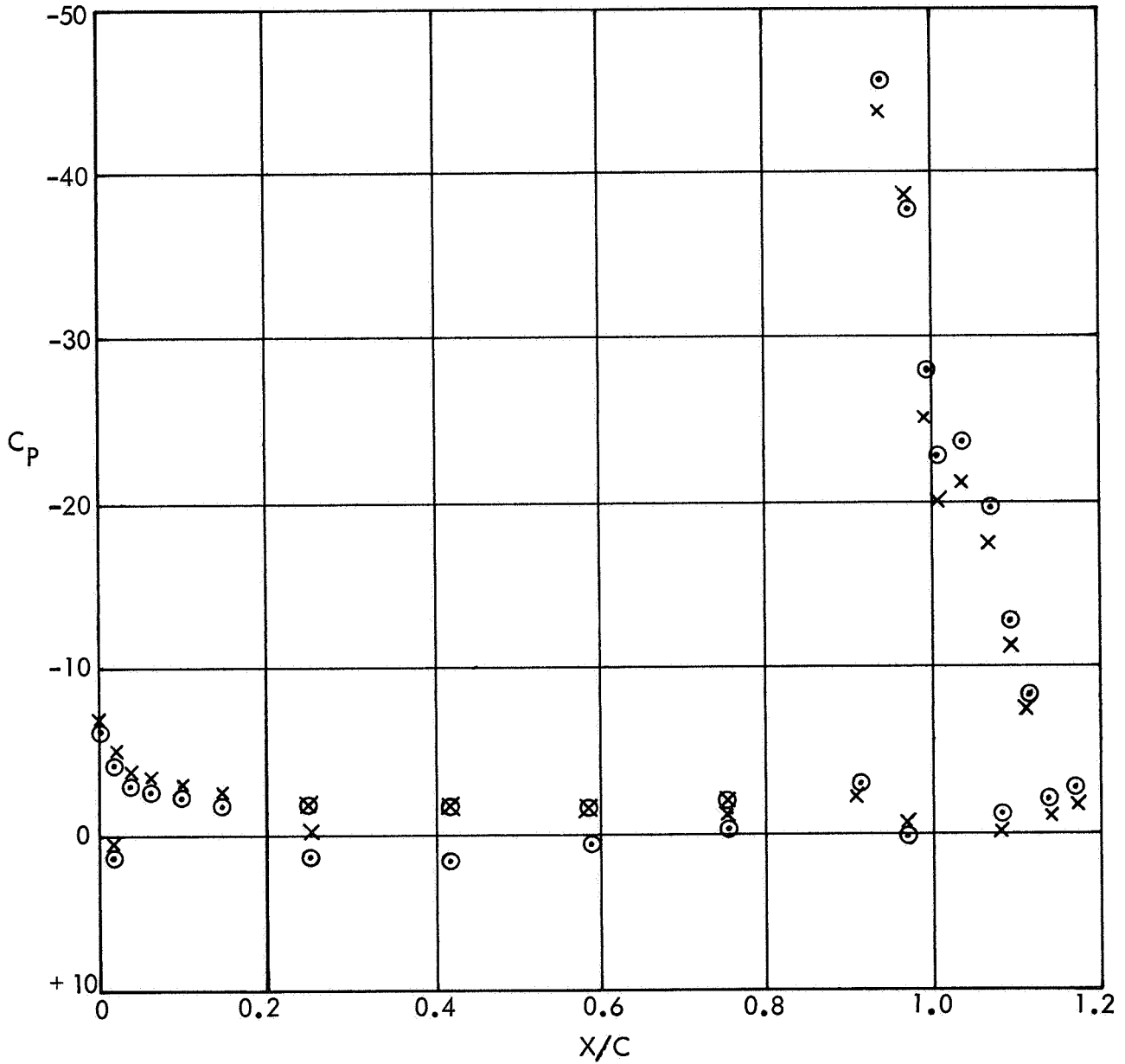


FIGURE 22. EFFECT OF FIXED-GROUND FLOW DISTORTION ON SURFACE PRESSURE DISTRIBUTIONS,
 $C_{\mu\text{NOM}} = 3.0 \quad \eta = 0.866$

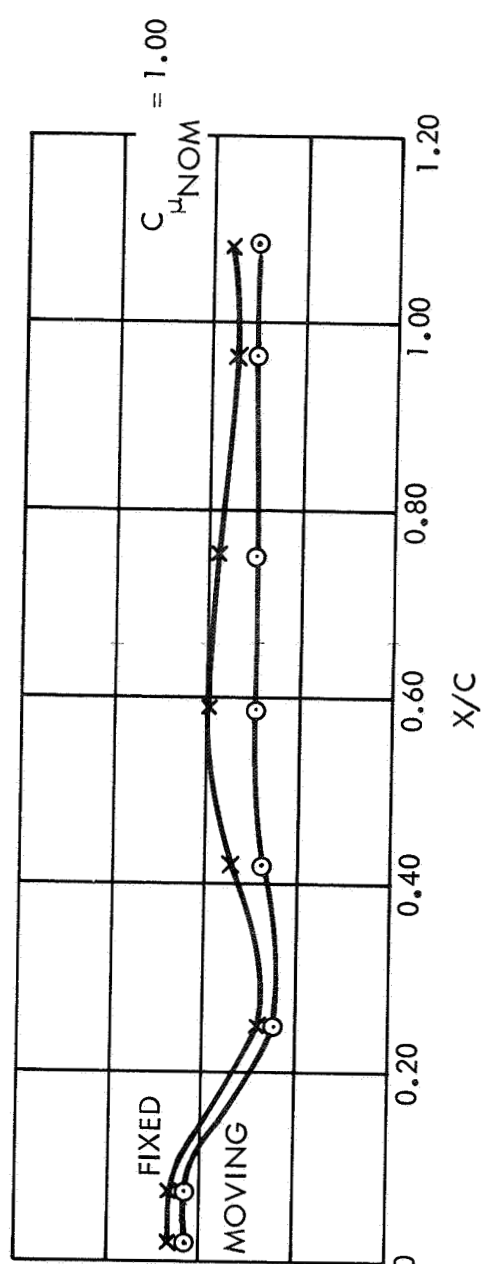
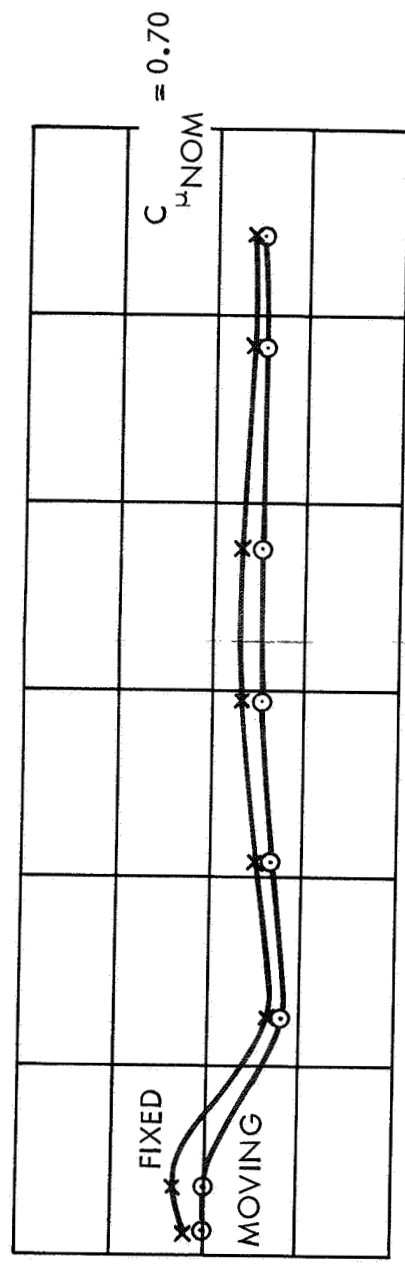
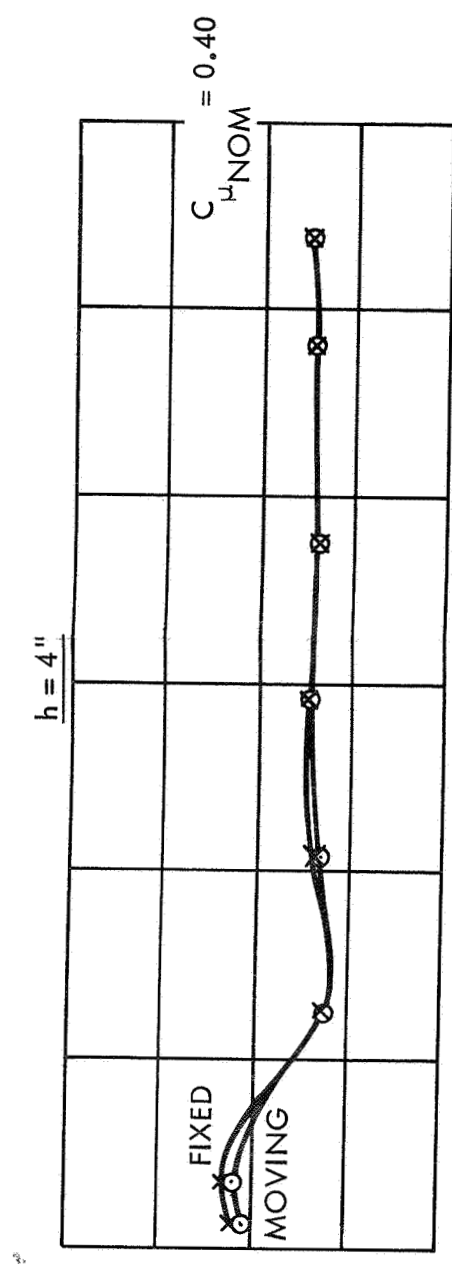
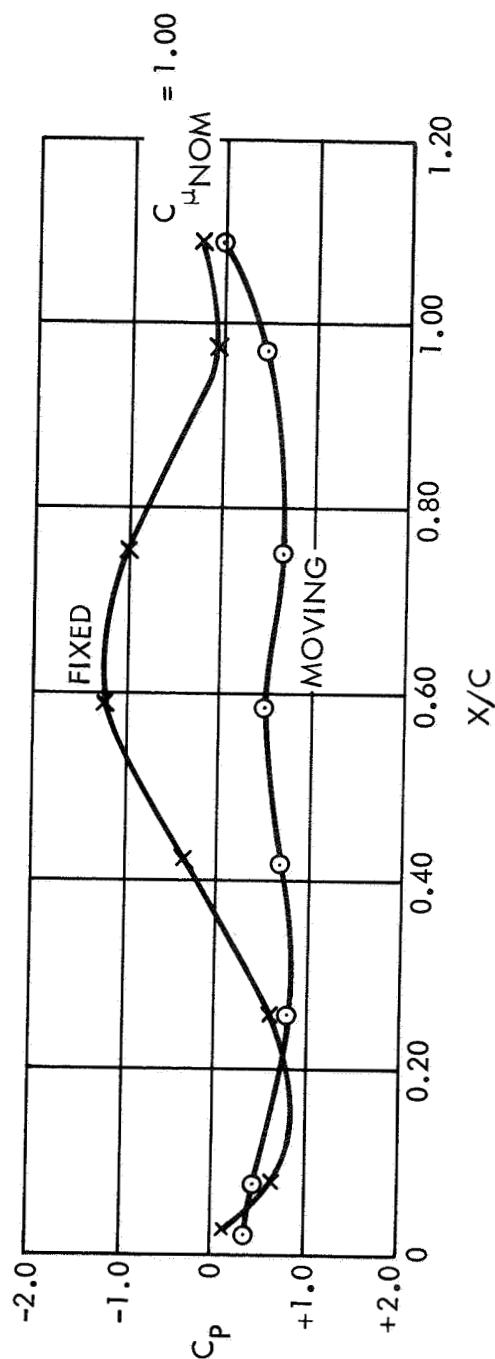
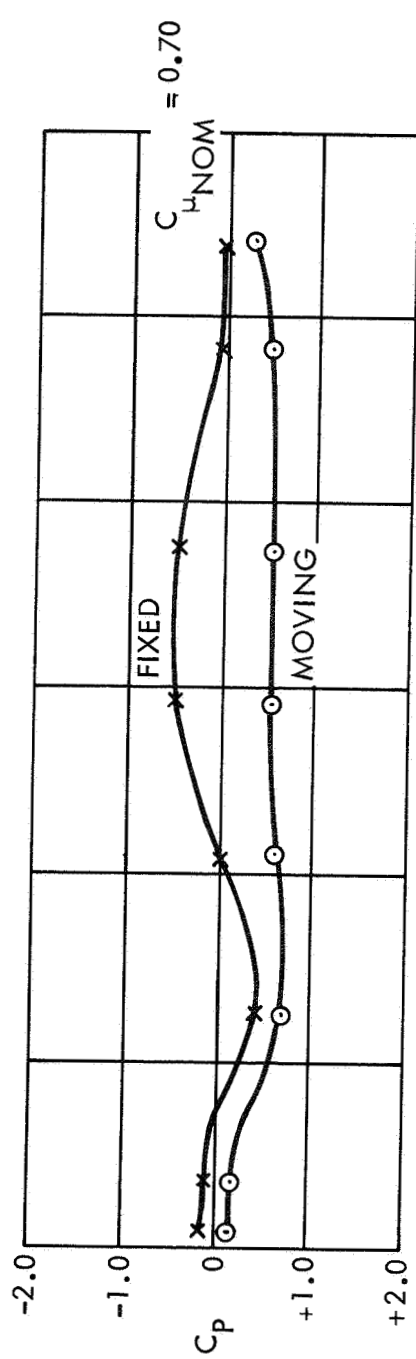
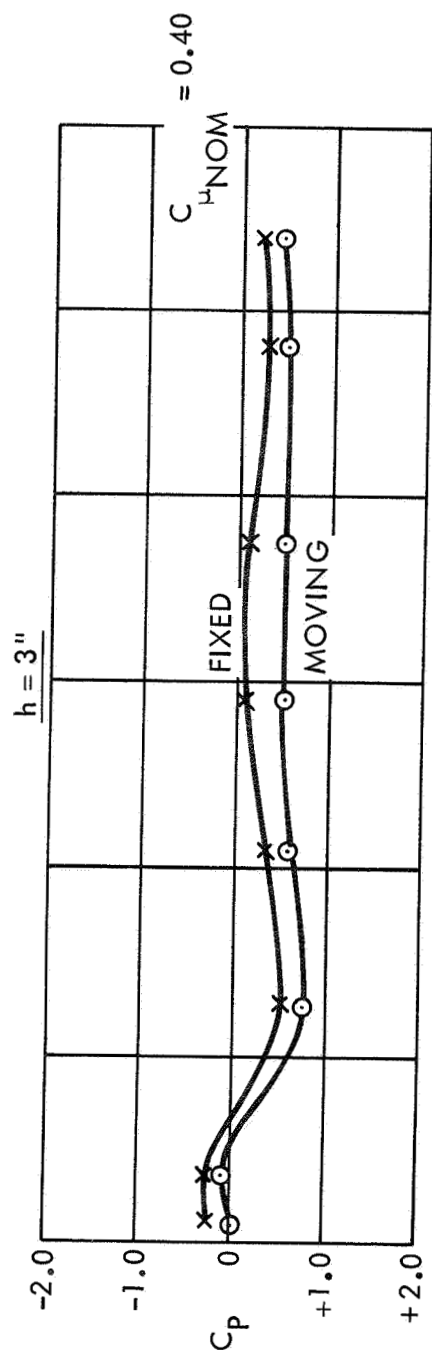
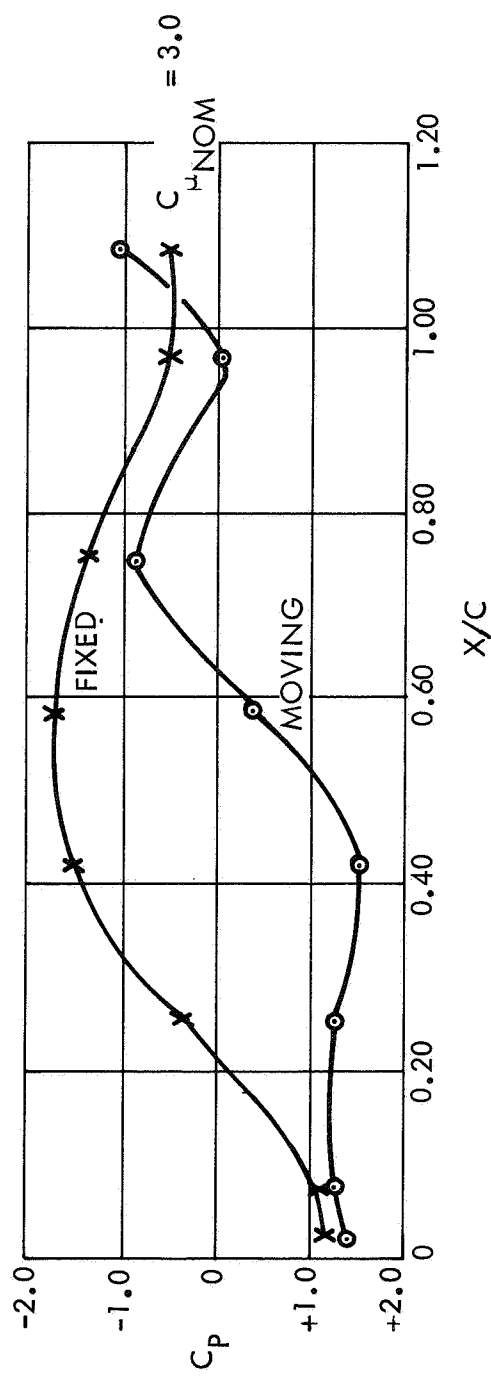
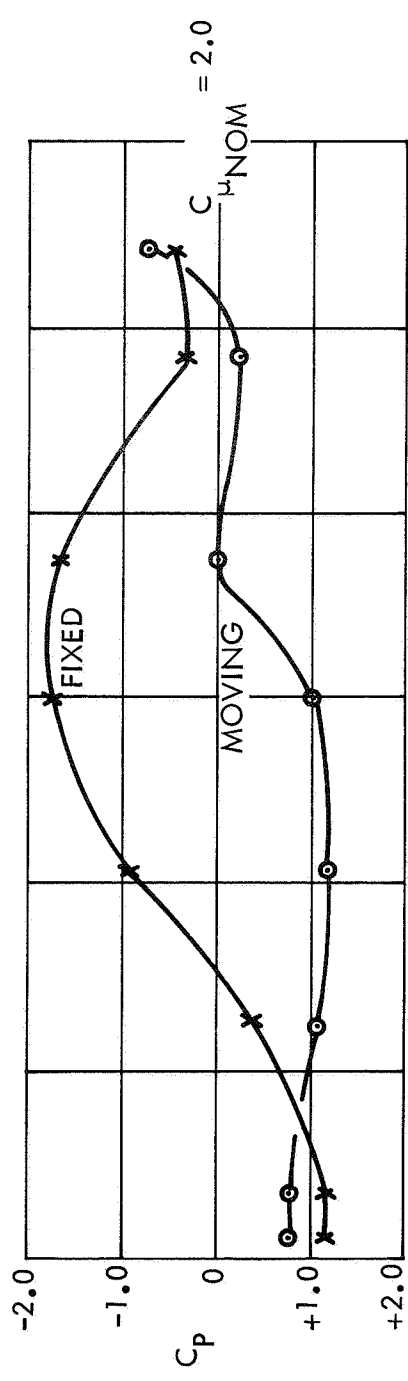
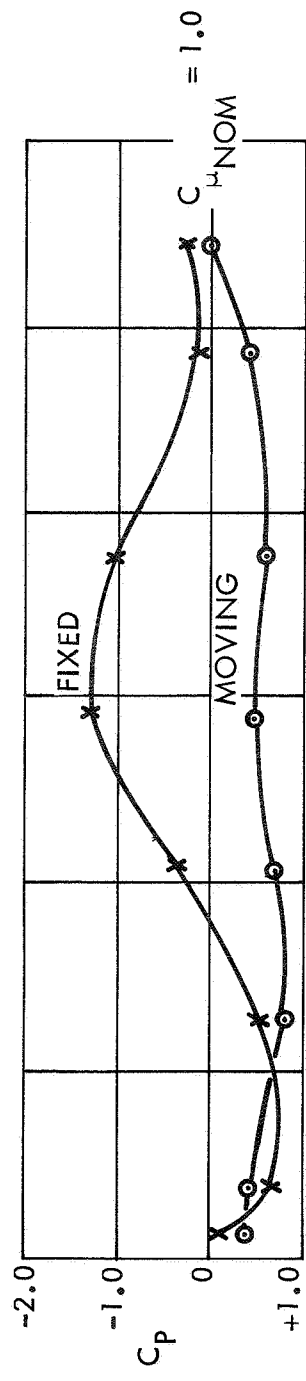


FIGURE 23. EFFECT OF FIXED-GROUND FLOW DISTORTION ON LOWER SURFACE STATIC PRESSURE DISTRIBUTIONS (i) $C_{\mu,NOM}$ BETWEEN 0.40 AND 1.00

$h = 3''$



$h = 4''$

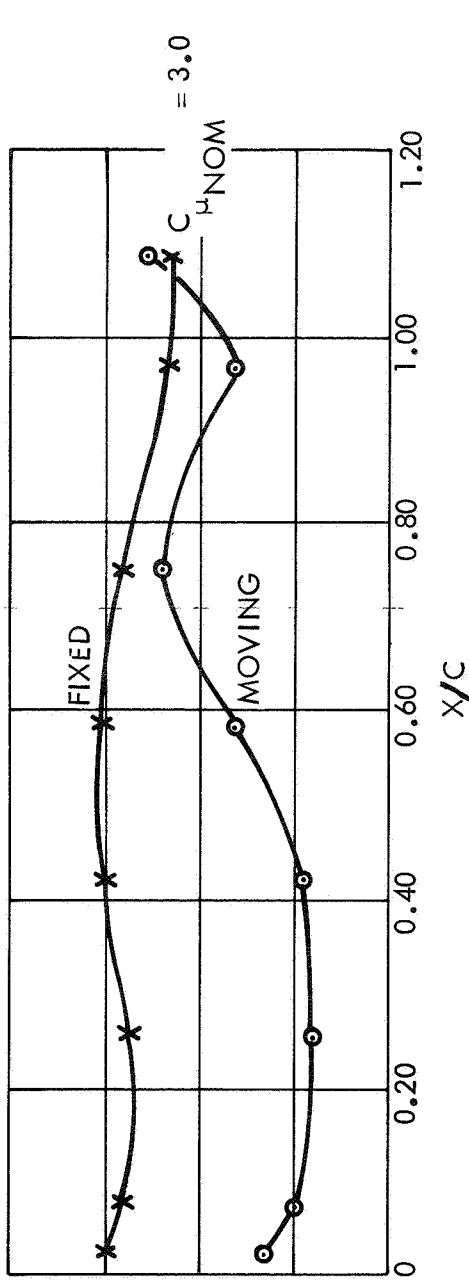
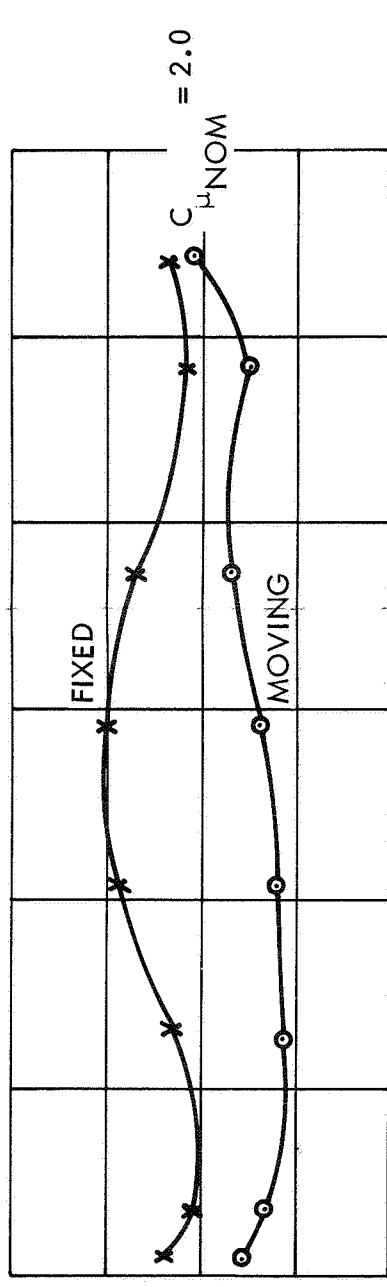
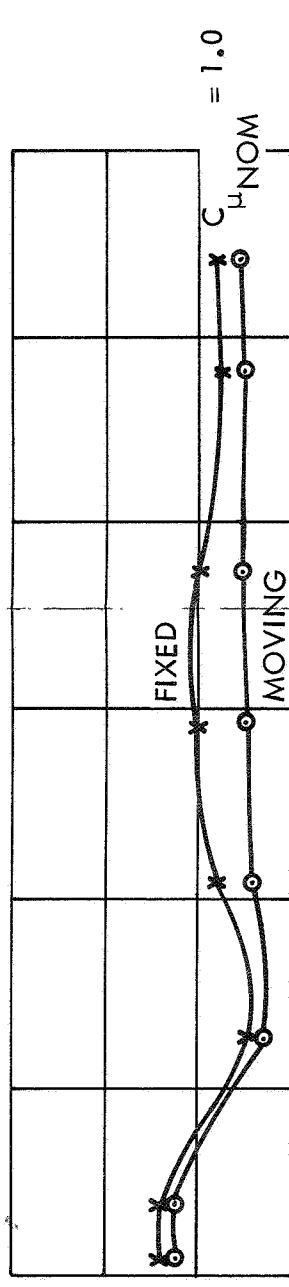


FIGURE 24. EFFECT OF FIXED-GROUND FLOW DISTORTION ON LOWER SURFACE STATIC PRESSURE DISTRIBUTIONS (ii) $C_{\mu NOM}$ BETWEEN 1.0 AND 3.0

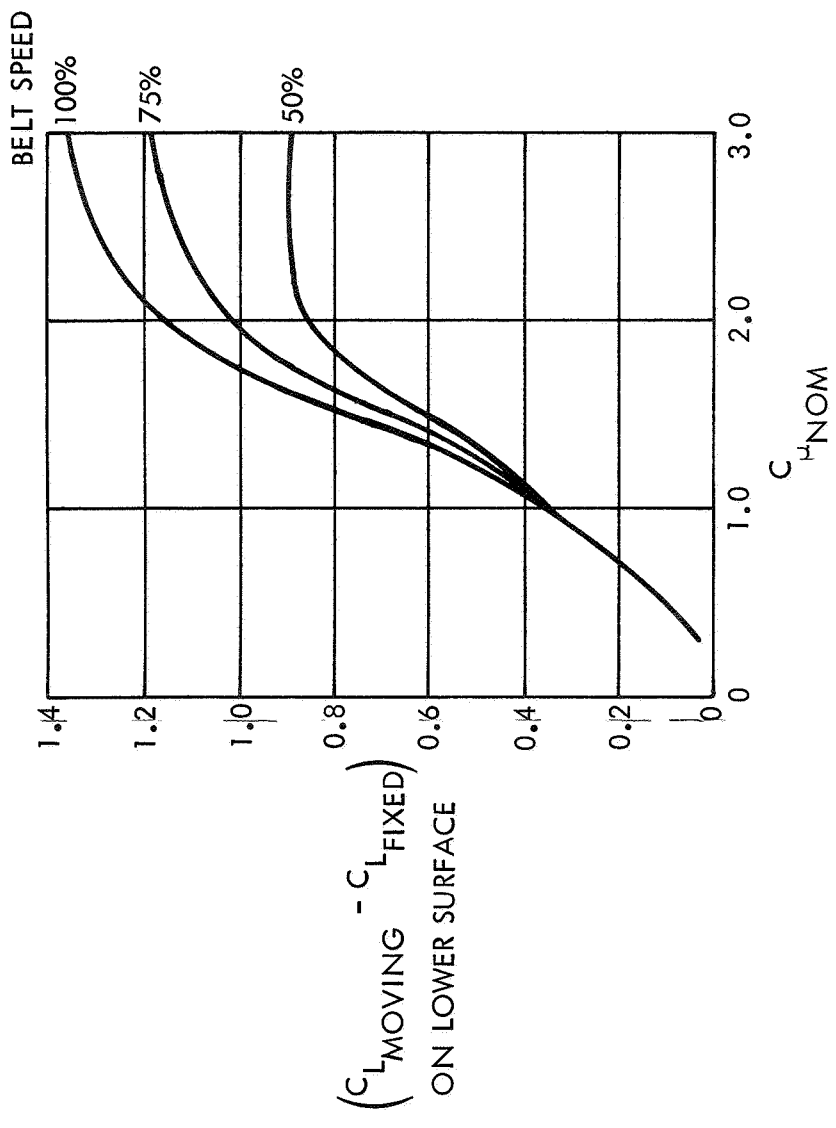
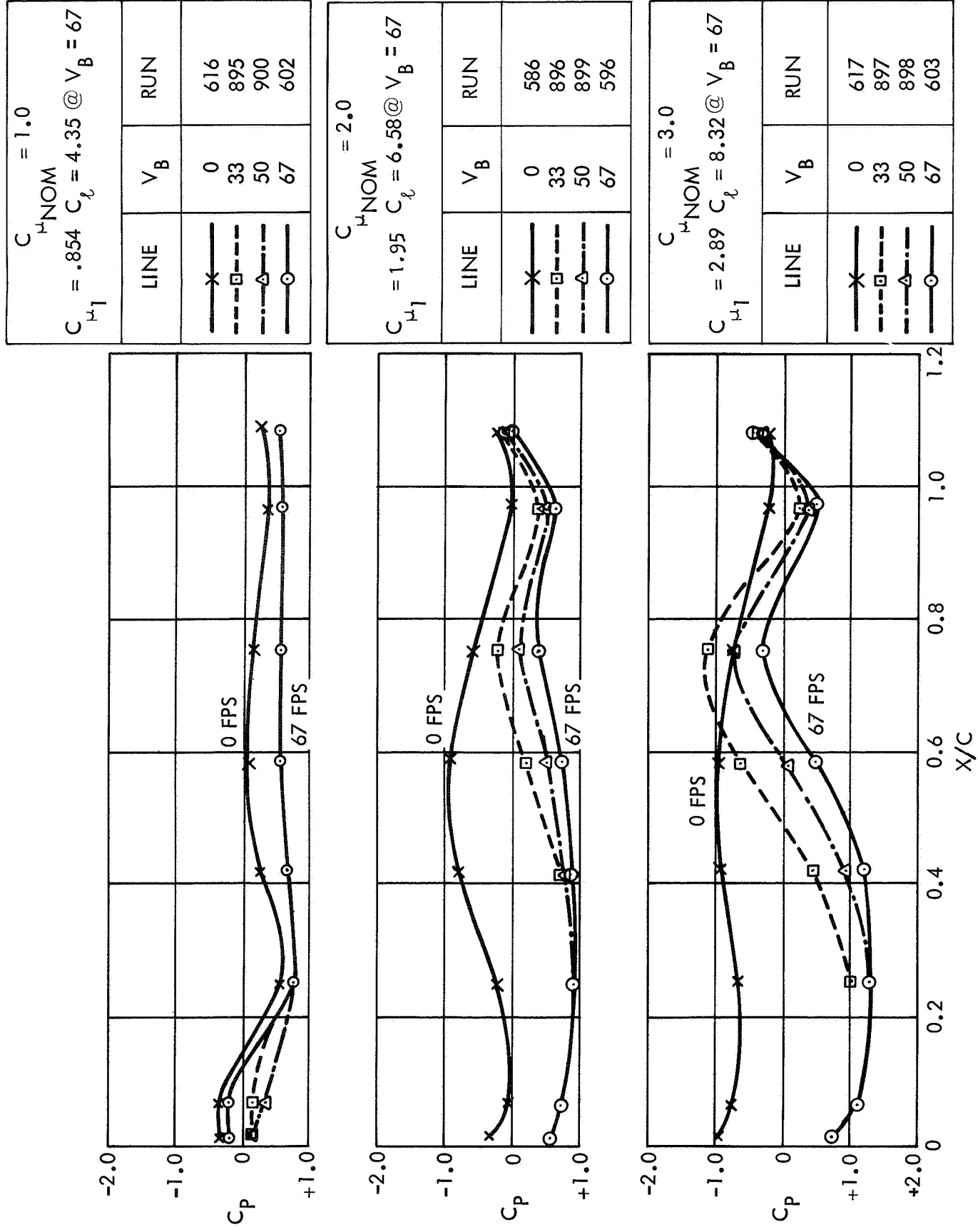
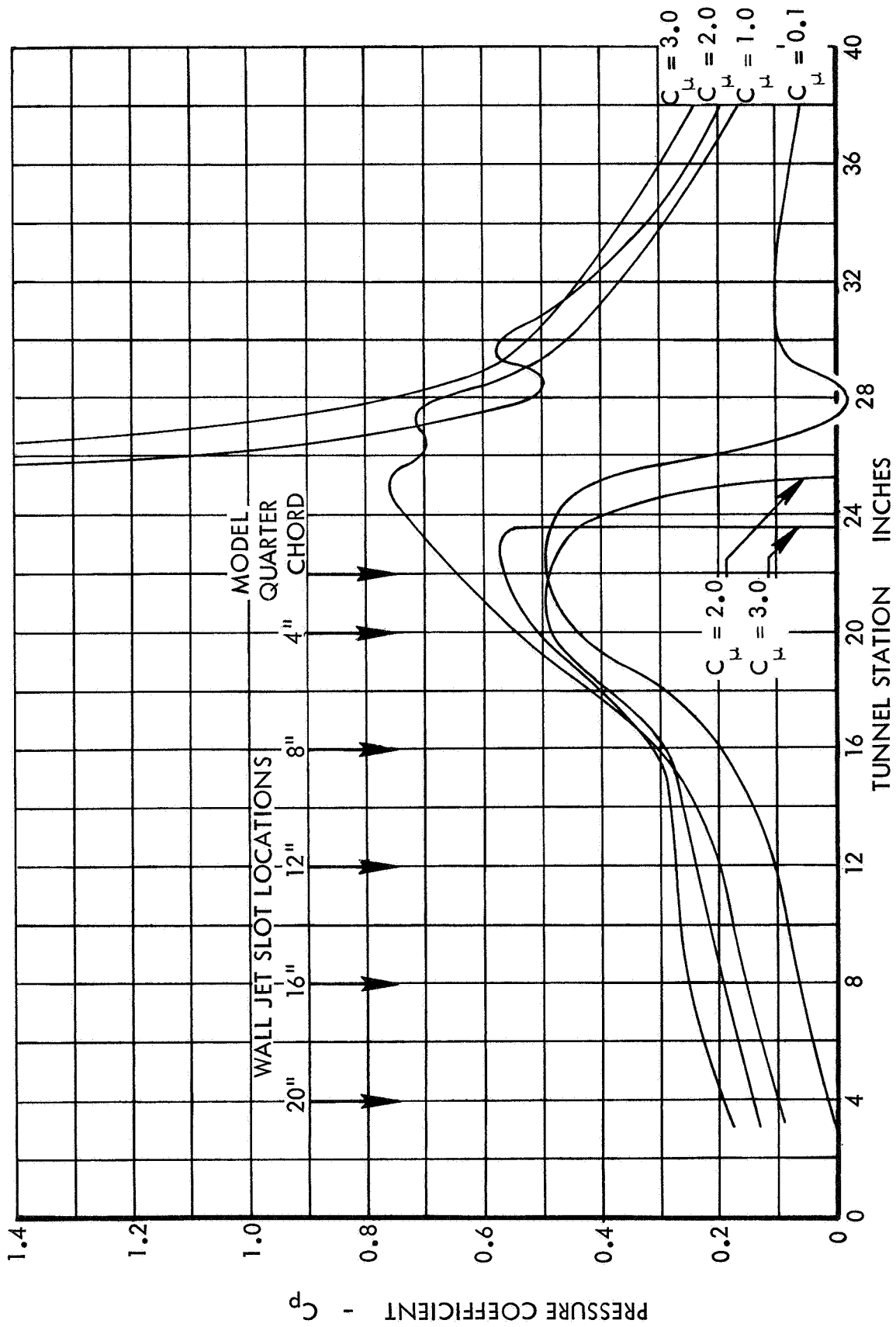


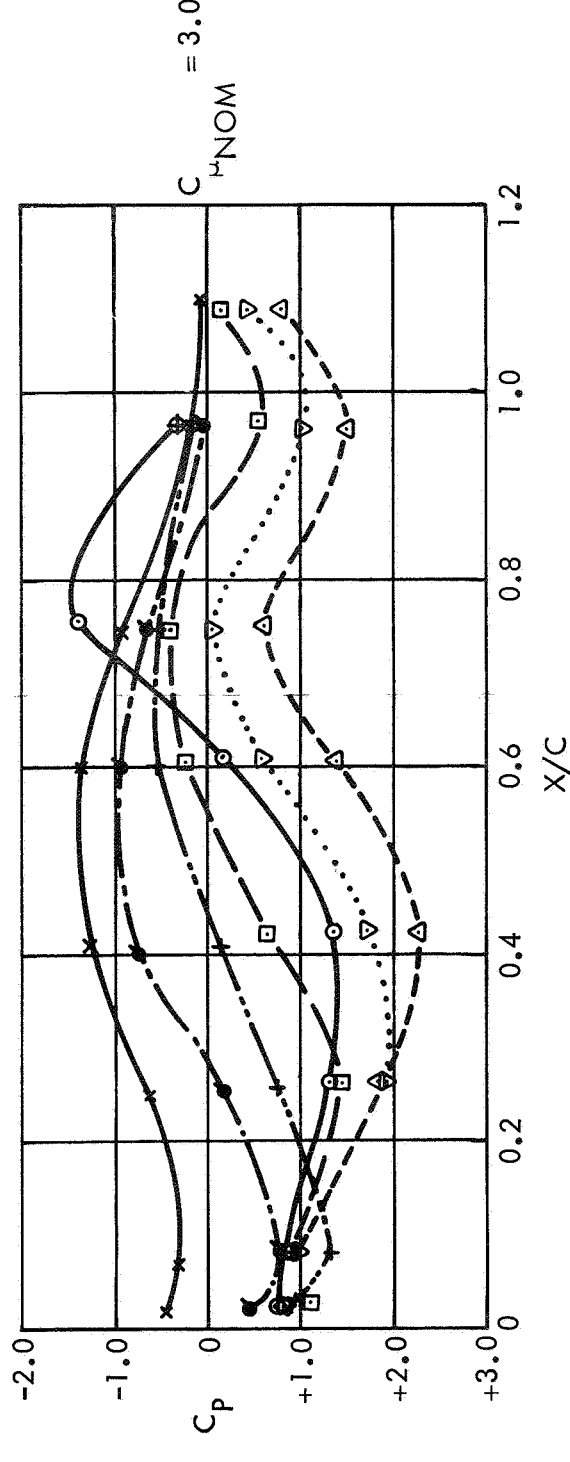
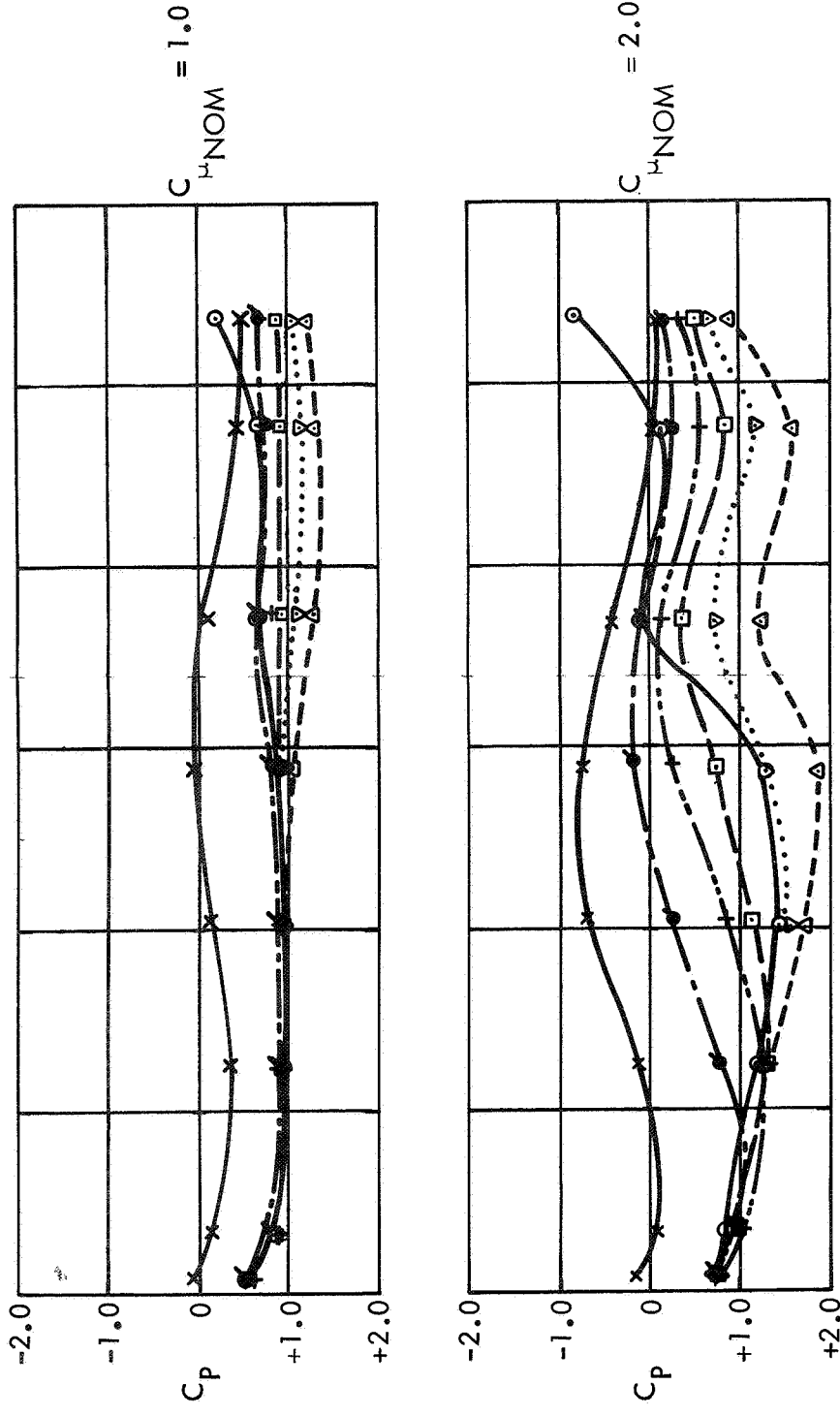
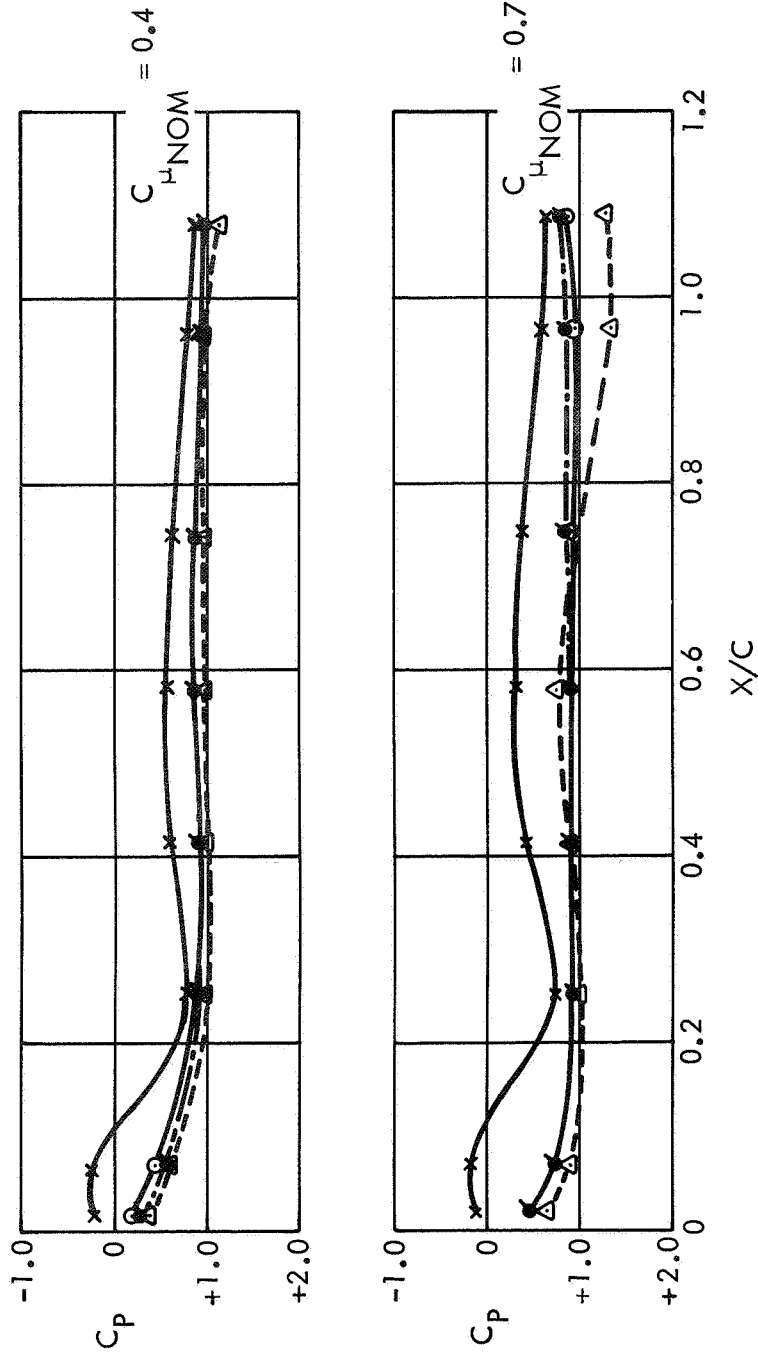
FIGURE 25. RESULTS OF BELOW-SPEED MOVING GROUND TESTS AT $\frac{h}{C} = 1.0$, $\eta = 0.866$



MODEL HEIGHT = 3"
 ANGLE OF ATTACK = 0°
 DYNAMIC PRESSURE = 5 PSF

FIGURE 26. STATIC PRESSURE DISTRIBUTION ON WIND TUNNEL FLOOR CENTERLINE

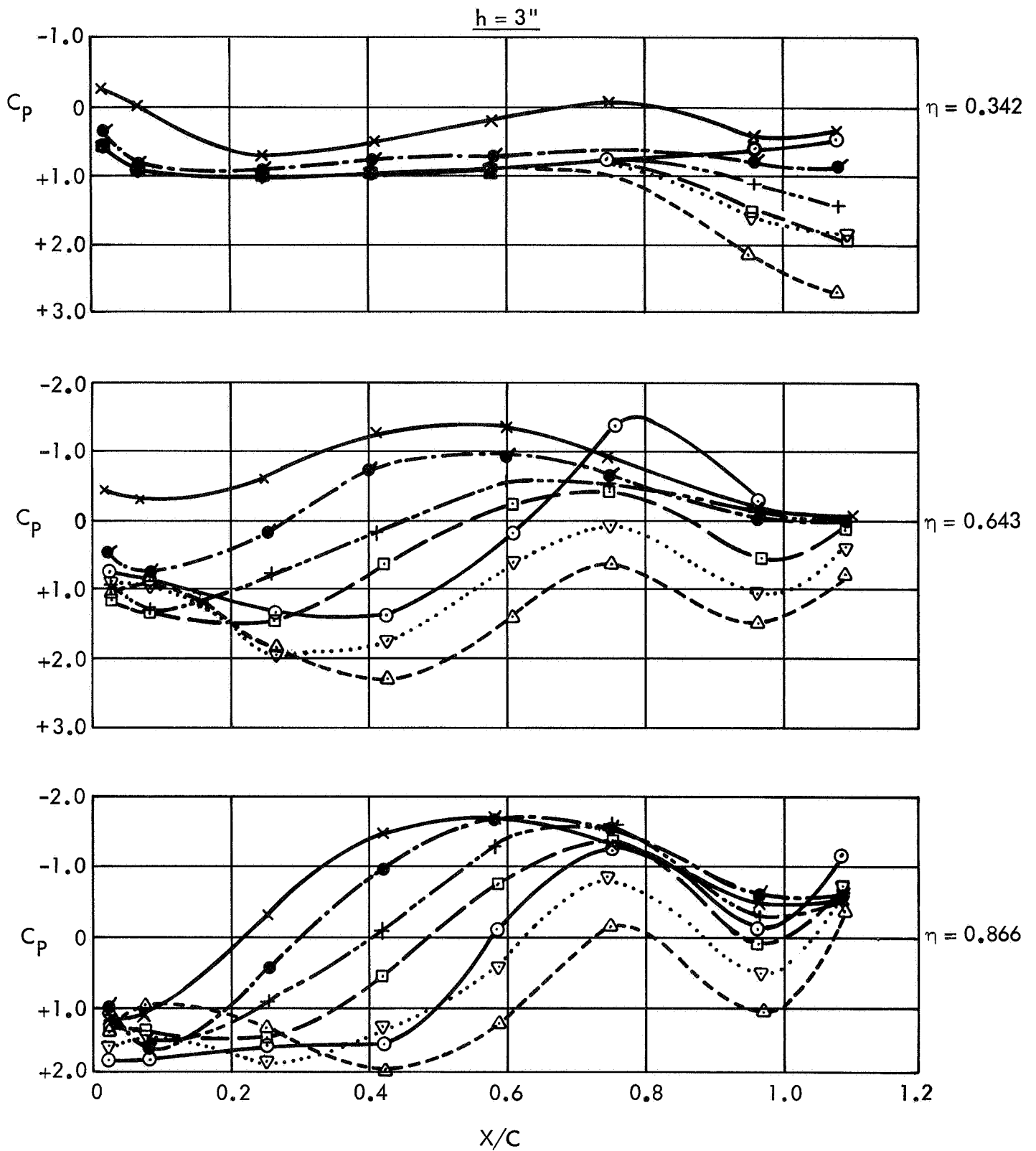
$h = 3''$



SYMBOL	N	RUNS	$C_{\mu 1}$	$C_{l, .643}$						
—x—	FIXED GRD.	385 TO 389	0.891	3.766	1.654	4.259	2.399	4.691		
—o—	MVG GRD.	394, 395 343, 349 350	0.940	4.617	1.942	5.650	2.860	6.517		
—•—	2.0	651 TO 655	0.918	4.378	1.990	5.362	2.924	5.807		
—+—	2.5	657 TO 661	0.921	4.467	1.864	5.500	2.826	6.125		
—□—	3.0	666 TO 668	0.919	4.451	1.864	5.752	2.866	6.511		
—∇—	3.5	691 TO 695	0.949	4.610	1.843	5.928	2.809	7.010		
—△—	4.0	697 TO 701	0.948	4.679	1.831	6.222	2.770	7.239		

THE 0.067" SLOT AT THE 8" POSITION WAS USED

FIGURE 27. EFFECT OF BLOWING B.L.C., AT THE GROUND, ON WING LOWER SURFACE PRESSURES; $h = 3''$, $\eta = 0.643$

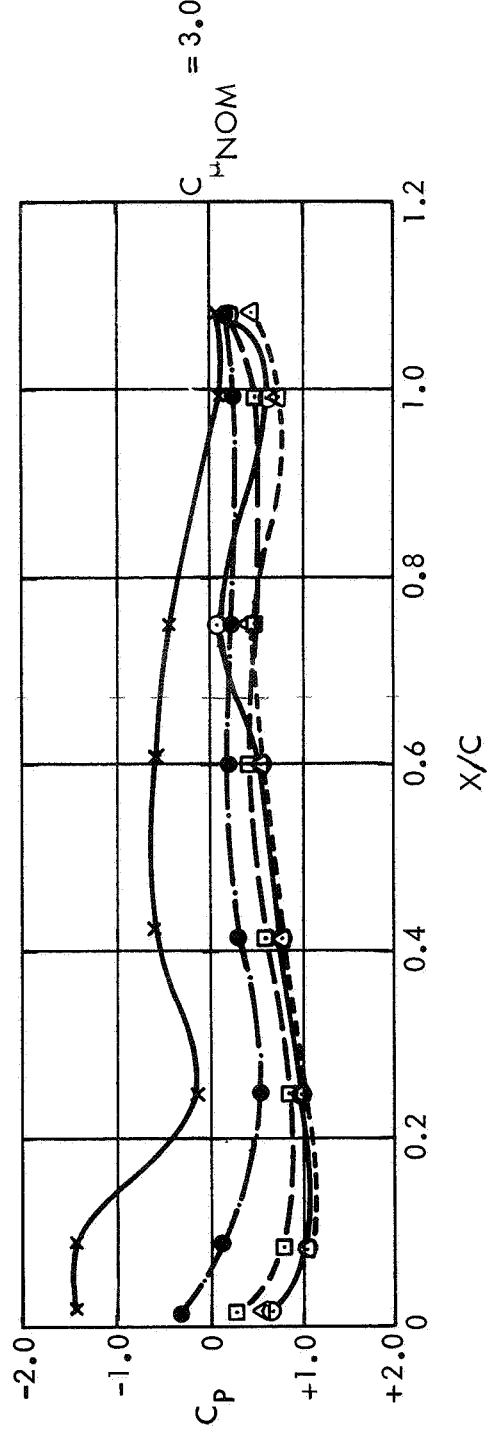
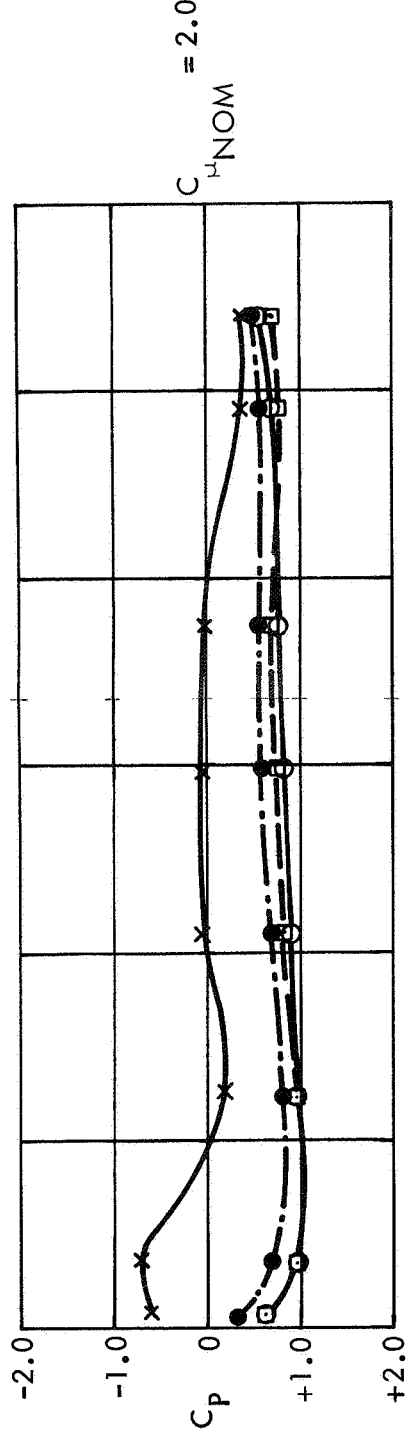
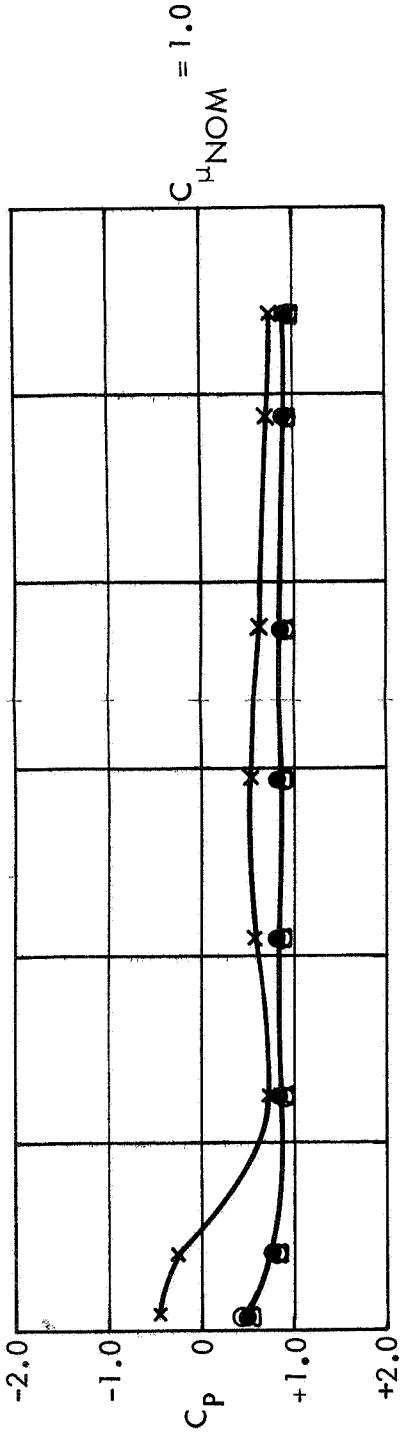
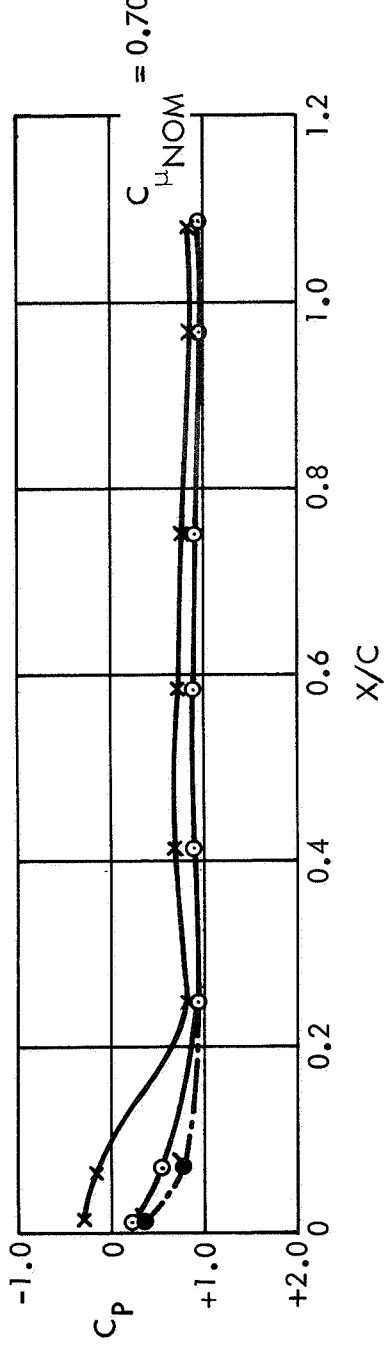
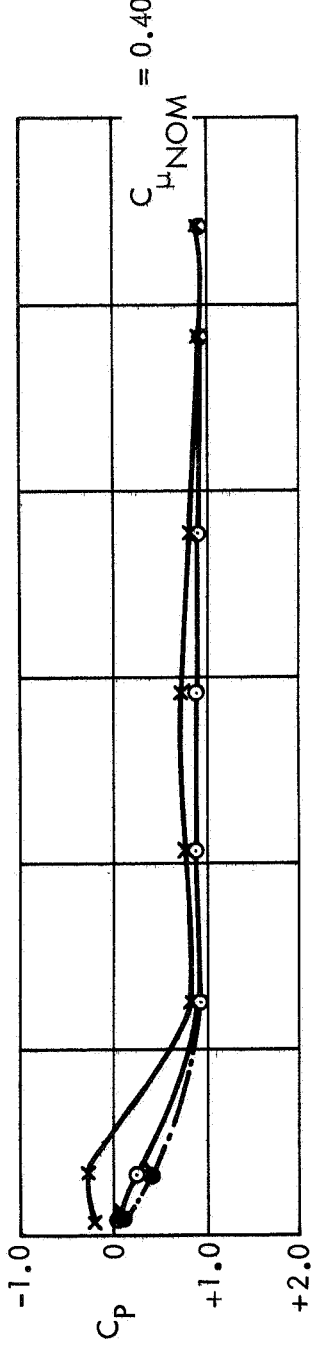


FOR SYMBOLS LIST, SEE FIGURE 27.

FIGURE 28. EFFECT OF BLOWING BLC, AT THE GROUND,
ON WING LOWER SURFACE PRESSURES;
 $h = 3''$ $C = 3.0$

NOM

$h = 4''$



SYMBOL	N	RUNS	$C_{\mu 1}$	$C_{l, .643}$						
—x—	FIXED GRD.	614 TO 616 586, 617	0.866	4.510	1.946	5.431	2.843	5.939		
—o—	MVG. GRD.	600 TO 602 596, 603	0.854	4.927	1.947	6.497	2.890	7.292		
—•—	2.0	849 851, 854 856, 858	0.963	5.030	1.917	6.109	2.965	6.862		
—□—	3.0	850 852, 855 857, 859	0.939	4.958	1.968	6.376	2.986	7.175		
—△—	4.0	772, 773 774	0.942	4.909	1.910	6.322	3.003	7.271		

THE 0.067" SLOT AT THE 12" POSITION WAS USED

FIGURE 29. EFFECT OF BLOWING B.L.C., AT THE GROUND, ON WING LOWER SURFACE PRESSURES; $h = 4''$, $\eta = 0.643$

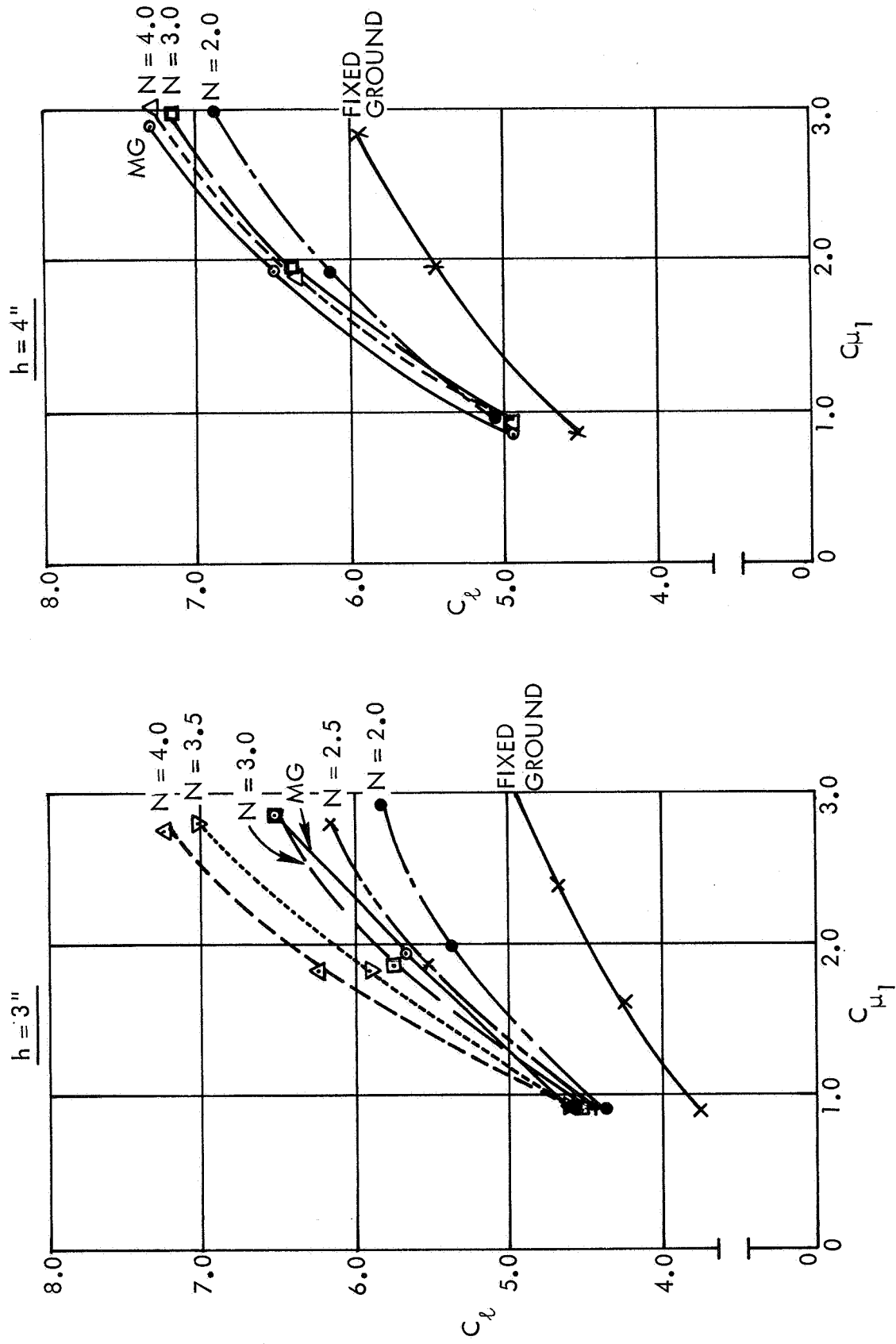


FIGURE 31. EFFECT OF GROUND BLC ON SECTIONAL LIFT COEFFICIENT, $\eta = 0.643$

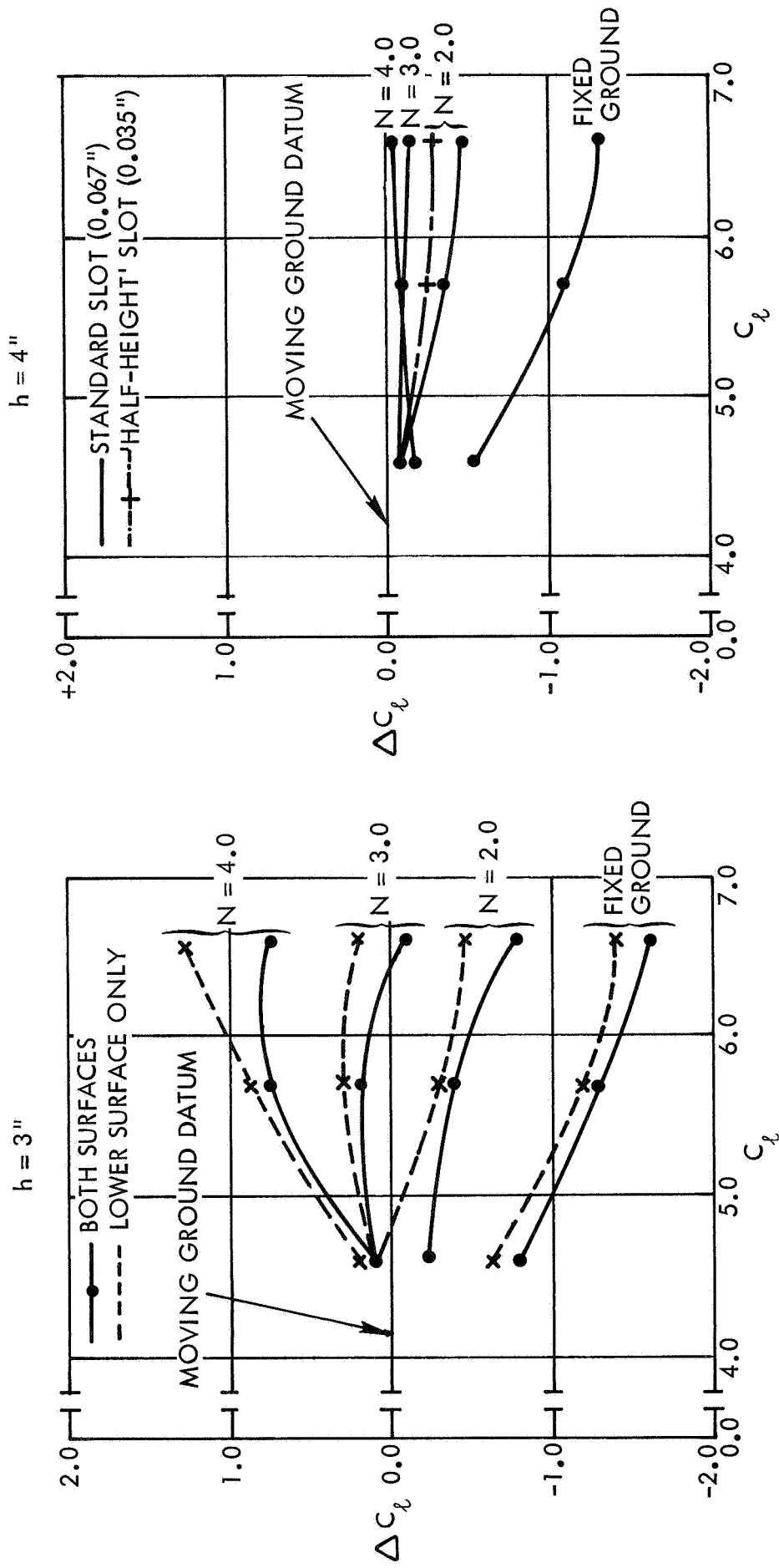


FIGURE 32. ERRORS IN SECTIONAL LIFT COEFFICIENT FOR FIXED AND BLC GROUND CONFIGURATIONS, $\eta = 0.643$

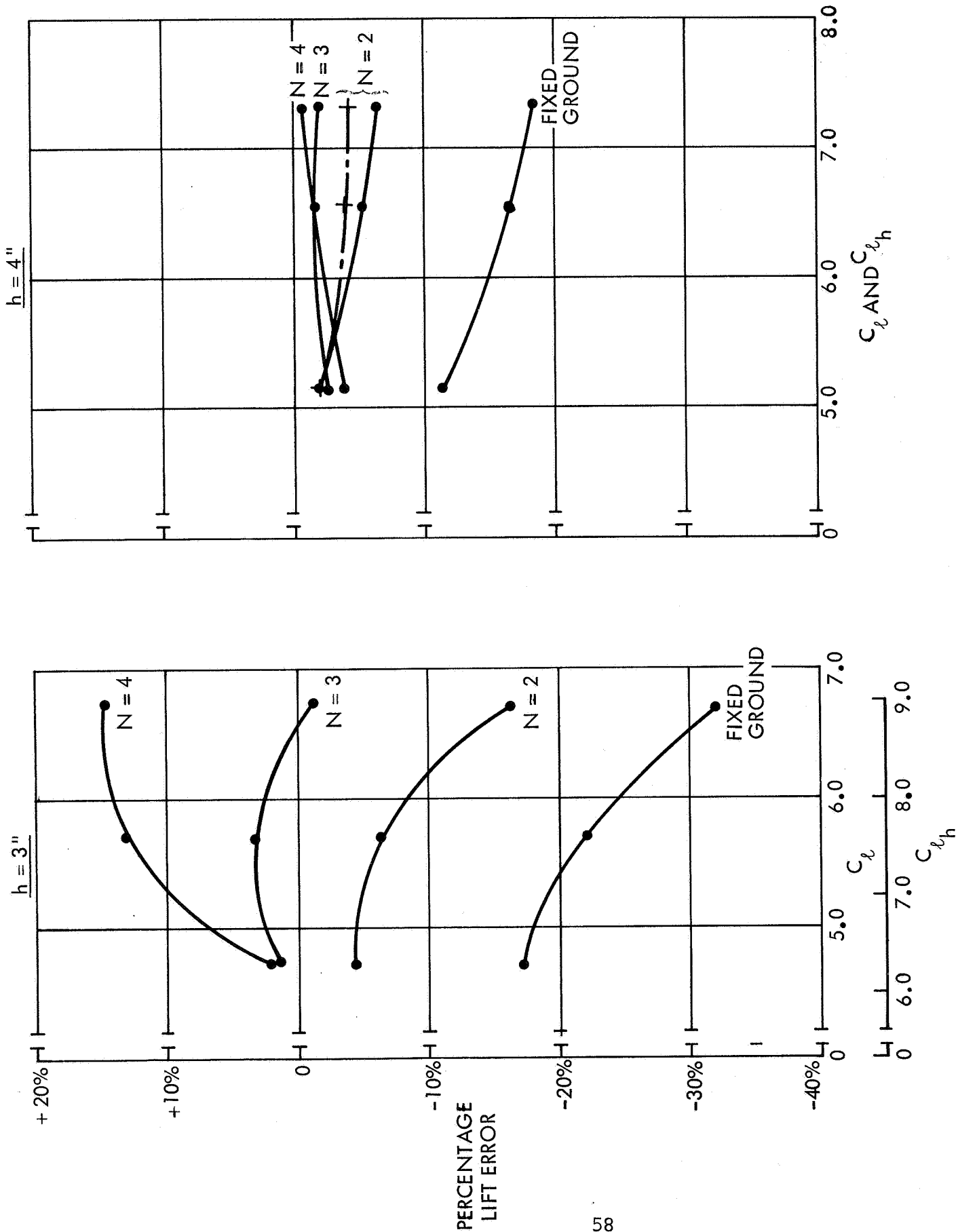
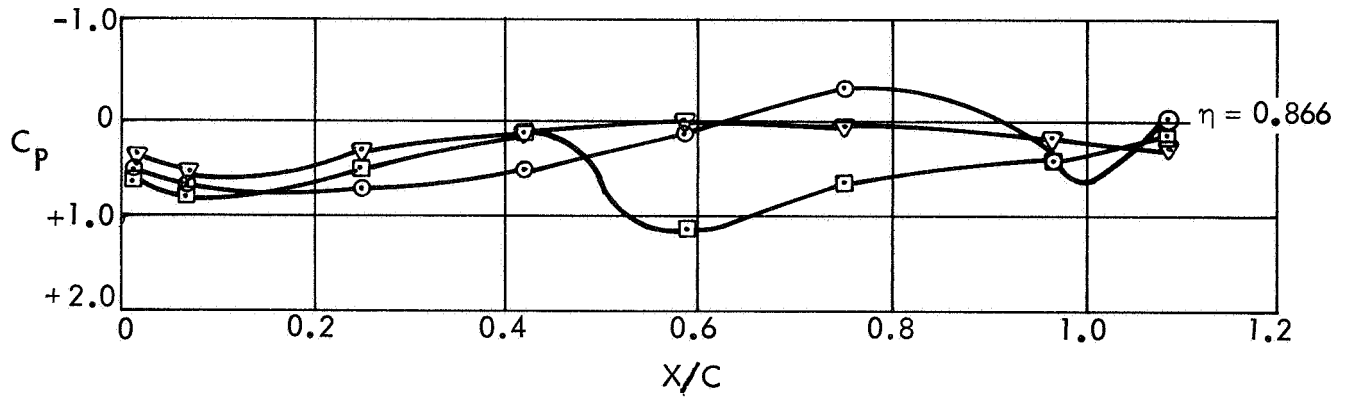
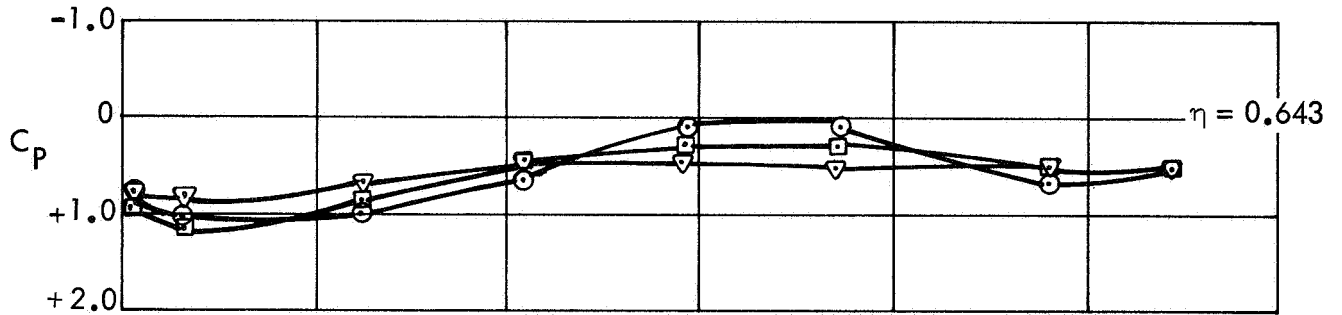
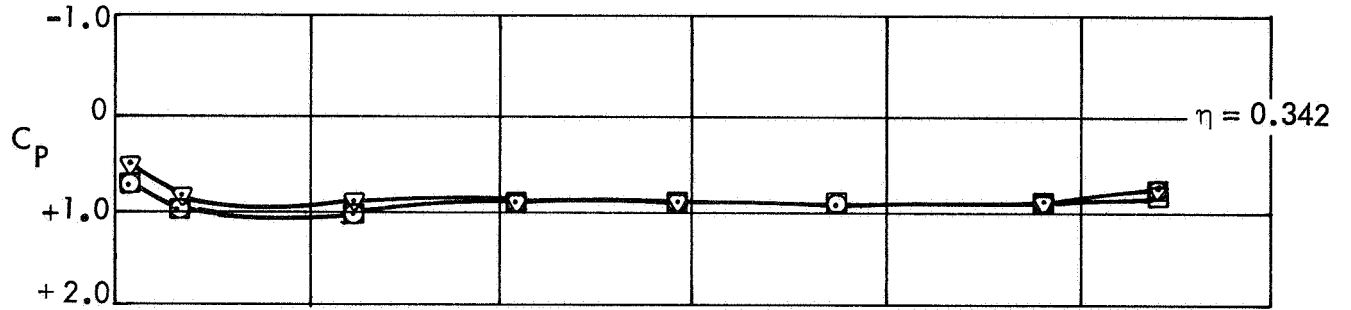


FIGURE 33. PERCENTAGE LIFT ERRORS FOR FIXED AND BLC GROUND CONFIGURATIONS, $\epsilon = 0.643$

h = 3"



SYM	STRUT CONFIGURATION
○	NO STRUT
▽	0° STRUT
□	45° STRUT

FIGURE 34. EFFECT OF DUMMY UNDERWING SUPPORT STRUT FAIRING (i) $C_{\mu_{NOM}} = 1.0$, $N = 2$

$h = 3''$

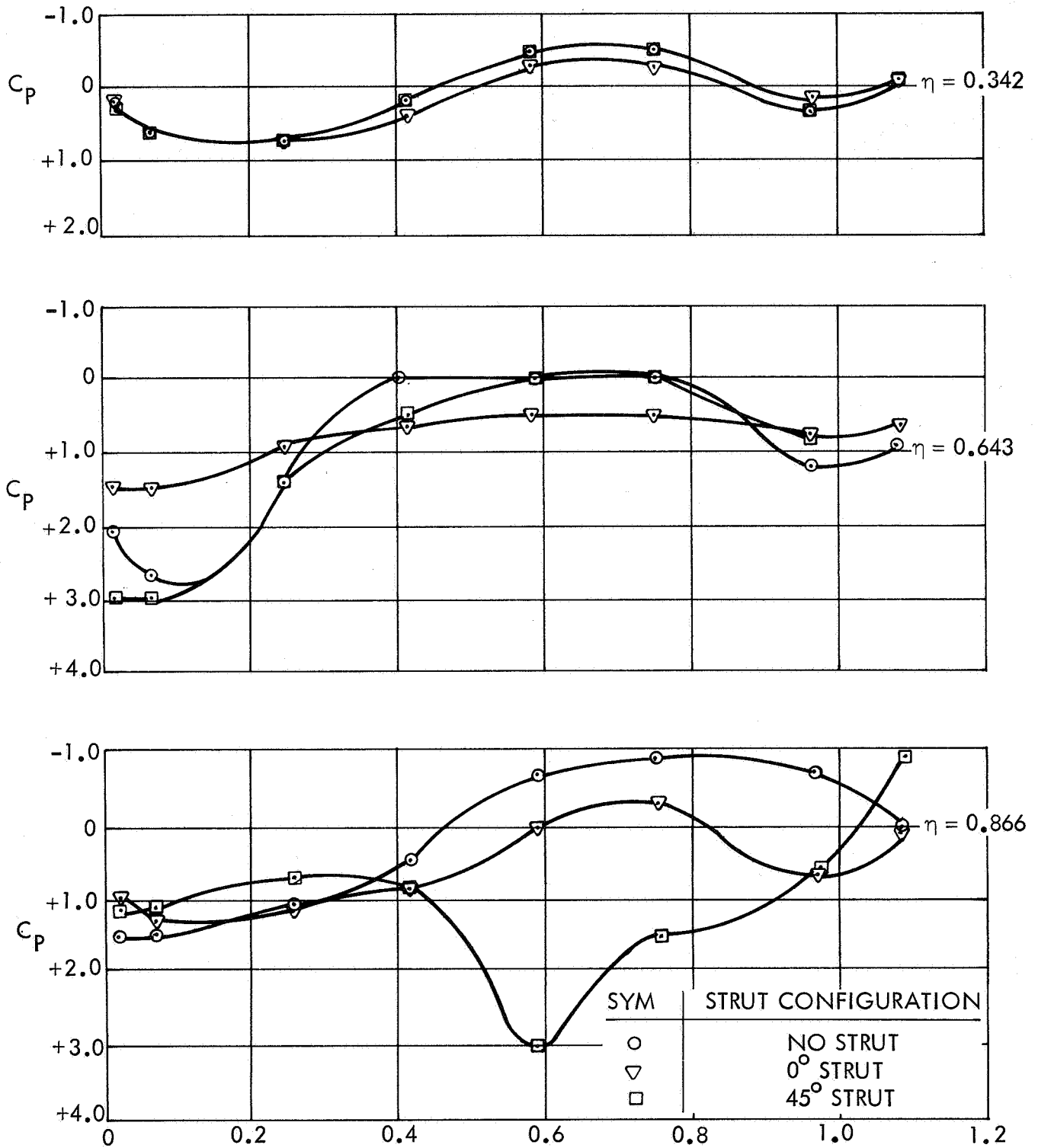


FIGURE 35. EFFECT OF DUMMY UNDERWING SUPPORT STRUT FAIRING (ii) $C_{u,NOM} = 3.0, N = 3$

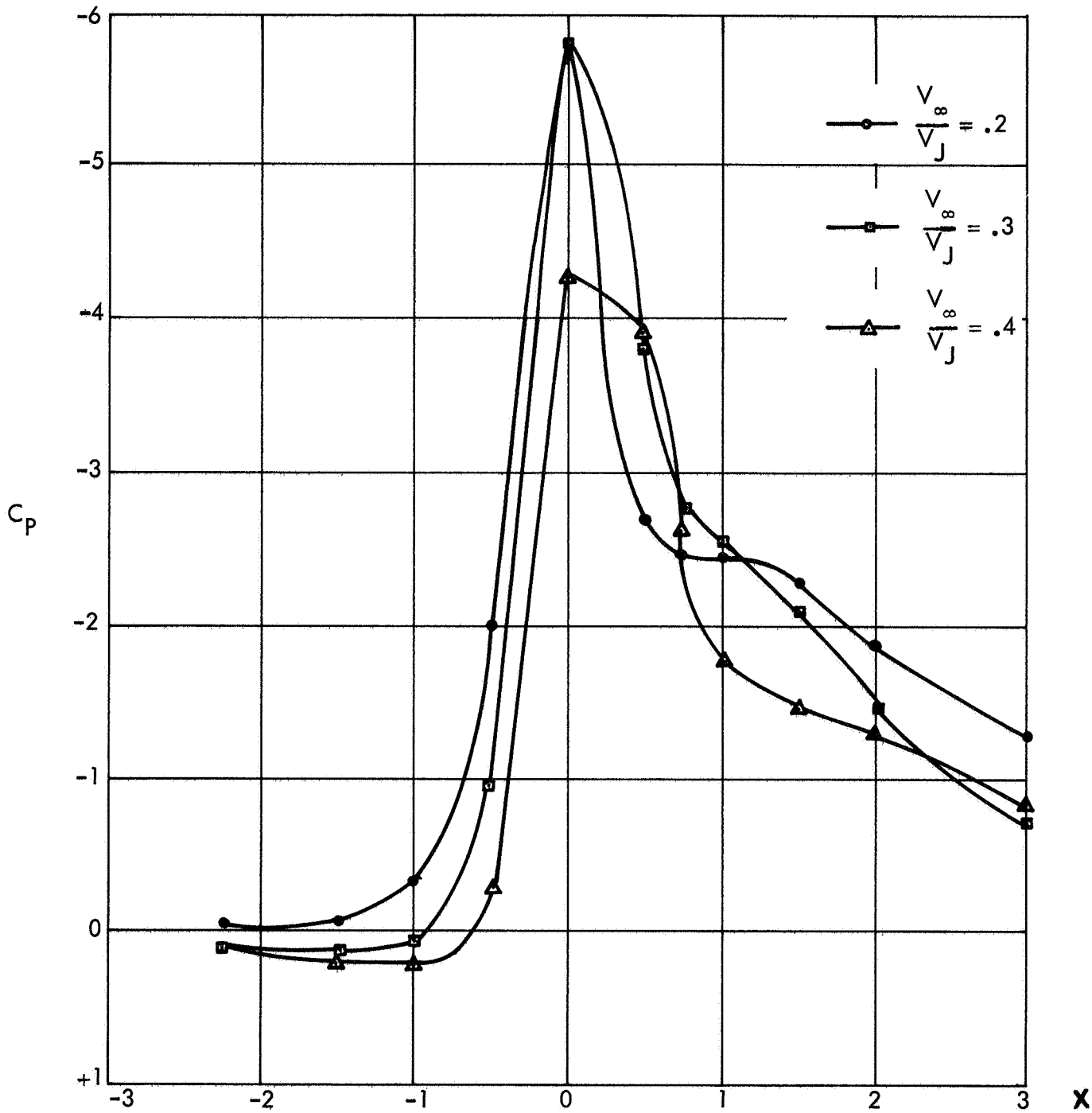
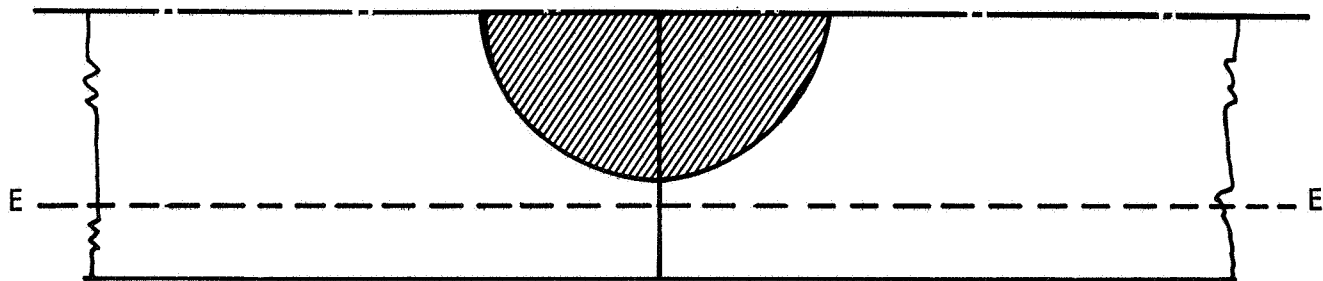
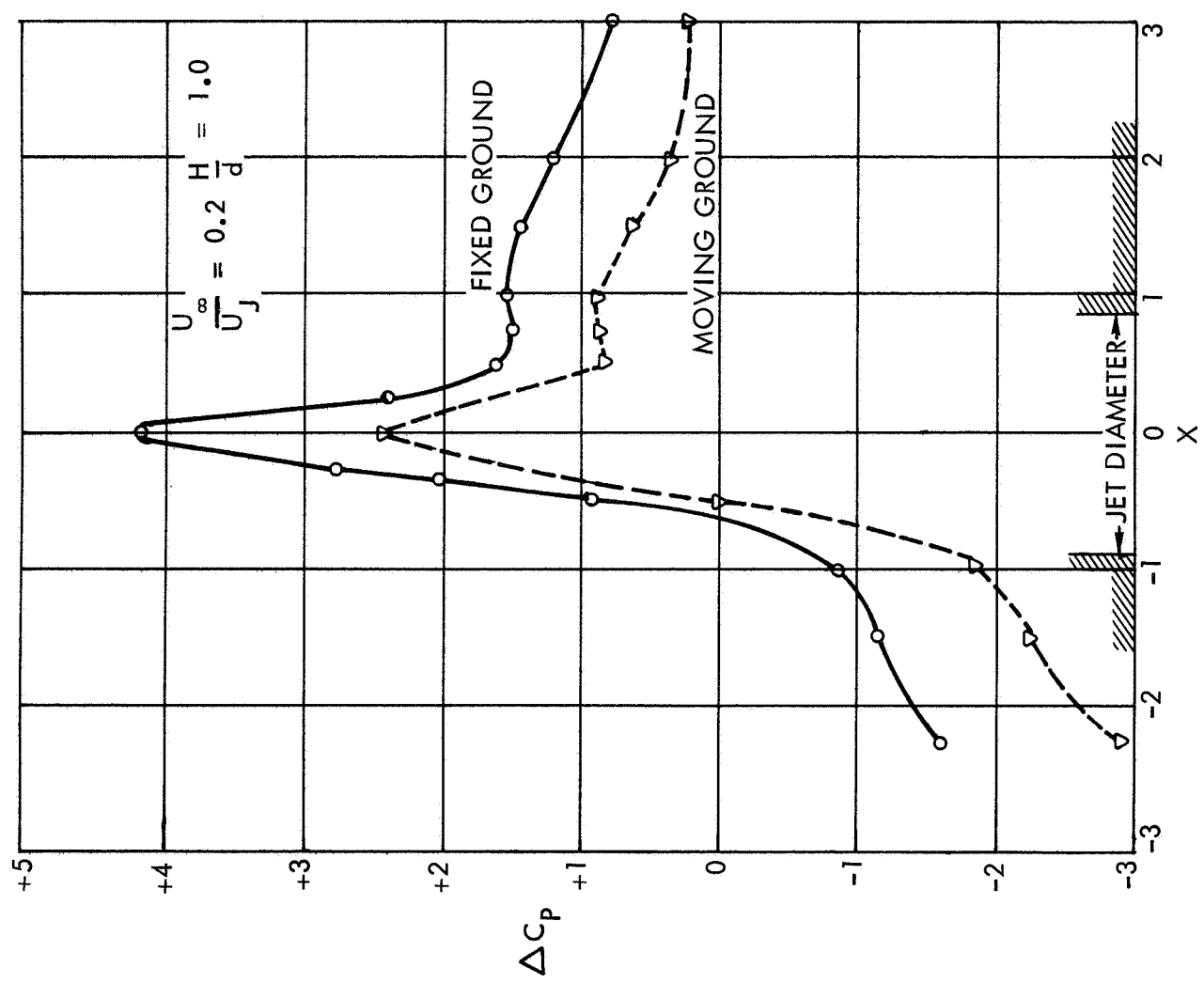
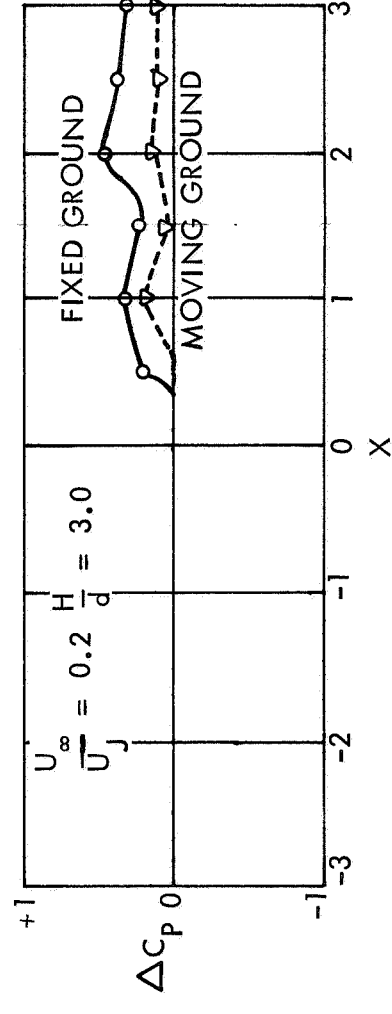
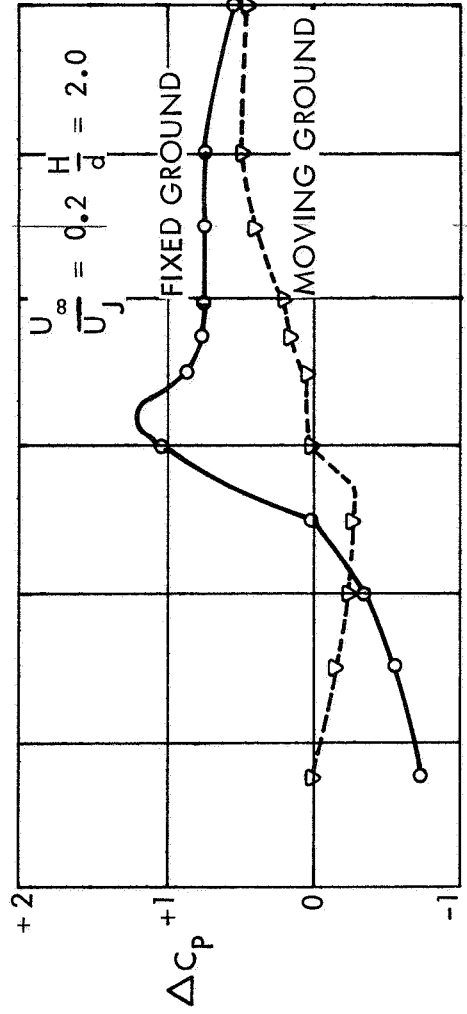
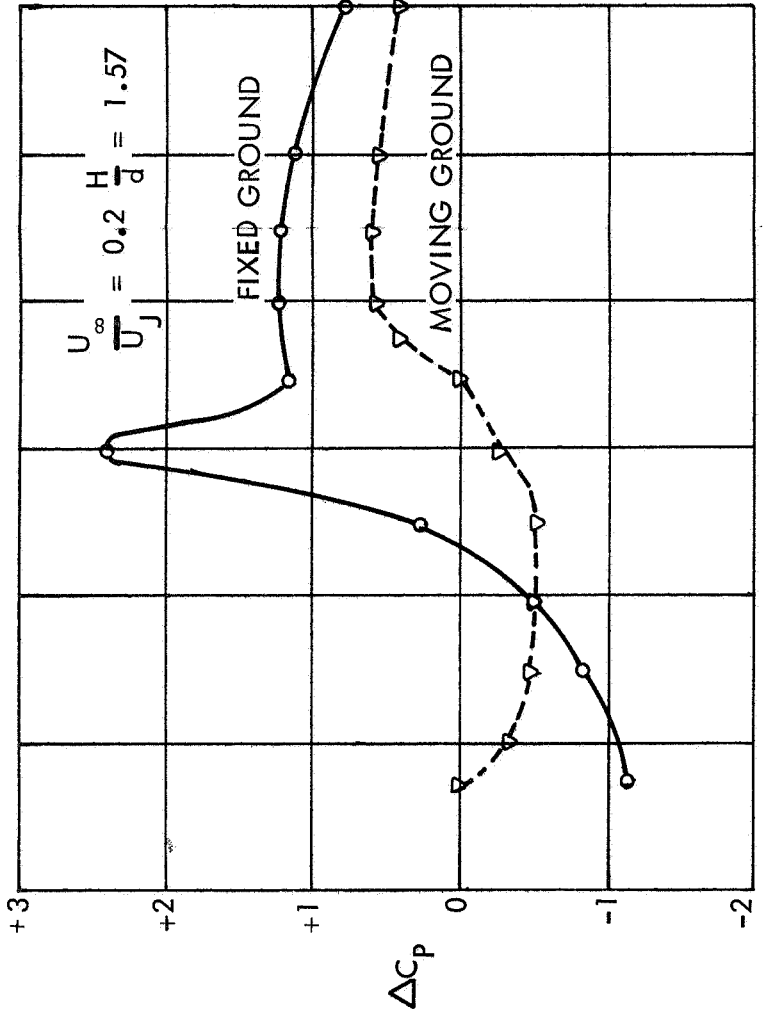


FIGURE 36. STATIC PRESSURE DISTRIBUTIONS FOR THE ROUND JET MODEL, CENTER-TUNNEL POSITION.



PRESSURES ARE FOR LINE EE, FIGURE 6

FIGURE 37. PRESSURE CHANGES, NEAR A ROUND LIFTING JET, CAUSED BY DESCENDING INTO GROUND EFFECT, (i) $\frac{U_\infty}{U_J} = 0.20$

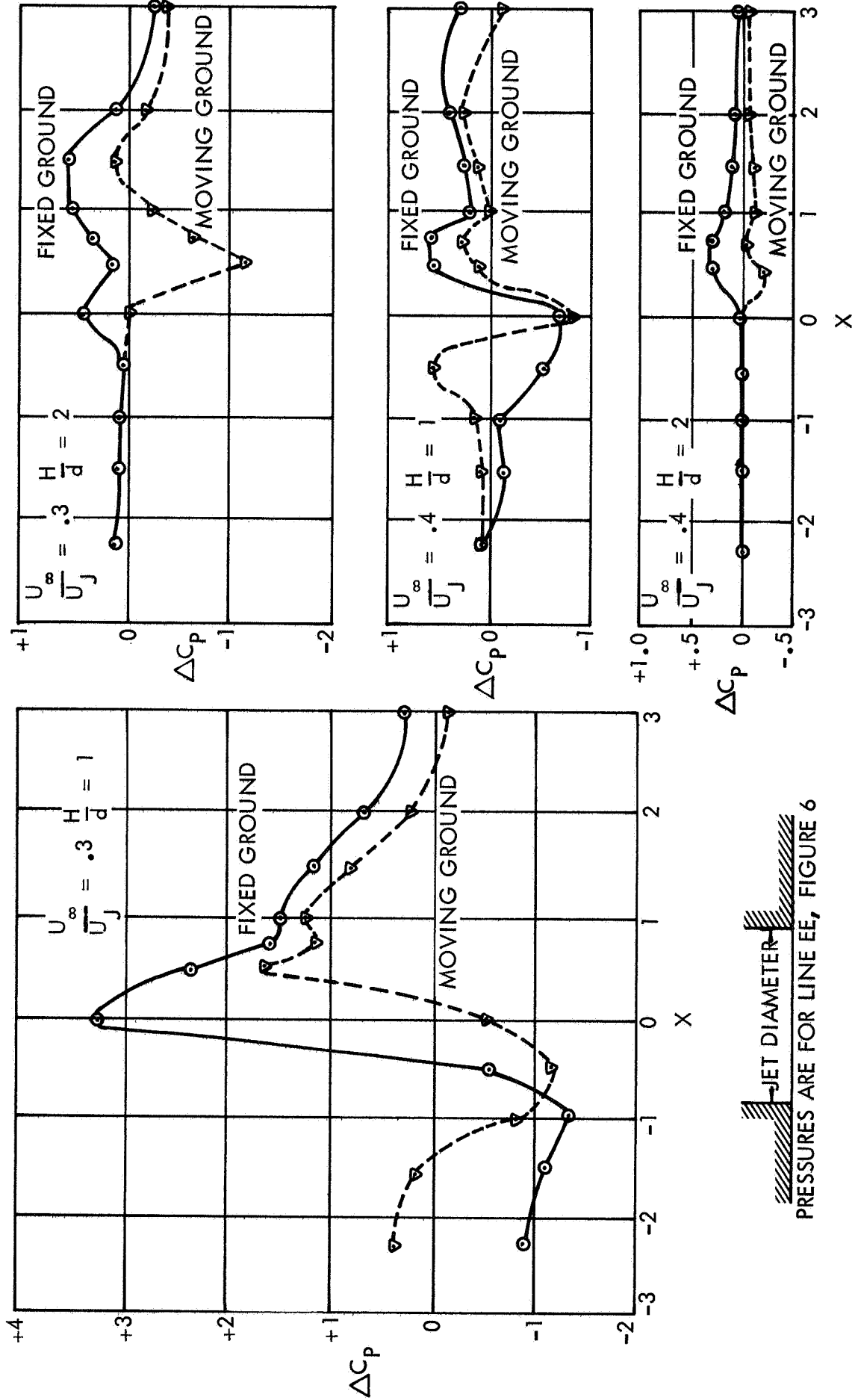
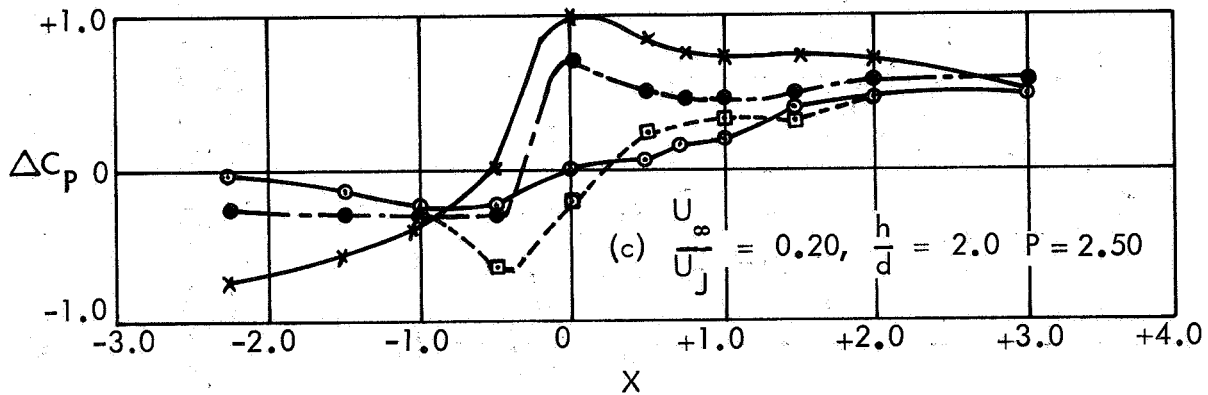
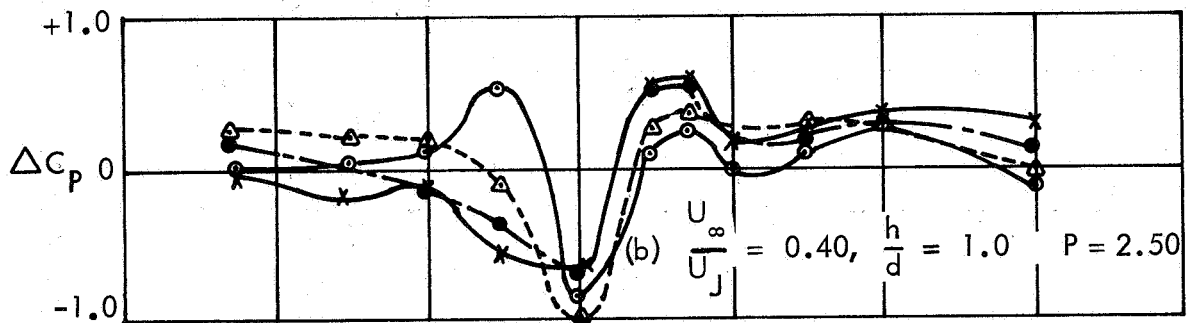
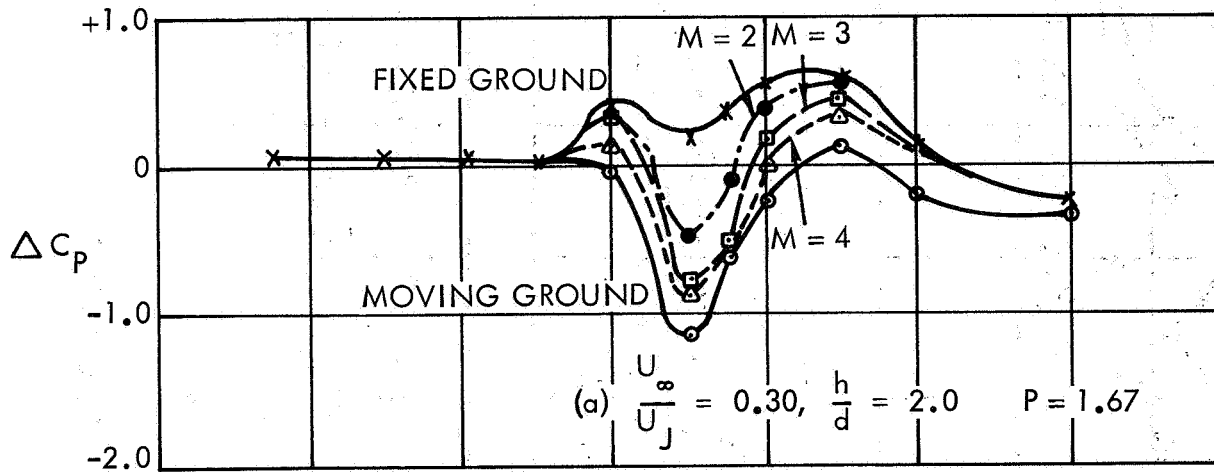


FIGURE 38. PRESSURE CHANGES, NEAR A ROUND LIFTING JET, CAUSED BY DESCENDING

INTO GROUND EFFECT, (ii) $U_\infty / U_j = 0.30$ AND 0.40



THE 0.032" SLOT AT THE 8" POSITION WAS USED

FIGURE 39. EFFECT OF BLOWING BLC, AT THE GROUND, ON LIFTING-JET EXIT PLANE PRESSURES:
(i) MODERATE JET PENETRATION CASES

THE 0.032" SLOT
AT THE 8" POSITION
WAS USED

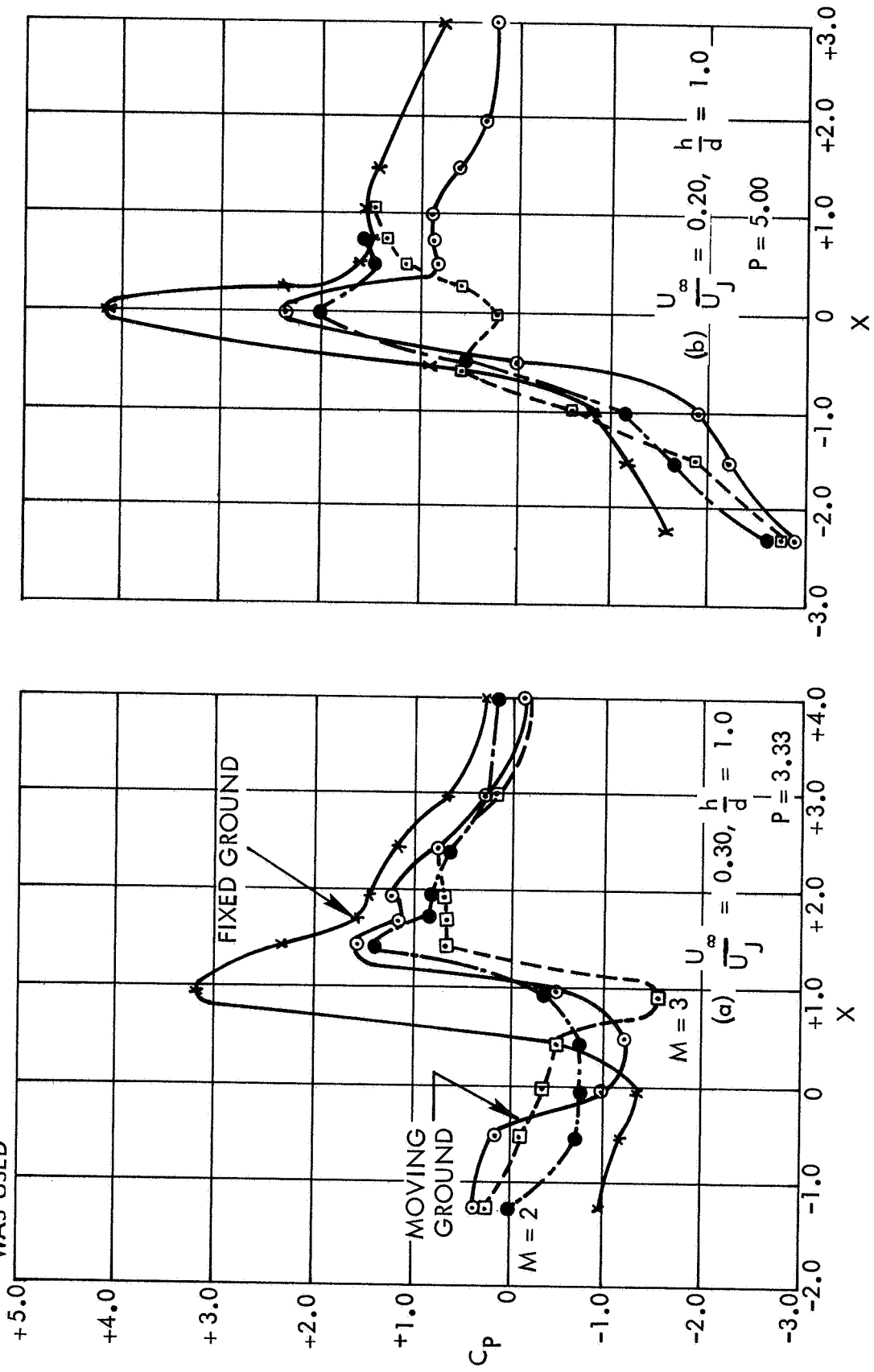


FIGURE 40. EFFECT OF BLOWING BLC, AT THE GROUND, ON LIFTING-JET
EXIT PLANE PRESSURES: (ii) STRONG JET PENETRATION CASES

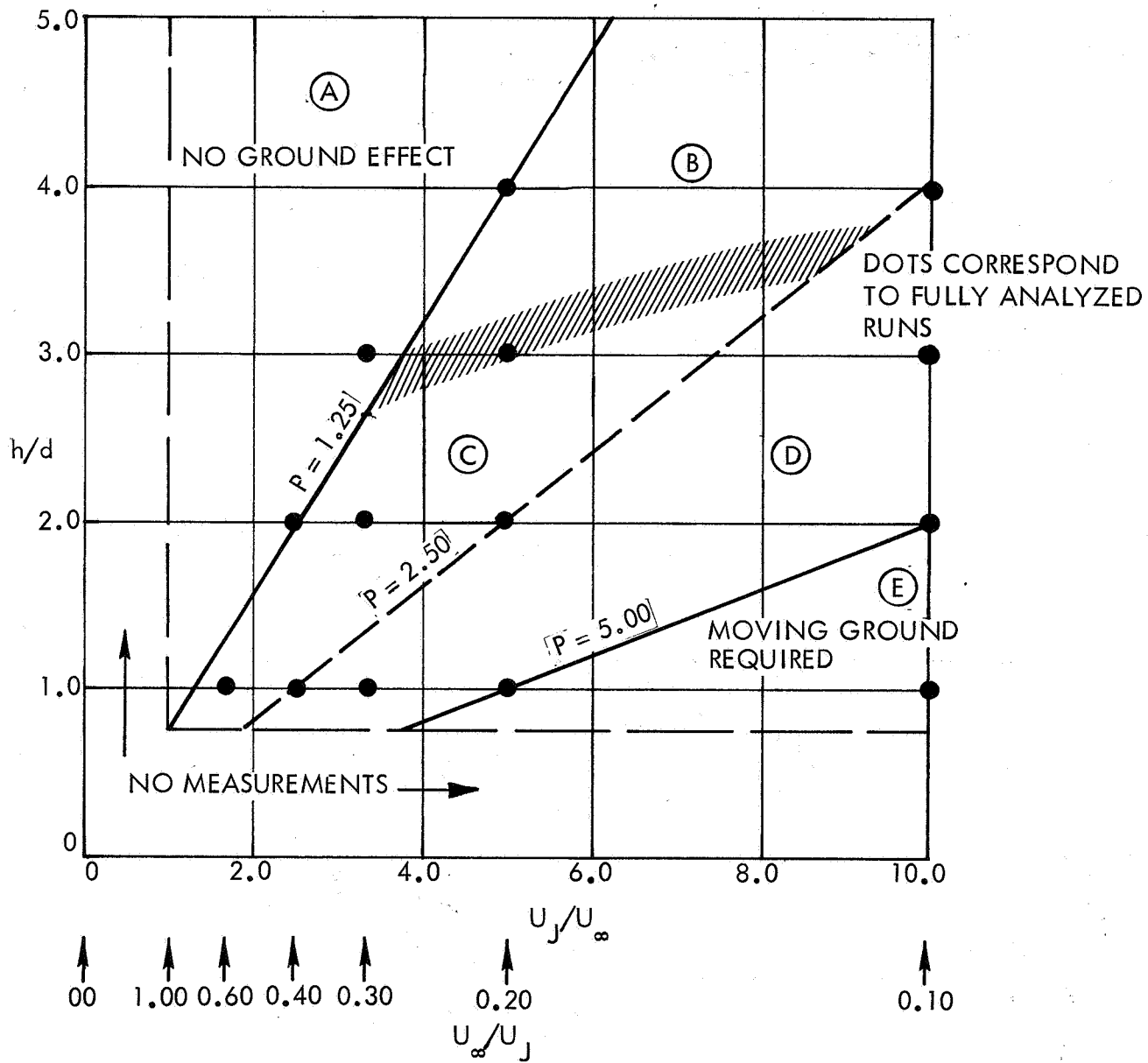


FIGURE 41. GROUND SIMULATION TECHNIQUES FOR ROUND, LIFTING-JET CONFIGURATIONS

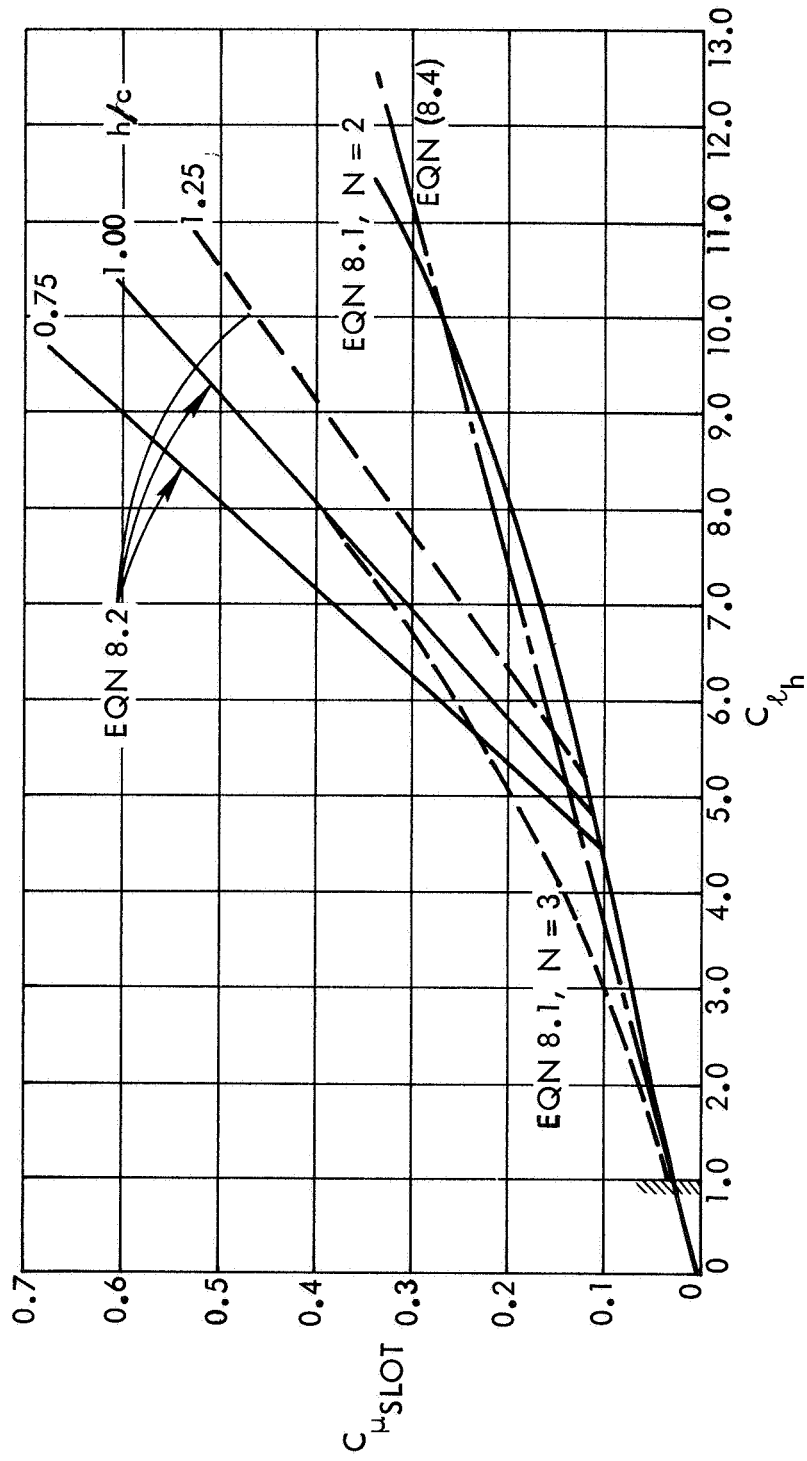


FIGURE 42. COMBINED FLOOR TANGENTIAL - BLOWING REQUIREMENTS